Performance of Cross-Corrugated Plate Heat Exchangers
Made of Polymeric and Metallic Materials

Asal Sharif

Promotor: prof. dr. ir. M. De Paepe
Proefschrift ingediend tot het behalen van de graad van
Doctor in de ingenieurswetenschappen: werktuigkunde-elektrotechniek

UNIVERSITEIT
GENT

Vakgroep Elektromechanica, Systeem- en Metaalengineering
Voorzitter: prof. dr. ir. L. Dupré
Faculteit Ingenieurswetenschappen en Architectuur
Academiejaar 2019 - 2020

ISBN 978-94-6355-298-1
NUR 961
Wettelijk depot: D/2019/10.500/106

Examination board

Prof. Dr. ir. Patrick De Baets (UGent, Chair)
Prof. Dr. ir. Michel De Paepe (UGent, Supervisor)
Prof. Dr. ir. Kamel Hooman (University of Queensland, Brisbane, Australia)
Dr. ir. Henk Huisseune (Novy, Kuurne)
Prof. Dr. ir. Jan Pieters (UGent)
Prof. Dr. ir. Bart Merci (UGent)
Dr. ir. Sven De Schampheleire (UGent)
Prof. Dr. ir. Joris Degroote (UGent, Secretary)

Promotor: Prof. dr. ir. M. De Paepe
Dissertation for obtaining the degree of
Doctor of Electromechanical Engineering

Department of Electromechanical, Systems and Metal Engineering
Faculty of Engineering and Architecture
Academic year 2019-2020

GHENT
UNIVERSITY

Acknowledgements

I would like to acknowledge Prof. Michel De Paepe for promoting this thesis and his time. My sincere gratitude to those without their support and guidance this work would not come to an end, the dean of the faculty of Engineering and Architecture, Prof. Patrick De Baets for his neutral judgment as the chairman of the jury committee, Prof. Bart Merci for his valuable technical feedbacks and support and Prof. Guy De Tré for his kind assistance and caring advice during the finalisation process of this work. Also, those jury members who believed in this work.

Additionally, I would like to acknowledge my colleagues for their encouragements. In particular I would like to thank Ilya and Willem for translating the summary to Dutch. Yves Maenhout for the IT support. Also I must acknowledge Griet Blonde, Annie Harri, Muriel Vervaeke and Annick De Coster for their administrative support.

Most importantly, my heartfelt gratitude to those who matter to me the most, Denis, my parents, Soheil, Francine and Edgar. Also my friends, Inès, Hossein, Golnoosh, Kathleen, Mariam, Mahta, Martin, Sarvenaz, Françoise, Christine and Ghazaleh.

Ghent, August 2019

Asal Sharif

Table of Contents

List of Figures

List of Tables

Nomenclature

A	area	m^2
B	base length	m
Bi	Biot number	-
c_p	specific heat capacity	J/kgK
D_h	hydraulic diameter	m
f	friction factor	-
F	safety factor for GCI	-
h	mean convective heat transfer coefficient	W/m^2K
H	grid spacing	m
Ht	height	m
j	Colburn j factor	-
K	thermal conductivity	W/mK
k	turbulent kinetic energy	m^2/s^2
L	flow length	m
Nu	Nusselt number	-
p	order of convergence	-
P	pressure	Pa
P^*	relative pumping power	m^{-2}
Pr	Prandtl number	-

q	mean heat flux	W/m^2
R	thermal resistance	K/W
r	grid refinement ratio	-
Re	Reynolds number	-
T	Temperature	K
t	thickness	m
U	overall thermal conductance	W/m^2K
u	velocity in x direction	m/s
u_c	Velocity in minimum cross-sectional area	m/s
v	velocity in y direction	m/s
V^*	relative heat exchanger volume (eq (2-30))	m^3
w	velocity in z direction	m/s
x, y, z	coordinates	m
x^*	dimensionless coordinate position over the flow length	-

Greek symbols

α	apex angle	*degrees*
β	non-periodic pressure gradient	Pa/m
γ	corrugation inclination angle	*degrees*
Δ	difference	-
ε	effectiveness	-
Θ	dimensionless temperature	-
μ	dynamic viscosity	Pas

ν	kinematic viscosity	m^2/s
ρ	density	Kg/m^3
σ	contraction factor	-
Φ	general dependent variable	-
ω	specific dissipation rate	$1/s$

Subscripts and Superscripts

b	bulk
c	minimum cross section
w	wall
ws	wetted surface
$'$	fluctuations
$*$	periodic

Acronyms

BC	boundary condition
CFD	computational fluid dynamics
GCI	grid convergence index
HVAC	heating, ventilation, air conditioning & refrigeration
LES	large eddy simulation
LKW	low Reynolds number k-ω
LMTD	logarithmic mean temperature difference
NTU	number of transfer units
PEC	performance evaluation criterion

RSM	Reynolds stress model
SST	shear stress transport model
TC	thermal conductivity

Samenvatting

De stijging van de globale energievraag is wijdverspreid over alle sectoren van de globale economie. Als gevolg daarvan stijgt de energiegerelateerde CO2-uitstoot over de gehele wereld. Verwarming en koeling is verantwoordelijk voor ongeveer de helft van het energiegebruik van de Europese Unie (EU). De Europese autoriteiten en regeringen hebben prioriteit gegeven aan strategieën voor meer efficiënte en duurzame verwarming en koeling. Het is algemeen geweten dat warmtewisselaars de werkpaarden zijn gerelateerd aan verwarming en koeling. Het is daarom zinvol om de focus te leggen op het design van energie-efficiëntere en duurzamere warmtewisselaars om het probleem van het hoge energiegebruik in verwarming- en koelsystemen aan te pakken.

Compacte warmtewisselaars worden steeds vaker gebruikt voor verscheidene toepassingen aangezien ze een hoge effectiviteit en klein volume hebben vergeleken met meer conventionele plaat- en buiswarmtewisselaars. Dwarsstroomwarmtewisselaars met geprofileerde platen (hierna aangegeven door de meer gebruikelijke Engelse term ‘cross-corrugated’ warmtewisselaar) zijn compacte warmtewisselaars die veelvuldig gebruikt worden in de industrie en dewelke zeer geschikt zijn voor toepassing bij een laag Reynolds (*Re*) getal zoals HVAC (verwarming, ventilatie en luchtbehandeling) toepassingen. Dit type warmtewisselaar genereert zelfs bij lage *Re* getallen turbulentie waardoor de warmteoverdracht wordt verbeterd. Momenteel worden deze warmtewisselaars gemaakt uit metalen zoals roestvrij staal en nikkel-gebaseerde legeringen. Metalen hebben een hoge thermische geleidbaarheid en goede mechanische sterkte. Deze eigenschappen zijn gewenst voor het design van warmtewisselaars voor vele verschillende industriële toepassingen. Er zijn echter ook drijfveren om alternatieve materialen zoals polymeren te overwegen, onder andere de Europese doelen tegen 2020 rond klimaatverandering en energie, bevuiling, corrosie, schaarste van edele metalen, het hoge gewicht en de hoge investeringskost van warmtewisselaars uit metaal. Er zijn verder voordelen geassocieerd met het gebruik van polymeren als materiaal ter vervanging van metaal in de productie van warmtewisselaars. Enkele voorbeelden zijn het lage gewicht, grotere vormvrijheid, lage productiekost, compatibiliteit met veel vloeistoffen en gassen en de bruikbaarheid in bevochtiging- en ontvochtigingsinstallaties.

Tijdens de voorbije jaren is de interesse in het gebruik van polymeren warmtewisselaars voor verscheidene toepassingen toegenomen. Er gaan echter enkele uitdagingen gepaard met het design van een warmtewisselaar gemaakt uit

polymeren door de lagere thermische geleidbaarheid van het materiaal en met het bewaren van de structurele integriteit van de warmtewisselaar. In het geval van metalen warmtewisselaars is het design gefocust op de convectieve warmteoverdracht, aangezien de conductieve warmteoverdracht zeer effectief is door de hoge thermische geleidbaarheid. De wetenschappelijke literatuur toont echter aan dat door de lage thermische geleidbaarheid van polymeren, de conductieve warmteoverdracht ook een probleem kan zijn voor het design van polymeren warmtewisselaars, waardoor het design een gecombineerd convectie-conductie probleem wordt. Onderzoekers zijn continu op zoek naar nieuwe concepten om het conductieprobleem te verhelpen door te werken rond de geometrie (dunnere wanden, 53 µm) of de materialen (thermisch verbeterde composieten). De numerieke en experimentele studies rond warmtewisselaars uit polymeren of composieten zijn grotendeels rond vlakke plaat- en buiswarmtewisselaars. Het grote potentieel van cross-corrugated plaatwarmtewisselaars gemaakt uit polymeren is nog niet uitgebreid bestudeerd. Er is slechts één experimentele studie gevonden rond de evaluatie van de thermo-hydraulische prestatie van een zuiver polymeren cross-corrugated platenwarmtewisselaar met sinusoïdale vorm. Dankzij de grotere geometrische flexibiliteit in de productie van polymeren en de eenvoudige productiemethoden is een plaat met zaagtandprofiel echter zeer bruikbaar. Cross-corrugated platenwarmtewisselaars met zaagtandprofiel ingezet bij Reynoldsgetallen lager dan 2300 zijn de focus van deze thesis. De prestatie van deze warmtewisselaars gemaakt uit metalen, zuivere polymeren en composieten zijn bestudeerd aan de hand van numerieke stromingssimulaties (CFD of computational fluid dynamics).

Deze thesis start met een uitgebreide literatuurstudie om de hiaten te vinden in het onderzoek rond platenwarmtewisselaars met zaagtandprofiel in het werkingsgebied bij lage Reynolds getallen. Om de convectieve stroming in dit soort warmtewisselaars numeriek op te lossen met CFD is er geen consensus onder onderzoekers rond het gebruiken van laminaire stromings- of turbulente stromingsoplossingsstrategieën. Verder volgt uit de literatuurstudie dat de prestatie van cross-corrugated warmtewisselaars, onafhankelijk van het profiel van de platen, zeer afhankelijk is van de geometrische parameters zoals de aspectverhouding (verhouding breedte tot lengte of aspect ratio) van het kanaal en de hoek tussen de gestapelde platen (corrugation angle). De beschikbare studies rond sinusoïdale profielen behandelen voornamelijk de invloed van de hoek tussen de platen. De correlaties die beschikbaar zijn uit de wetenschappelijke literatuur zijn steeds toepasbaar voor slechts een bepaalde aspectverhouding van de kanalen, dewelke standaard is voor de productie van dit soort geometrie uit metaal. De invloed van de hoek op de thermohydraulische prestatie van cross-corrugated platenwarmtewisselaars is aanwezig in deze correlaties, de invloed van de aspectverhouding is echter niet toegevoegd. Het design van zaagtand cross-

corrugated platenwarmtewisselaars is echter flexibeler in aspectverhouding als er polymeren worden gebruikt voor de productie van de platen. De aspectverhouding is voor deze geometrieën proportioneel aan de tophoek van het zaagtandprofiel (apex angle). Voorgaande studies rond cross-corrugated warmtewisselaars met zaagtandprofiel gebruikten twee tophoeken (60° en 90°). Er is geen informatie te vinden in de wetenschappelijke literatuur rond de invloed van de tophoek op de drukkrachten, turbulente intensiteit en wervelsterkte en de verbanden met de stromings- en warmteoverdrachtkarakteristieken in deze geometrieën. Er is ten slotte beperkte informatie te verkrijgen rond de vergelijking van de prestatie van verschillende geometrieën, daarbij gebruik makende van toepasselijke prestatie evaluatie criteria (PEC) en de daaruit volgende keuze van de optimale geometrie voor het beschouwde systeem.

Om de voorheen vermelde hiaten in de wetenschappelijke literatuur weg te werken, zal deze thesis de keuze van een laminaire stromingsoplosser en van het Reynolds stress model (RSM) als turbulente stromingsoplosser voor numerieke simulaties evalueren. Uit een-op-een vergelijkingen tussen RSM simulaties en experimentele resultaten volgen afwijking kleiner dan 5%, wat binnen de meetnauwkeurigheid van het experiment valt. De invloed van een groot bereik van tophoeken (45° tot 150°) op de thermohydraulische prestatie is geanalyseerd met numerieke simulaties met RSM. Verder wordt de invloed van de intensiteit en complexiteit van de recirculatiezones en de turbulente intensiteit op de thermohydraulische prestatie en die hiermee gerelateerde viskeuze en drukkrachten bestudeerd. De keuze van het simulatiegebied als de elementaire cel met periodieke randvoorwaarden ten opzichte van een kanaal met meerdere opeenvolgende cellen wordt besproken. Drukval en warmteoverdrachtscoëfficiënt stijgen met groter wordende tophoek, door de verhoging van de drukkrachten en de wervelsterkte in de stromingsrichting. In tegenstelling tot de stroming in buizen, zijn voor deze stroming de drukkrachten dominant ten opzichte van de viskeuze krachten. De invloed van de tophoek op de wrijvingscoëfficiënt (f) en de Colburn j factor volgt twee duidelijke trends. De tophoeken rond 90-100° zijn de transitiehoeken voor het stromingsregime. Maxima van turbulente intensiteit, wrijvingscoëfficiënt en Colburn j factor worden waargenomen rond deze hoeken. De verhouding tussen de druk- en viskeuze krachten daalt als de tophoek groter wordt dan 100°, wat een kleinere recirculatiezone en lagere turbulente intensiteit met zich meebrengt. Verder wordt de thermohydraulische prestatie van de geanalyseerde geometrieën bepaald gebaseerd op een prestatie evaluatie criterium. Hieruit volgt dat de geometrie met de grootste tophoek het beste presteert. Ten slotte worden gegeneraliseerde correlaties voor het Nusselt getal (Nu) en wrijvingscoëfficiënt voorgesteld om het effect van de tophoek in rekening te brengen. De resultaten van de simulaties en van de voorgestelde correlaties zijn in

goede overeenkomst, er is een maximale afwijking van 9% voor Nu en van 13% voor f.

Ten tweede wordt in deze thesis het gecombineerd convectie-conductie warmteoverdrachtsprobleem voor cross-corrugated platenwarmtewisselaars uit polymeren opgelost met de hulp van CFD. Het CFD model houdt specifiek rekening met de thermische eigenschappen van het gebruikte materiaal (zuiver polymeer of composiet De haalbaarheid van het gebruik van CFD om stroming en warmteoverdracht in een polymeren cross-corrugated warmtewisselaar te bepalen is gevalideerd met experimenten. De keuze van twee verschillende rekendomeinen voor het CFD model en de voor- en nadelen van deze keuze worden besproken. De resultaten tonen aan dat er een significante invloed is van het temperatuurprofiel aan de plaat op de lokale en gemiddelde warmteoverdrachtscoëfficiënten bij lage Reynolds getallen. De thermische prestatie van een nieuw ontwerp van dit soort warmtewisselaar, ontworpen om te concurreren met een uit metaal, is bestudeerd. Verder is ook de invloed van de plaatdikte en de thermische geleidbaarheid op de prestatie onderzocht. De conclusie van dit onderzoek luidt dat het nieuwe ontwerp veel potentieel heeft om de metalen warmtewisselaar te vervangen voor een groot bereik van toepassingen door zijn voordelen omtrent bevuiling, corrosie en productiekost. Het voorgestelde CFD model is in staat om nauwkeurig de prestatie van dit soort warmtewisselaars uit polymeer te voorspellen. Het is echter cruciaal dat voor elke specifieke toepassing de structurele integriteit, de kostenanalyse van de polymeren of composieten en de materiaaleigenschappen zoals permeabiliteit en absorptiviteit worden geanalyseerd naast het voorgestelde thermische CFD model.

Summary

Rise in global energy demand is widespread across all the main sectors of the global economy. Consequently, the energy-related CO_2 emissions worldwide is increased. Heating and cooling is responsible for about half of the European Union's (EU) final energy consumption. The EU authorities and governments have a priority on developing strategies which lead to more efficient and sustainable heating and cooling. There are different approaches in order to tackle the energy use issue in heating and cooling systems. The design of more energy efficient and sustainable heat exchangers is one of them.

Compact heat exchangers are increasingly used for different applications due to their high efficiency and small size compared to conventional plate and tubular heat exchangers. Cross-corrugated plate geometry is a type of compact heat exchangers that is widely used in industry and particularly is suitable for low *Re* applications such as HVAC (heating, ventilation and cooling) applications. This type of geometry generates turbulence even at a very low Reynolds number, which enhances the heat transfer. Moreover, the corrugation pattern provides a large heat transfer area, structural strength and enhancement of heat transfer. Currently, metallic materials such as stainless steel and nickel-based alloys are used to produce this type of heat exchanger. Metallic materials have high thermal conductivity and high material strength. These properties are favourable for designing heat exchangers for many different industrial applications. However, factors such as the 2020 targets of the EU on climate change and energy, fouling, corrosion, the scarcity of precious materials, and the heavy weight and high capital cost of metallic heat exchangers are all incentives towards considering alternative materials such as polymers. There are advantages associated with the use of polymeric materials in place of metallic materials in heat exchanger manufacturing. For example, their light weight, great geometric flexibility, low manufacturing cost, ability to handle both liquids and gases, and ability to be used in both humidification and dehumidification systems.

In recent years, significant interest has been shown in using polymeric heat exchangers for different applications. However, there are challenges with designing heat exchangers with polymeric materials due to their low thermal conductivity and structural performance. For metallic heat exchangers the design problem mainly is limited to the convective heat transfer, as there is no issue with the conduction due to the high thermal conductivity of metals. However, based on the literature, due to the low thermal conductivity of polymers, low conduction can be an issue in the polymeric heat exchangers, therefore the heat transfer

problem is combined convection-conduction. Researchers are constantly looking for new solutions to overcome the conduction problem by either working on the geometries (thinned wall, 53 μm) or polymeric materials (thermally enhanced composites). The existing numerical and experimental studies on pure polymeric or composite heat exchangers are mainly associated with the flat plate or tube heat exchangers. The great potential of cross-corrugated plates with polymer materials is not studied enough. There is only one experimental study on evaluation of the thermo-hydraulic performance of pure polymeric cross-corrugated plate heat exchangers with sinusoidal corrugation and thinned wall. In general cross-corrugated plate geometries are traditionally manufactured and studied with sinusoidal corrugations. However, thanks to the great geometric flexibility that polymers provide and the ease of manufacturing the manufacture of cross-corrugated with triangular corrugation is feasible. Cross-corrugated plate heat exchangers with triangular corrugation used in low Reynold applications (less than 2300) is the focus of this thesis. Performance of triangular cross-corrugated plate heat exchangers made of metallic, pure polymeric and composite materials are investigated using computational fluid dynamics (CFD).

Firstly, in this thesis, an extensive literature review is performed to identify the research gaps concerning the convection problem in triangular cross-corrugated plate heat exchangers at low range of Reynolds number. In order to solve the convective flow problem in the cross-corrugated plate geometries using CFD, the researchers do not agree on whether to use laminar or turbulent flow solver. In addition, based on the literature, the performance of cross-corrugate plate geometries independent of the corrugation type strongly depends on the geometrical parameters being the aspect ratio of the channel and the angle between the plates that are stacked (corrugation angle). The available studies on sinusoidal corrugation mainly report the influence of the corrugation angle. The available correlations in the literature are only related to a specific aspect ratio of the channels which is common for manufacture of this type of geometry with metallic materials. The influence of different corrugation angle on the thermo-hydraulic performance of cross-corrugated plate heat exchangers are included in these correlations but not the influence of the channel aspect ratio. For the design of triangular cross-corrugated geometries with polymeric materials there are more flexibilities in terms of channels aspect ratio. For the geometries with triangular corrugation, the aspect ratio of the channel is proportional to the apex angle of corrugation. The existing studies on triangular cross-corrugated plates are associated with two apex angles being 60° and 90°. Moreover, in the literature, no such study is available which deals with the effect of the apex angle on the pressure force, turbulence intensity, and vorticity magnitudes and links those to the flow and heat transfer mechanisms of triangular cross-corrugated plates. Finally, there is little information available in the

literature on comparing the performance of several geometries using an appropriate performance evaluation criteria (PEC) and selecting the optimal geometry for a specific system.

To close the aforementioned gaps in the literature, in this thesis, the choice of laminar solver and Reynolds stress models (RSM) as turbulent solver for the CFD model are evaluated. One on one comparison between the RSM and experimental results shows less than 5% deviation, which is within the uncertainty of the experiment. The influence of a wide range of apex angles from 45° to 150° on the thermo-hydraulic performance is analysed using CFD with RSM flow solver. Furthermore, the influence of the intensity and complexity of the recirculation zones along with the turbulence intensity on the thermo-hydraulic performance and corresponding viscous and pressure forces are studied. The choice of the computational domain as a unitary cell with periodic boundary condition versus a long channel with several cells is discussed. By increasing the apex angle both pressure drop and heat transfer coefficient increase, due to the increase of the pressure force and the vorticity magnitude along the flow direction. The pressure force is the dominant force, contrary to pipe flow, where the viscous force is dominant. The influence of the apex angle on the friction factor (f) and the Colburn j factor follows two distinguished trends. The apex angles around of 90-100° are the transitional angles for the flow regime. Peak of turbulence intensity, friction factor and Colburn j factor are observed around these angles. The ratio between pressure and viscous forces decays after angle 100°, resulting in a smaller recirculation zone and lower turbulence intensity. In addition, the thermo-hydraulic performance of the considered geometries is compared with respect to each other based on a performance evaluation criterion. It is found that the geometry with the largest apex angle has the highest performance. Finally, generalized correlations for Nusselt number (Nu) and f are presented to specifically take into account the effect of the apex angle. The data from the simulations and generalized correlations are in a good agreement, with a maximum deviation of 13% for Nu and 11.7% for f.

Secondly, in this thesis, the combined convection-conduction (conjugate) heat transfer problems on polymeric cross-corrugated plates is solved with the aid of CFD. The CFD model specifically takes into account the thermal properties of the heat exchanger material (pure polymer and composite). The feasibility of the application of the CFD model to solve the flow and conjugate heat transfer problems of polymeric cross-corrugated heat exchangers is validated against experimental results. The choice of two different computational domain for the CFD model and their advantages are discussed. The thermal performance of a new polymeric cross corrugate heat exchanger designed to be thermally competitive with a metallic one at the component level is studied. Furthermore, the influence

of wall thickness and thermal conductivity on thermal performance are investigated. In conclusion, the new design for a polymeric cross-corrugated heat exchanger has great potential to replace the metallic cross-corrugate for a wide range of applications due to its advantages regarding fouling, corrosion, and manufacturing cost. The proposed CFD model is able to accurately predict the performance of these type of geometries composed of polymeric material. However, it should be ensured that for each specific application the structural performance, cost analysis of composite materials and material performance in terms of permeability and absorption are coupled with the proposed CFD thermal model.

1

Introduction

1.1 Why this PhD?

Based on recent energy policy reports and assessments provided by international authorities such as the International Energy Agency (IEA), energy efficiency remains a crucial issue in energy policy agendas at both national and international levels [1, 2]. The rise in global energy demand is widespread across all main sectors of the global economy. According to Figure 1-1, which was published by the IEA, the global energy demand increased by 2.3% in 2018 compared to 2017, reaching the highest demand of this decade. This is almost twice the average rate of growth since 2011. Due to economic growth, improvements in the standard of living, and stronger heating and cooling needs in some regions, the annual energy demand has increased [3].

Figure 1-2 shows that, according to the report published by IEA [3], energy-related CO_2 emissions have increased globally from 1990 to 2018. Consequently, energy-related CO_2 emissions worldwide have increased to 33.1 Gt in 2018, which is 1.7% higher than in 2017 and the highest rate since 2013.

From 2014 to 2016, although the global economy continued to grow, CO_2 emissions stagnated. This trend was mainly due to strong energy efficiency improvements and the deployment of low-carbon technology. However, this was not the case in 2017 and 2018, when the energy efficiency measures and the implementation of low-carbon options did not compensate for the rise in energy-related CO_2 emissions caused by higher economic growth. Therefore, CO_2 emissions increased by nearly

0.5% for every 1% gain in global economic output in 2017 and 2018, while the average annual increase since 2010 is only 0.3% [3].

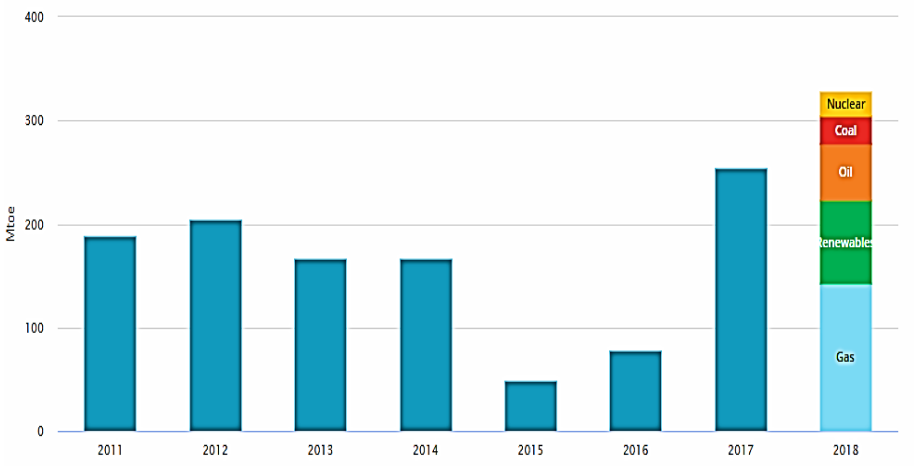

Figure 1-1. Annual change in global primary energy demand, 2011-18 [3].

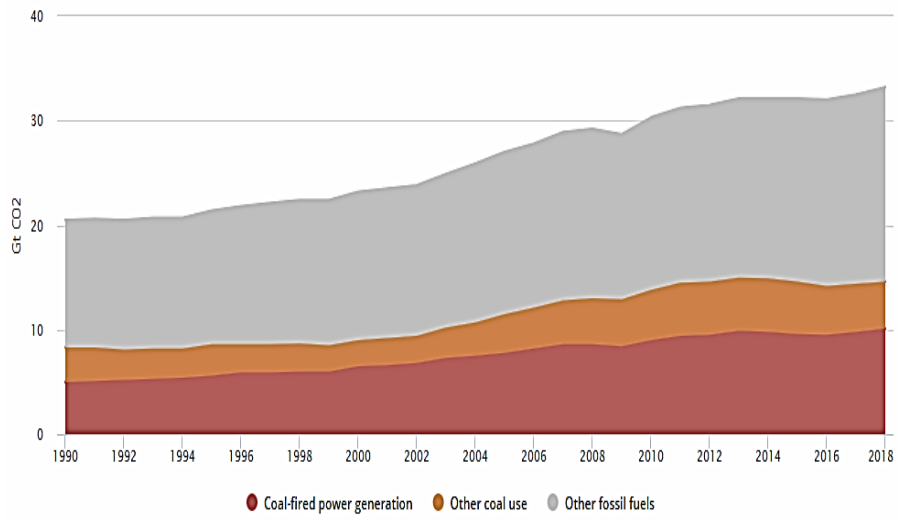

Figure 1-2. Energy-related CO_2 emissions by different sources, 1990-2018 [3].

The European Union (EU) authorities and governments are increasingly striving to reinforce policies aimed at reducing energy use. For instance, in 2008, a set of climate and energy-related targets (Figure 1-3) were set to be met by 2020 [4].

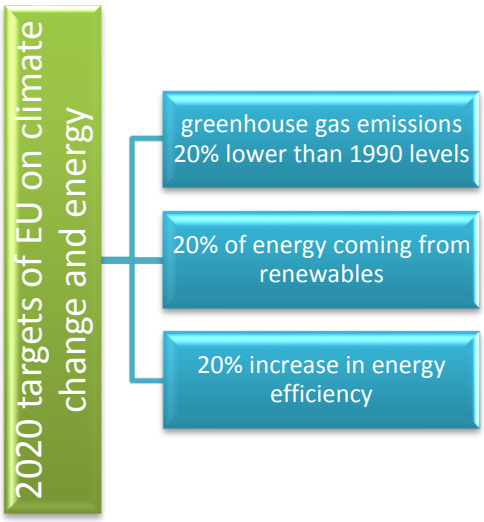

Figure 1-3. The 2020 targets of the EU on climate change and energy.

Energy products are categorized as electricity, heating and cooling, and transportation fuels [5]. Heating and cooling is responsible for about half of the EU's final energy use. It is the highest energy user ahead of transport and electricity. Therefore, the EU has a priority on developing strategies which lead in more efficient and sustainable heating and cooling [6].

There are different approaches in order to tackle the energy use issue in heating and cooling systems. The design of energy efficient heat exchangers is one of them [7].

In general, the heat exchanger market is an enormous market that consumes primarily precious materials such as aluminium. In 2012, the market size was US$ 42.7 billion, and was predicted to reach US$ 57.9 billion by 2016 and increase to US$ 78.16 billion by 2020. This indicates a growth rate of approximately 7.8% per year [8].

According to Hesselgreaves et al. [9], compact heat exchangers are increasingly being used for different applications due to their high efficiency and small size compared to conventional plate and tubular heat exchangers. They are characterized by a high heat transfer surface area density and a high heat transfer intensity despite their small physical size [10]. Currently, theses heat exchangers are mainly made of metallic materials.

There are various types of compact heat exchangers in the heat exchanger industry. Cross-corrugated plate heat exchangers are the main focus of this research. They are widely used in industry and are particularly suitable for low Reynolds (*Re*) applications such as HVAC (heating, ventilation and cooling) applications. Focke and Knibbe [11], used flow visualisation experiments to understand the flow phenomena in corrugated channels at a very low range of *Re* (less than 200). It was found that the existence of secondary swirling flow patterns and vortices increase turbulence production at this range of *Re*. Moreover Focke and Knibbe [11], Blomerius et al. [12], Focke et al. [13] and Shah and Wanniarachchi [14] acknowledged that the transition to the turbulence takes place at a low range of *Re*. They identified that the critical *Re* is in the range of 170 to 270 depending on the channel aspect ratio. With increasing the *Re* flow tends to become chaotic and the flow structure changes drastically which improves the heat transfer and pressure drop. Moreover, the corrugation pattern provides a large heat transfer area, structural strength and enhancement of heat transfer. The heat transfer is enhanced in this kind of geometry due to the repeated disruption of boundary layers, promotion of secondary flow and by using flow passages with small hydraulic diameter [15].

Figure 1-4 shows an example of a metallic sinusoidal cross-corrugated plate heat exchanger manufactured by the Alfa Laval Company. Among the various corrugation types, a sinusoidal corrugation profile is traditionally used in industry. Currently, metallic materials such as stainless steel, nickel-based alloys, and copper are used to produce this type of heat exchanger [15]. However, there are operating constraints related to metallic materials in some industrial applications due to phenomena such as corrosion and fouling. Currently, for those applications, the manufacturers of heat exchangers use nickel and titanium as these materials are more resistant to corrosion compared to the other metallic materials. However, they are expensive due to scarcity and they are difficult to process.

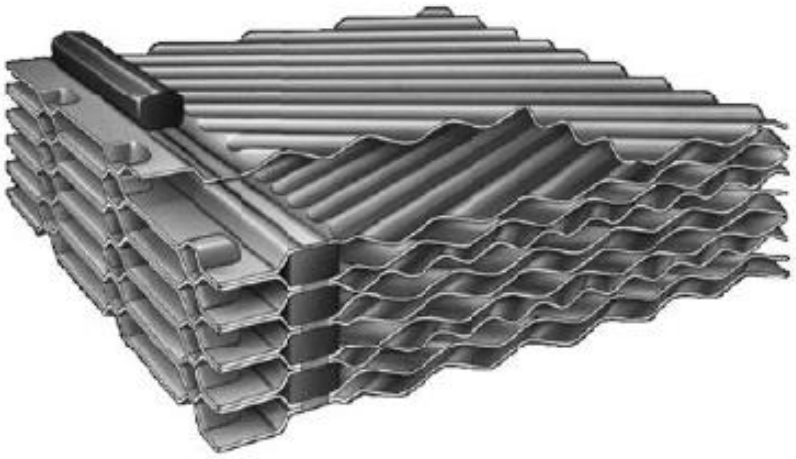

Figure 1-4. Section of a cross-corrugated plate heat exchanger [15].

The current supply of metallic raw materials is not to scale with the growing necessity of the heat exchanger market. One possible approach to this problem is to find alternative materials [7].

Polymers and polymer compounds are possible alternative materials. While corrosion is a prominent issue with metallic materials, polymers are known to be corrosion and fouling resistant [16, 17]. There are other advantages associated with the use of polymeric materials instead of metallic materials in heat exchanger manufacturing. For example, their light weight, great geometric flexibility, low manufacturing cost, ability to handle both liquids and gases, and ability to be used in both humidification and dehumidification systems [17]. Moreover, they are more environmentally attractive than the metallic materials, as the energy required to produce a unit mass of polymer is about half of that required to produce a unit mass of common metallic materials [18].

Heat exchanger manufacturers are constantly searching for new and improved designs in order to reduce the precious material and energy use of their products. Increasingly energy-efficient and enhanced heat exchangers help to meet the 20-20-20 targets of the EU.

As mentioned above, manufacturing of heat exchangers from polymeric materials has advantages. Moreover, cross-corrugated plate's geometry has advantages over the conventional plates and tubes as described earlier. The application of the injection moulding process with polymeric materials extends the flexibility of the corrugation shape. Therefore, manufacturing of cross-corrugated plates with triangular

corrugation from polymeric materials is an interesting idea and easy to build. The focus of this study is the cross-corrugated plate heat exchangers used for low *Re* applications specifically for HVAC.

In summary, this idea is interesting because of the following reasons. First of all the geometry induces turbulence especially at low Reynolds number which improves the heat transfer. This characteristic is especially interesting for low *Re* applications. Second, the compactness provides a large area density. Therefore, a higher heat transfer rate is expected compared to the conventional plates and tubes heat exchangers. Third, the corrugation patterns improve rigidity of the plates and a mechanical means of maintaining the channel gaps [13]. The last two properties of cross-corrugated plate geometry are especially interesting when cross-corrugated plate heat exchanger is manufactured from polymers because of the limitations associated with polymers which will be explained later in this chapter.

1.1.1 State of the art of polymeric heat exchangers

In recent years, significant interest has been shown in using polymeric heat exchangers in applications such as HVAC [17], heat recovery, sea water and water desalination, material separation and purification [19], electronics cooling [20], and automotive manufacturing [21]. Since 1988, extensive reports by Reay [22], Zaheed and Jachuck [16], T'Joen et al. [17], Cevallos et al. [23], Chen et al. [24], Hussain et al. [25] and Deisenroth et al. [26] have been published. These reports aim to provide updates on the research progress and development in the use of pure polymers and especially thermally enhanced polymers in heat exchangers. Moreover, various polymer material characteristics and their effect on performance for a range of operating pressures and temperatures are discussed. A summary of the operating conditions, heat exchanger geometry types, and research methods from various polymer heat exchanger applications is shown in Table 1-1.

References	HEX geometry	Application	Temperatue range	Research method
Zaheed and Jachuck [16], Burns and Jachuck [27]	Cross-corrugated film plate	Process intensification, Fuel-cells, HVAC, automobile, aviation	27–55 ˚C Max 220 °C	Experimental
Lowenstein et al. [28]	Parallel plates	Liquid desiccant cooling/HVAC	30–100 ˚C	Experimental
Cheng and GELD [29]	Plate-fin	HVAC applications	25–90 ˚C	Experimental
Luckow [30]	Doubly finned plates	Natural gas liquefaction/Cooling	35–90 ˚C	Numerical
Bar-Cohen et al. [31]	Doubly finned wall	Cooling/Refrigeration	35–90 ˚C	Analytical
Laaber and Bart [32]	Film plates with milled channels	Chemical industry for solvent condensation	Max 100 ˚C	Experimental
Christmann et al. [33], [34]	Film plates with milled channels	Water desalination	51–101 ˚C	Experimental
Alizadeh [35]	Crossflow plates	Liquid desiccant cooling/HVAC applications	14–90 ˚C	Experimental
Harris et al. [36]	Crossflow micro plates	Cooling Automobile radiators	20–95 ˚C	Analytical Experimental
Glouannec et al. [37], Noel et al. [38]	Tube	Electrical heating device	28–45 ˚C	Experimental
Bourouni et al. [39]	Tube	Water desalination	20–80 ˚C	Experimental
Ghosh et al. [40]	Webbed tube	Natural gas liquefaction	26–60 ˚C	Numerical
Cevallos et al. [41]	Webbed tube	Natural gas liquefaction	15–125 ˚C	Numerical Experimental
Chen et al. [42]	Finned tube	Liquid desiccant cooling/HVAC applications	8–34 ˚C	Experimental
Song et al. [43]	Tube-in-Shell	Water desalination	8–98 ˚C	Experimental

Liu et al. [44], Wu et al. [45]	Tube-in-Shell	Hot water heating system	20–30 ˚C	Experimental
Zarkadas and Sirkar [46]	Tube-in-Shell	Cooling/Refrigeration	20–35 ˚C	Experimental
Zhao et al. [19]	Tube-in-Shell	Cooling/Refrigeration	20–85 ˚C	Numerical
Yan et al. [47]	Tube-in-Shell	Industrial application	18–82 ˚C	Experimental
Shives et al. [48]	Plate fin heat sink	Electronics cooling	23–55 ˚C	Numerical Experimental
Bahadur and Bar-Cohen [20]	Pin fin heat sink	Electronics cooling	10–70 ˚C	Numerical
Kasza and Królikowski [49]	Pin fin heat sink	Electronics cooling	35–80 ˚C	Numerical
Hoerber et al. [50]	Pin fin heat sink	Electronics cooling	20–180 ˚C	Experimental

Table 1-1. Summary of research studies on development of polymeric heat exchangers.

According to Table 1-1, the existing studies on polymeric heat exchangers are mainly associated with the flat plate or tube heat exchangers. The great potential of cross-corrugated plates with polymer materials is not studied enough. The only available studies on pure polymeric cross-corrugated are Burns and Jachuck [27], Zaheed and Jachuck [16] and Zaheed-Maheswaran [51]. These experimental studies are published by a research group in the University of Newcastle.

The thermal conductivity and tensile strength of metallic materials are high. Both characteristics are favourable for the heat exchanger design. For instance, the thermal conductivity of stainless steel and nickel are respectively 50 W/mK and 90 W/mK at room temperature [52]. This high thermal conductivity leads to a high heat transfer rate through the wall of heat exchanger, meaning the wall has low thermal resistance. The conductive resistances of metallic heat exchangers are typically several orders of magnitude smaller than their convective resistances [15]. Hence, the heat transfer problem for metallic heat exchangers is the convection problem.

Polymeric materials have very low thermal conductivity and tensile strength compared to metallic materials. The thermal conductivities of most polymers are lower than 1 W/mK, which is 100 times lower than most metals [24]. Designing a polymeric heat exchanger is especially challenging since the conductive heat transfer resistance becomes significant or even dominant due to the low thermal conductivity

of the polymeric heat exchanger wall. A list of the numerical studies on polymeric heat exchangers is mentioned in Table 1-1. Based on these studies, the conductive heat transfer resistance of polymeric material cannot be ignored and must be taken into account. Therefore, in order to solve the heat transfer problem, combined convection-conduction problems must be studied, while for the metallic heat exchangers, the heat transfer problem is limited to the convection problem [19, 31, 40, 41, 49]. Zhang et al. [53] mentioned that the boundary conditions on the wall of polymeric heat exchanger are neither uniform temperature nor uniform heat flux. The boundary conditions on the wall are formed by the coupling between the two flows. The conductive resistance of heat exchanger also has an influence on boundary conditions.

When replacing metals with polymers in heat exchanger applications, the thermal and structural performance will strongly depend on the wall thickness. For polymeric heat exchangers, the wall thickness and structural performance are directly proportional, while the wall thickness and thermal performance are inversely proportional. Thus, a trade-off must be made. The focus of this thesis is the thermal performance of polymeric heat exchangers, and such structural analysis is not within the scope of this work.

Based on the experimental study conducted by Zaheed and Jachuck [16], the wall thickness of pure polymeric cross-corrugated plate heat exchangers must be smaller than 100μm (100μm for non-corrugated plate) in order to retain the thermal efficiency of the heat exchanger for heat recovery applications. This raises questions concerning the tensile strength of polymer materials. Depending on the operational conditions and type of polymeric materials, the wall thickness cannot be reduced beyond the limit of mechanical strength. Therefore, it is worthwhile to investigate whether it is feasible to design a polymeric cross-corrugated plate with a wall thickness higher than the limit identified by Zaheed and Jachuck [16].

According to the recent studies by Bar-Cohen et al. [54], Ghosh et al. [40] and Deisenroth et al. [26], one promising approach to overcoming the low thermal conductivity of polymers is the enhancement of polymer materials through the addition of thermally conductive fillers, which can lead to novel heat exchanger designs. The authors claim polymer composite materials enhanced with thermally conductive fillers have great potential to replace metallic or pure polymeric heat exchangers. However, their full potential has not yet been exploited. Designing heat exchangers using composite materials is still a new field and requires further research. Several researchers studied the performance of pure polymeric or thermally enhanced composite heat exchangers with different geometries [17, 19, 24, 41]. However, as mentioned before (Table 1-1) the geometries studied thus far are mainly composed of tube or flat plate components. There is currently no study on the composite cross-

corrugated plate heat exchangers. It is interesting to investigate how far the thermally enhanced composite materials compared to pure polymers improve the thermal performance of cross-corrugated plate heat exchangers for HVAC applications.

Computational fluid dynamics (CFD) is a very powerful tool, and its use can be very helpful for heat exchanger analysis and the design of industrial heat exchangers. The CFD model is an alternative to experimental tests since it provides speedy solutions to the design of heat exchangers and parametric studies.

In section 2.1 of this thesis, an extensive literature review is performed to identify the research gaps concerning the convection problem in cross-corrugated plate heat exchangers and the performance of cross-corrugated plates with metallic materials. This review has found that the flow in this type of heat exchanger has a complex three-dimensional nature even at a very low Reynolds number. Therefore, selecting a flow solver for CFD modelling is not straightforward. Different authors chose different flow solvers. In addition, the geometrical parameters can play an important role in the further enhancement of performance [55, 56]. Most of the studies on cross-corrugated plate heat exchangers are associated with sinusoidal corrugation and the influence of the corrugation angle on thermo-hydraulic performance of this type of corrugation [14, 57-60]. Sundén and Manglik [61], reported all the available correlations on sinusoidal cross-corrugated in their book. However, these correlations are only related to a specific aspect ratio of the channels which is common for this type of geometry with metallic materials. The influence of different corrugation angle on the thermo-hydraulic performance of cross-corrugated plate heat exchangers are included in these correlations but not the influence of channel aspect ratio. For the design of cross-corrugated geometries with polymeric materials there are more flexibilities in terms of channels aspect ratio and corrugation type compared to rigid metallic materials. Recently, the use of cross-corrugated films with triangular corrugation has attracted attention in membrane technology and HVAC applications [55, 56]. But, there is not enough study on the thermo-hydraulic characteristics of cross-corrugated geometry with triangular corrugation. Hence, it is necessary to first understand the flow phenomena and convection problem in cross-corrugated plate heat exchangers with triangular corrugation. Furthermore, to understand how the performance of this geometry can be enhanced based on the geometrical parameters of the corrugation profile, more specifically the channel aspect ratio. In addition developing new correlations for different aspect ratio allows designers to correctly size their heat exchanger and to compare the performance of different geometries.

In order to study the convection problem, the effect of solid material is neglected (conduction). The convection problem can be modelled using CFD simulations by assuming either a uniform temperature or uniform heat flux boundary conditions on

the wall adjacent to the fluid . Subsequently, convective heat transfer coefficients are calculated under these ideal boundary conditions. Thanks to CFD, it is feasible to evaluate the influence of the geometrical parameters, especially the aspect ratio of the channels in cross-corrugated plates, on the performance of the heat exchanger.

Moreover, contrary to metallic heat exchangers, as previously mentioned (Table 1-1), the available CFD studies on polymeric heat exchangers suggest the combined convection-conduction CFD model to solve the heat transfer in polymeric heat exchangers including both hot and cold flows in the computational domain because the conductive resistance is not negligible. According to Zhao et al. [19], in the case of polymeric heat exchangers not including the solid wall and applying empirical parameters such as constant temperature and constant heat flux on the wall adjacent to the fluid in the CFD model cause error in thermal performance prediction of heat exchanger. However, the value for the error is not indicated. It is known that the conductive resistance depends on the thermal conductivity and thickness of the solid wall [15]. Therefore, the question is how much is the error on the thermal performance of heat exchanger by not including the solid wall in the model and whether this error is dictated by thermal conductivity or thickness of the solid wall.

1.2 Objectives

The main objective of this thesis is to predict the thermal hydraulic performance of cross-corrugated plate heat exchangers fabricated from polymeric/composite materials using numerical method. This objective will contribute to establish credibility for polymeric cross- corrugated plate design in heat exchanger technology. In addition, the aim is to understand the extent to which the performance of this novel heat exchanger can be improved by using thermally enhanced composite materials in place of pure polymers.

In order to reach the main objective a secondary objective is defined as following and must be fulfilled first. As a secondary objective, this doctoral thesis aims for better understanding of the convection problem in triangular cross-corrugated heat exchangers and the physics governing the convective heat transfer and hydraulic behaviour. In order to achieve this goal, the heat transfer problem will be constrained to the convection problem only. Therefore, the solid material of the heat exchanger will be assumed to be metallic, and a CFD model will be developed to accurately predict the thermo-hydraulic performance of a cross-corrugated heat exchanger. Furthermore, the potential performance improvements resulting from changes in the geometrical parameters are investigated, particularly the aspect ratio of the channel.

Consequently, the aim is to develop a set of correlations where the influence of the aspect ratio is integrated in the equations.

This doctoral research will be limited to the low air velocities often encountered in HVAC applications, such as those found in buildings and industry. The high air velocities encountered in car radiators are not included in this work.

Both aforementioned objectives of this thesis are motivated by the 20-20-20 targets of the EU. The first objective focuses on the use of alternative materials in the design of cross-corrugated heat exchangers to reduce the use of precious materials and costs. The second objective focuses on the thermo-hydraulic enhancement of the cross-corrugated heat exchanger, which contributes to the overall system efficiency.

1.3 Outline

The manuscript is composed according to the following outline.

First, the focus is placed on solving the convection problem in cross-corrugated plate heat exchangers (Chapter 2). An extensive literature review on cross-corrugated plate heat exchangers composed of metallic materials is given. The CFD design method for heat exchangers is explained, and the model is validated with the available experimental results from the literature. The choice of different flow solvers for CFD modelling is discussed. The thermo-hydraulic performance of the heat exchangers with different aspect ratios is compared based on a performance evaluation criterion. Furthermore, the physics behind the different trends seen in heat transfer and flow characteristics are explained. The influence of turbulence intensity on those characteristics and corresponding viscous and pressure forces is studied.

In Chapter 3, several correlations are developed for each channel aspect ratio based on the heat and flow characteristic results derived from the parametric study of cross-corrugated plates presented in Chapter 2. A set of generalized correlations is developed to integrate the influence of the aspect ratio.

In Chapter 4, the combined convection-conduction heat transfer problems for the polymeric/composite cross-corrugated plates is solved with the aid of CFD. The choice of different computational domains is discussed, and the CFD model is validated with the available experimental results. The influences of different thermal conductivities of materials and variations in wall thickness are investigated. The thermal performance of a new polymeric cross-corrugated heat exchanger designed to be thermally competitive with a metallic one at the component level is studied.

In Chapter 5, conclusions are drawn and recommendations for future work are proposed.

2

Performance Assessment of Metallic Cross-Corrugated Plate Heat Exchangers

2.1 Introduction

Energy use in society is often divided into three sectors: industry, transportation, and buildings. Currently, among these three key sectors, buildings are the dominant energy consumers, accounting for approximately 40% of energy use and 36% of CO_2 emissions in the EU. The transportation sector is responsible for 33% of energy use [62, 63]. Therefore, it is meaningful to primarily target the buildings sector when taking measures to reduce energy use.

One particular application of interest where heat exchangers are used extensively is heating, ventilation, and air conditioning (HVAC) in buildings. HVAC accounts for approximately 40% of the energy use in buildings [64] and around 11% of the total energy use in Europe [65]. Most often in these applications, heat is exchanged between the air and a liquid carrier. Therefore, HVAC system designs for buildings present major opportunities for energy conservation today [66].

Cross-corrugated plates are a type of heat exchanger in which the two unmixed hot and cold stream flows exchange heat by passing through the channels. The direction of the main flow from the inlet to the outlet of each channel for both hot and cold streams are shown with arrows. The corrugated plates are stacked on top

of each other with different orientation angles (Figure 2-1). Over 60 different corrugated patterns have been produced during the past century [67]. A corrugation pattern provides a large heat transfer area, structural strength, and enhancement of heat transfer. The heat transfer is enhanced in this kind of geometry due to the repeated disruption of boundary layers, the promotion of secondary flow, and the use of flow passages with small hydraulic diameters [15].

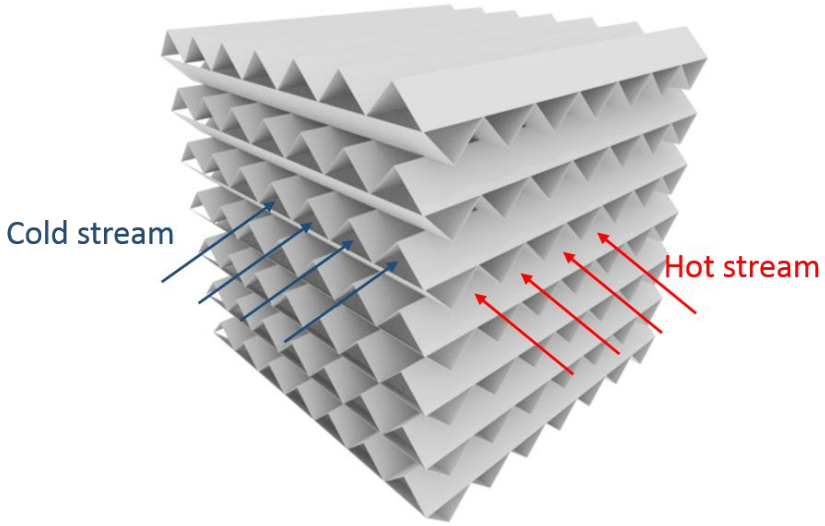

Figure 2-1. Schematic of a triangular cross-corrugated heat exchanger

CFD is an effective tool for the study of the thermal and hydraulic characteristics of corrugated channels. Due to the very high computational effort required for simulations of a complete heat exchanger, researchers such as Mehrabian and Poulter [68], Fernandes et al. [69], Freund and Kabelac [70], Han et al. [71] and Etemad and Sundén [57] have employed one periodic unitary cell or several cells as their computational domain.

Authors such as Ghaddar et al. [72] ($0<Re<2000$), Sundén and Trollheden [73] ($50<Re<1250$), Pereira and Sousa [74] ($0<Re<1200$), and Adachi and Uehara [75] ($50<Re<500$), used CFD to study the flow with low to moderate *Re* in channels with rectangular corrugation. It was found that the flow exhibits complex behaviours such as separation, recirculation, reattachment, and deflection. Moreover, self-sustaining geometrically induced oscillations present in the flow work to increase the heat transfer performance. Depending on the geometry under consideration, different transitional Reynolds numbers are reported in the literature. It is important to note that most of the studies agree that the transition from laminar flow to turbulent flow in cross-corrugated geometries occurs at relatively low Reynolds numbers compared to the case of a straight tube. For example, Ghaddar et al. [72] reported the transitional *Re* as approximately 900. According to Shah and Wanniarachchi [14], the flow in a cross-corrugated channel features a transition at a Reynolds number between 100 and 1500. According to Heggs et al. [76], purely laminar flow does not exist for Reynolds numbers larger than 150. Later, Shah et al. [77] confirmed that for $Re > 200$, the flow is turbulent in the cross-corrugated channel. Furthermore, Focke et al. [13] and Liu and Tsai [78] reported that the flow becomes turbulent at the low Reynolds number of 400 and 300, respectively.

Both steady-state laminar and turbulence models are used by different authors to solve for the flow in cross-corrugated channels at low to moderate *Re* ($0<Re<2000$). Yin et al. [79] investigated the flow and heat transfer in corrugated channels with sinusoidal waves. The authors implemented a steady-state laminar model for Reynolds numbers in the range of 100–1500. Guo-Yan et al. [80], studied a sinusoidal cross-corrugated heat exchanger for Reynolds numbers between 84 and 1168, both numerically and experimentally. They claimed that a steady-state laminar model is a reasonable choice for this range of Reynolds numbers. The deviation between the numerical and experimental results for Colburn j factor and friction factor was found to be around 15%. Chen [81] employed a steady-state laminar model to analyse the flow and heat transfer in a triangular cross-corrugated plate for Reynolds numbers in the range of 100–2000.

Conversely, other researchers state that a steady-state laminar model is not an appropriate flow model for the aforementioned *Re* range. For example, Ciofalo et

al. [82] and Ciofalo et al. [83] found that for *Re* in the range of 1000–10000, the laminar model significantly underpredicts the Nusselt number. Furthermore, they reported that the most common two-equation turbulence model (i.e. the standard k–ε model with wall functions) overpredicts both the Nusselt number and the friction factor, especially for the lower range of *Re*. It was stated that a low Reynolds number k–ε model with a resolved boundary layer or a large eddy turbulence model (LES) fit the experimental results best. The low Reynolds k–ε model still underpredicts the Nusselt number by up to 20% for the corrugation angles higher than 90°. Ciofalo et al. [84] reported that for a corrugated heat exchanger with the corrugation angle of 70° at *Re*=2080, the low Reynolds number k–ε model slightly overpredicts the average Nusselt number (by 6%) and underpredicts the friction factor by 25%. Another two-equation turbulence model, the Shear-Stress Transport model (SST) was implemented by Kanaris et al. [85] and Pelletier et al. [86] for *Re* in the ranges of 500–6000 and *Re* of 3500, respectively. However, Dietz et al. [87] claim that for complex flows, the isotropic turbulence assumption which is used in two-equation turbulence models is not justified. The Reynolds stress model (RSM) [88], does not use the isotropic assumption at the cost of requiring more equations to be solved. The study by Freund and Kabelac [70] on a chevron-type plate heat exchanger reports that the RSM model is 8% more accurate than the SST model in predicting the average heat transfer coefficient for this type of heat exchanger. Due to the anisotropic nature of Reynolds stress and the complexity of the flow in cross-corrugated plates, the RSM model is more accurate than the k–ε model [89]. Moreover, Liu and Niu [90], calculated the Nusselt number in the cross-corrugated geometry using several turbulence models such as standard k–ε model, Re-Normalisation Group (RNG) k–ε model [91], realizable k–ε model (RLZ), and RSM model for the *Re* in the range of 200-3000. They compared the simulated results with a set of experimental results. It was found that the Nu values calculated based on RSM model fits the experimental results the best with 7% deviations. The simulated results based on the RNG model have the highest deviations with the experimental results by 30%.

The most popular corrugation profile that has been studied numerically and experimentally is sinusoidal. The main focus of study has been the influence of corrugation angle (illustrated in section 2.2.1) on the thermo-hydraulic characteristics of cross-corrugated heat exchangers. All researchers reported that by increasing the corrugation angle, the Nusselt number and friction factor increase [58, 60, 92-94]. According to Zhang and Che [95] and Zaheed-Maheswaran [51], the corrugation angle of 90° is the optimal angle in terms of the thermo-hydraulic performance of sinusoidal heat exchangers. Despite all the efforts towards the study of sinusoidal cross-corrugated heat exchangers mentioned above, only a few researchers have investigated the performance

characteristics of triangular heat exchangers. Scott et al. [96] compared the mass flux through the flat and triangular corrugated membrane for different corrugation angles with an apex angle of 90˚ (500<*Re*<2500), where a substantial increase in the mass fluxes across the latter geometry is obtained. Moreover, the highest mass fluxes were achieved with the corrugation angles of 45˚ and 90˚. Due to the analogy between heat and mass transfer, similar effects can be expected for the heat flux. Hall et al. [97] provided a correlation for the mass transfer coefficient by performing experimental tests on a triangular cross-corrugated heat exchanger with an apex angle of 90˚ at low to moderate *Re* (200–2300). It was found that the flow regime in the mentioned *Re* range is not laminar. Subsequently, Scott and Lobato [56] proposed some correlations for Sherwood numbers using electrochemically measured mass flux data from a triangular membrane with an apex angle of 90˚ for low *Re* (100–1400). They confirmed that the irregular flow path caused by the membrane corrugation promotes the turbulent flow condition which consequently improves the mass transfer. Leung and Probert [98] studied the thermal behaviour of turbulent air flow (*Re* = 5000–20000) for three heat exchangers with isosceles triangular corrugations and apex angles of 40˚, 60˚, and 90˚. Zhang [99] investigated numerically the flow and heat transfer for Reynolds numbers in range of 100–6000 in a triangular cross-corrugated heat exchanger with an apex angle of 60˚. They used the low Reynolds number k-ω (LKW) turbulence model and proposed two correlations for Nusselt number at constant temperature and heat flux boundary conditions.

When it comes to comparing the performance of several heat exchangers and the selection of the optimal heat exchanger for a particular system, there are many different criteria to consider. It is a multi-objective optimisation problem with some constraints. The most important objectives and constraints to consider for compact heat exchangers with gas flow are a minimum frontal area and the volume requirements for a given heat transfer rate and pumping power[15]. Therefore, a performance evaluation criterion (PEC), which is a scalar value, is required to compare one of these objectives while the rest of design variables are held constant. Several PEC for compact heat exchangers have been proposed by various authors such as London [100] (JF criterion= j/f) and Webb [101]. However, based on Ameel et al. [102], for some criteria, such as the JF criterion, the physical interpretations of fan power and volume are not included. Therefore, several designs with different pumping power and volume can have the same JF value. Additionally, changing the geometry causes changes in the pumping power, mass flow rate, and outlet temperature. Therefore, it is unrealistic to identify the best design based solely on the JF criterion. The most comprehensive PEC for compact heat exchangers was introduced by Cowell [103], and brings together different methods to resolve their individual limitations [102, 104].

As discussed above, the flow and heat characteristics of cross-corrugated heat exchangers strongly depend on the geometrical parameters. The existing studies on triangular cross-corrugated plates are associated with two apex angles being 60° and 90°. Therefore in this study, the influence of a wider range of apex angles from 45° to 150° on the heat transfer and hydraulic characteristics is analysed numerically. In literature, no such study is available which deals with the effect of the apex angle on the pressure force, turbulence intensity, and vorticity magnitudes and links those to the flow and heat transfer mechanisms of triangular cross-corrugated plates. Finally, there is little information available in the literature on comparing the performance of several geometries using an appropriate PEC and selecting the optimal geometry for a specific system. Therefore, in this chapter, an appropriate PEC is used to achieve a realistic comparison between different geometries.

2.2 CFD Method for Convection

2.2.1 Geometry and Computational Domain

To limit computational cost, a periodic unitary cell, which is shown in Figure 2-2(a), was chosen as the computational domain. In order to validate the use of a periodic unitary cell as the computational domain, a set of simulations was also conducted for a triangular cross-corrugated channel with several cells (Figure 2-2(b)). According to Zhang [99], after 3-5 cells in a channel with several repetitive cells, the flow is fully developed. Therefore, in this study, eight repetitive cells are considered.

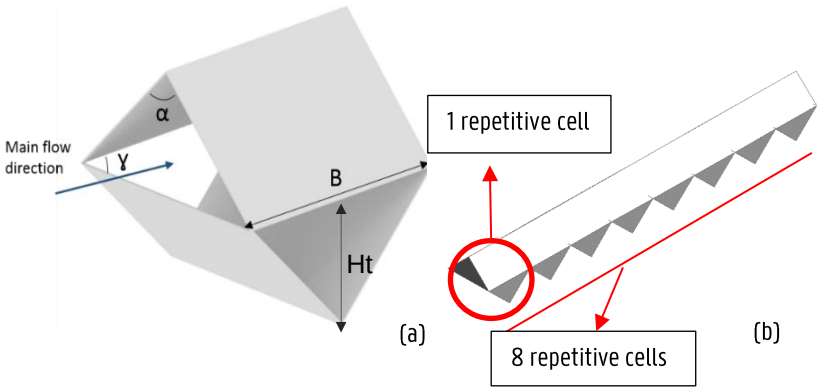

Figure 2-2. Computational domain: (a) a unitary cell, (b) Channel with 8 repetitive cells.

The geometrical parameters of the triangular corrugation are given as the base length (B) and the apex angle (α), which is directly related to the aspect ratio (base to height ratio) of the channel. The corrugation inclination angle (ɣ) is the angle between the axes of the triangular prisms and is fixed at 90˚ in this study. The reason for this choice is that the corrugation angle of 90˚ has the highest performance among all of the corrugation angles [51, 95].

Twelve geometries are created by varying the apex angles while the base length is held at 5 mm. The apex angles are 45˚, 55˚, 65˚, 75˚, 90˚, 100˚, 110˚, 120˚, 125˚, 130˚, 140˚ and 150˚. Note that for a given apex angle, the variations of the base can be captured by setting different *Re*, and thus only one base length is considered here.

2.2.2 Boundary Conditions and Fluid Properties

The boundary conditions imposed for geometry (a) in Figure 2-2 are shown in Figure 2-3.

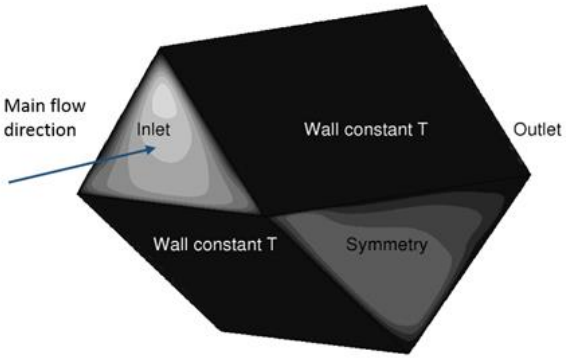

Figure 2-3. Boundary conditions for the unitary cell.

The no-slip boundary condition for the flow velocity components is applied at the wall ($u = v = w = 0$). For the temperature component, a constant temperature is imposed at the wall.

At the left and right sides of the domain, symmetry conditions are used. The normal velocity components are set to zero at the boundary and the normal component of the gradient of all scalar quantities is also equal to zero. This implies no flow and no flux across the boundaries.

It is assumed that the flow is fully developed throughout the computational domain. Therefore, stream-wise periodic boundary conditions with constant temperature are imposed along the flow direction, linking the inlet and outlet. This means that the velocity field entering the domain is identical to the one leaving the domain.

$$u_{inlet} = u_{outlet}\,,\ v_{inlet} = v_{outlet}\,,\ w_{inlet} = w_{outlet}\,.$$

(2-1).

The non-periodic part of the pressure (βL) is assumed to vary linearly with the length in the flow direction. The pressure can then be written as

$$p = -\beta L + p^{*},$$

(2-2).

In this equation, β is a constant representing the non-periodic pressure gradient and p^* is the periodic part of the pressure. A periodic dimensionless temperature is defined as

$$\Theta = \frac{T - T_w}{T_b - T_w},$$

(2-3).

where T_b is the local bulk temperature and A is the minimum cross sectional area (eq. (2-4)).

$$\boldsymbol{T_b = \frac{\int \rho u T dA}{\int \rho u dA}}$$

(2-4).

The dimensionless temperature of the flow entering the domain is equal to the dimensionless temperature of the flow leaving the domain:

$$\Theta_{inlet} = \Theta_{outlet}.$$

(2-5).

For the channel with several cells, the same boundary conditions mentioned above are used. Instead of periodic boundary conditions, uniform velocity and atmospheric pressure are imposed at the inlet and outlet of the channel, respectively.

The fluid considered in this study is air with constant properties (Table 2-1). Notice that because the temperature variations are relatively small within the flow domain, constant dynamic viscosity is a valid assumption.

ρ (kg/m^3)	c_p (J/kgK)	K (W/mK)	μ (kg/ms)	Pr
1.225	1006.43	0.0242	1.789e-5	0.74

Table 2-1. Air properties.

2.2.3 LMTD Method

Figure 2-4 shows a simple flow diagram of a heat exchanger. A hot fluid enters the heat exchanger and its heat is transferred to a cold fluid. Hence, the temperature of the hot fluid decreases and the temperature of the cold fluid increases while flowing through the heat exchanger, as is shown in Figure 2-5. The arrangement of flow is called counterflow: the two fluids flow parallel to each other but in opposite directions. In a coflow arrangement both fluids flow parallel to each other in the same direction [105].

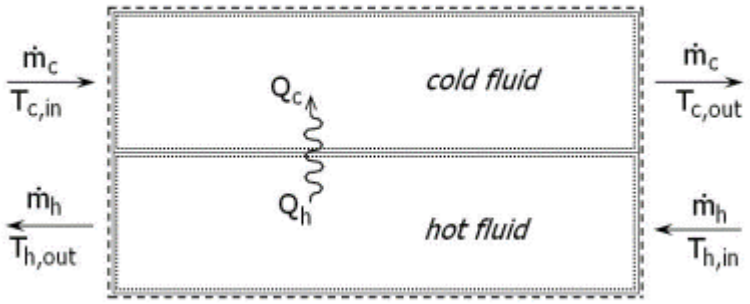

Figure 2-4. Flow diagram of a counterflow heat exchanger [105].

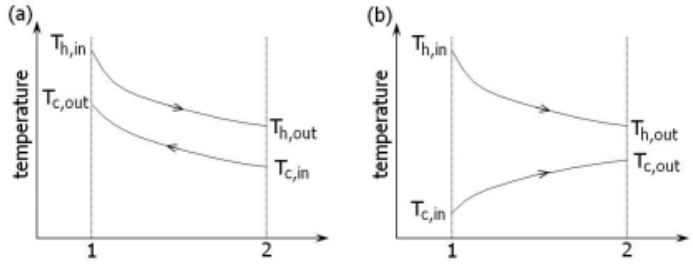

Figure 2-5. Temperature distribution for (a) a counterflow heat exchanger and (b) a coflow heat exchanger [105].

LMTD is the logarithmic mean temperature difference for the two fluid streams assuming counterflow. Based on Figure 2-5a, the LMTD expressed as

$$LMTD = \frac{(T_{hot,inlet} - T_{cold,outlet}) - (T_{hot,outlet} - T_{cold,inlet})}{\ln\left(\frac{T_{hot,inlet} - T_{cold,outlet}}{T_{hot,outlet} - T_{cold,inlet}}\right)},$$

(2-6).

And the corresponding heat transfer rate equation is defined as

$$Q = UA\ F\ LMTD,$$

(2-7).

The thermal performance of a heat exchanger is determined by its thermal conductance (UA), which gives the relation between the logarithmic mean temperature difference and the heat transfer rate.

The LMTD is a measure for the driving force of heat transfer. It is maximal in a counterflow heat exchanger. However, many heat exchangers do not have a counterflow arrangement due to other design constraints. To correct for a layout different from counterflow, the correction factor F is introduced in equation (2-7). F is dimensionless and dependent on the flow arrangement and the inlet and outlet temperatures. Charts to determine the correction factor F for many commonly used heat exchanger designs were developed by Bowman and Mueller [106].

2.2.4 Data Reduction

The Reynolds number is calculated (2-8) based on the average core velocity (velocity in the minimum cross-sectional flow area), u_c and the hydraulic diameter. The hydraulic diameter for the unitary cell is defined by (2-9), wherein A_c is the minimum cross sectional area, L the flow length (here is equal to the base), and A_{ws} is the wetted surface area. The hydraulic diameters for all different geometries simulated in this study are shown in Table 2-2.

α [◦]	D_h [m]
45	0.0046
55	0.0044
65	0.0042
75	0.0040
90	0.0035
100	0.0032
110	0.0029
120	0.0025
125	0.0023
130	0.0021
140	0.0017
150	0.0013

Table 2-2. Hydraulic diameter for different geometries.

$$Re = \frac{u_c D_h}{\nu},$$

(2-8).

$$D_h = \frac{4LA_c}{A_{ws}},$$

(2-9).

In order to characterize the heat transfer phenomena, the average heat transfer coefficient (h) and Nusselt number are defined in the following equations. In following equations, q_w is the average wall heat flux.

$$h = \frac{q_w}{LMTD_{sim}},$$

(2-10).

$$Nu = \frac{q_w D_h}{K\ LMTD_{sim}},$$

(2-11).

In the CFD simulation a constant wall temperature is imposed at the wall. Applying the equation for LMTD, equation (2-6) to this specific case with a single fluid in contact with a constant wall temperature, results in equation (2-12). In order to avoid the confusion between the actual LMTD formula (equation (2-6)) and the reduced LMTD formula for the CFD simulation (equation (2-12)), the equation (2-12) is called $LMTD_{sim}$ in this doctoral thesis.

$$LMTD_{sim} = \frac{(T_w - T_{cold,outlet}) - (T_w - T_{cold,inlet})}{\ln(\frac{T_w - T_{cold,outlet}}{T_w - T_{cold,inlet}})},$$

(2-12).

Also the Colburn j factor, is analysed in this study.

$$j = \frac{Nu}{Re\ Pr^{1/3}},$$

(2-13).

Furthermore, the friction factor f, the dimensionless representations of pressure drop, is given by

$$f = \frac{\Delta p \, D_h}{\rho \frac{u_c^2}{2} L}.$$

(2-14).

2.2.5 Computational Model for Convection

In order to solve a convection problem, the nature of the flow inside the heat exchanger needs to be determined first. In practice, the Reynolds number is used to predict whether the flow is laminar or turbulent. Thanks to the pioneer pipe flow visualisation by dye injection of Reynolds [107], it is possible to identify a so-called critical Reynolds number where the transition from laminar to turbulence occurs [108] by performing experimental studies for any fluid system. For a *Re* lower than the critical Reynolds number, the flow is laminar. This means that no instabilities are possible in the flow as they are damped due to the high viscosity. The adjacent layers of fluid are highly ordered, the velocity is parallel to the wall and varies only in the direction normal to the wall. For a *Re* above the critical Reynolds number value, the onset of turbulence starts growing and transitional regime begins where the flow is unsteady, sometimes exhibiting laminar behaviour and sometimes turbulent flow characteristics. The transition from laminar to turbulent triggered by mechanisms such as interaction of unsteady flow that develops naturally, small disturbance induced by geometry surface or vibration which creates the instability in the flow. By increasing the *Re,* the flow instability continues growing until the flow becomes fully turbulent. The fully turbulent flow has irregular velocity fluctuations in all directions which are superimposed on the main flow velocity. In this type of flow, the fluctuations travel randomly in the flow by the rotational fluid structures called eddies with varying size [108-110]. Moreover, in the fully turbulent flow, a broad range of sizes of eddies exist, while the self-sustained unsteadiness usually generates larger eddies with a small eddy-size distribution [15].

Based on the literature study in the section 2.1, the flow in cross-corrugated plate heat exchangers is complex and the transitional regime initiates between $10<Re<200$ depending on the corrugation angle and the aspect ratio of the channel [77]. In this study, a *Re* range of 310–2064 is considered. As previously mentioned in section 2.1, for this range of *Re* and this geometry, the self-sustained unsteadiness exist and are periodic. However based on Shah and Sekulic [15], the irregularity of the fluctuations in the turbulent flow distinguishes turbulence from self-sustained oscillations which exist in the transitional regime. In the literature, the flow in this range of *Re* in the heat exchanger is often referred to as "turbulent" or "low-Reynolds-number turbulent" ($Re<3000$) [15], although it is not entirely clear to what extent the unsteadiness is fully turbulent.

The steady-state three-dimensional numerical simulations of flow and heat transfer in the corrugated channel are obtained with the aid of the commercial CFD code FLUENT 16.2. As will be investigated later in the results section, the steady-state laminar flow assumption may not be accurate in the *Re* range of this study. Thus, in combination with the three-dimensional geometry, the dynamic LES model seems like a natural choice since it can deal with transitional/weakly turbulent flow through the dynamic viscosity. However, the LES model requires longer calculation times (in particular for second order flow characteristics to converge) compared to the turbulence models, as both the time steps and the mesh size must be sufficiently fine compared to the Kolmogorov scale to resolve enough of the turbulence [111]. On the other hand, based on the literature study discussed in the section 2.1, for the same range of *Re* as this study, it is found that the RSM model yields more accurate results compared to the other turbulence models for predicting the flow and heat transfer phenomena in cross-corrugated plate geometries [70, 87, 89]. Therefore, as a large number of simulations needs to be performed (55 simulations) for this study, the RSM model is employed as the flow solver. Later on, in the section 2.3.1, it will be illustrated that the results of simulations using RSM model are in a good agreement with the experimental results.

Different partial differential governing equations have to be considered for the laminar or RSM models [111]. For example, the governing Reynolds-averaged balance laws for the mass, momentum for velocity in directions x_j (j=1,2,3), and energy are summarized in Eq. (2-15) – (2-17). Here ($-\overline{\rho \acute{u}_\iota \acute{u}_j}$) and ($-\overline{\rho c_p \acute{u}_j \acute{T}}$) are Reynolds stress and turbulent heat flux. Furthermore, an RSM closure can be used to close the turbulent terms.

$$\frac{\partial(\rho u_i)}{\partial x_i} = 0, \qquad (2\text{-}15).$$

$$\frac{\partial \rho u_i u_j}{\partial x_j} = -\frac{\partial P}{\partial x_i} + \frac{\partial}{\partial x_j}\left[\mu\left(\frac{\partial u_i}{\partial x_j} + \frac{\partial u_j}{\partial x_i}\right)\right] + \frac{\partial}{\partial x_j}(-\overline{\rho \acute{u}_\iota \acute{u}_j}), \qquad (2\text{-}16).$$

$$\frac{\partial \rho u_j c_p T}{\partial x_j} = \frac{\partial}{\partial x_j}\left[(\frac{\mu c_p}{\mathrm{Pr}}\frac{\partial T}{\partial x_j} + (-\overline{\rho c_p \acute{u}_j \acute{T}})\right]. \qquad (2\text{-}17).$$

The exact transport equations for the transport of the Reynolds stresses – $\overline{\rho \acute{u_\iota} \acute{u_j}}$ can be solved by the following Reynolds stress transport equation (equation (2-18). WhereP_{ij}, Ω_{ij}, $D_{T,ij}$, $D_{L,ij}$, ε_{ij} and Π_{ij} represent the Reynolds stress production, production by system rotation, turbulent diffusion, molecular diffusion, dissipation rate tensor and pressure-strain terms.

$$\frac{\partial}{\partial x_k}(\rho u_k \overline{\acute{u_\iota} \acute{u_j}}) = P_{ij} + \Omega_{ij} + D_{T,ij} + D_{L,ij} - \varepsilon_{ij} + \Pi_{ij},$$

(2-18).

For the three terms of P_{ij}, $D_{L,ij}$ and Ω_{ij} no additional models are required and they can be obtained from the exact equations of (2-19)–(2-21). More detailed information regarding theses equations can be found in the book of Malalasekera and Versteeg [108]. The rotation vector is ω_k [112].

$$P_{ij} = -\rho \left(\overline{\acute{u_\iota} \acute{u_k}} \frac{\partial u_j}{\partial x_k} + \overline{\acute{u_j} \acute{u_k}} \frac{\partial u_i}{\partial x_k} \right),$$

(2-19).

$$\Omega_{ij} = -2\omega_k \left(\overline{\acute{u_j} \acute{u_m}}\, e_{ikm} + \overline{\acute{u_\iota} \acute{u_m}} e_{jkm} \right),$$

(2-20).

$$D_{L,ij} = \frac{\partial}{\partial x_k}\left(\mu \frac{\partial}{\partial x_k}(\overline{\acute{u_\iota} \acute{u_j}})\right),$$

(2-21).

Additional assumptions and models are required for the turbulent diffusion ($D_{T,ij}$), dissipation rate tensor ε_{ij} and pressure-strain Π_{ij} terms to close the equation (2-18).

The turbulent diffusion terms is solved by the model proposed by Lien and Leschziner [113] (equation (2-22)). This equation, is the simplification of the generalized gradient-diffusion model of Daly and Harlow [114]

$$D_{T,ij} = \frac{\partial}{\partial x_k}\left(\frac{\mu_t}{\sigma_k} \frac{\partial \overline{\acute{u_\iota} \acute{u_j}}}{\partial x_k}\right),$$

(2-22).

The turbulent viscosity (μ_t) in equation (2-23) is calculated from the turbulent kinetic energy (k) and the dissipation rate (ε) (equation (2-24)). In equation (2-24),

the constants of $C_{1\varepsilon}$ and $C_{2\varepsilon}$ are respectively 1.44 and 1.92 and the Prandtl number for ε (σ_ε) is 1. Also, the mean strain rate is represented by Sij. The turbulent Prandtl number for k is σ_k, which is equal to 0.82.The turbulent kinetic energy is solved in the whole domain including the wall adjacent cells.

$$\mu_t = \rho C_\mu \frac{k^2}{\varepsilon}, \; C_\mu = 0.09, \tag{2-23}$$

$$\frac{\partial}{\partial x_i}(\rho \varepsilon u_i) = \frac{\partial}{\partial x_j}\left[\left(\mu + \frac{\mu_t}{\sigma_\varepsilon}\right)\frac{\partial \varepsilon}{\partial x_j}\right] + C_{1\varepsilon}\frac{\varepsilon}{k}\mu_t S_{ij}.S_{ij} - C_{2\varepsilon}\rho\frac{\varepsilon^2}{k}, \tag{2-24}$$

The pressure strain interactions term, Π_{ij} is modelled by the linear pressure-strain model which was proposed by Gibson and Launder [112], Fu et al. [115] and Launder [88]. Based on Malalasekera and Versteeg [108], their effect on the Reynolds stress is caused by two distinct processes . A slow process that reduces anisotropy of turbulent eddies due to their mutual interaction. And a rapid process due to the interactions between turbulent fluctuations and the mean flow strain that produces the eddies such that the anisotropic production of turbulent eddies is opposed. Their overall effect of both processes is to redistribute energy amongst the normal Reynolds stresses (i=j) so as to make them more isotropic and to reduce the Reynolds shear stresses (i≠j) [108].

The dissipation rate tensor term is modelled as in equation (2-25). Where, Y_M is an additional dilatation dissipation term based on the model proposed by Sarkar and Balakrishnan [116].

$$\varepsilon_{ij} = \frac{2}{3}\delta_{ij}(\rho\varepsilon + Y_M), \tag{2-25}$$

Earlier in the section 2.2.2, the boundary conditions at the wall are described. Immediately adjacent to the wall, the viscosity affected inner region which includes an extremely thin viscous sub-layer followed by the buffer layer exists. The near wall modelling approach which combines two-layer modelling [117] is applied to completely resolve the viscosity affected inner region all the way to the wall. This represents an enhanced treatment of near wall region for turbulent flows at low Reynolds number. Therefore, for all the simulations, the near-wall mesh is refined so that the first wall adjacent cell is placed in the viscous sublayer ($y^+<1$).

The discretization of the convective terms in the governing equations is performed via a second-order upwind scheme due to the higher stability. A coupled pressure-velocity algorithm (projection method) is used [118]. The gradients are evaluated via the least square cell-based method. The pressure gradient in the momentum equations is treated by a second-order discretization scheme to obtain more accurate results. The convergence criterion is set to 10^{-6} for the continuity and momentum and to 10^{-9} for the energy equation. The inlet temperature (mass weighted average temperature at inlet), velocity (area weighted average velocity), pressure drop and heat flux are monitored. Setting lower values for the convergence criterion did not lead to any changes of the monitored quantities. For each simulation, the mass balance was checked. The difference between the inlet and outlet mass flow rates was 3.38e-15. The error on enthalpy was 3.3e-6 %. Since all balances are closed well, this is an indication that the solution to the set of discretised Navier-Stokes equations is obtained within a small error due to the iterative convergence.

2.2.6 Grid Discretization Error

The flow domain is discretized using structured grids consisting of hexahedral and wedge elements. Conformal meshing is used to avoid interpolation errors on the interface where the periodic boundary condition is imposed. A coarse and a fine mesh are generated for each geometry. The number of grids for the fine mesh is 8 times larger than the coarse mesh. The number of grids for each geometry and mesh are indicated in Table 2-3. The number of elements for the coarse meshes vary from 5.6M to 1M. The number of elements for the fine meshes vary from 45M to 8.6M. The highest value of the cell skewness and the lowest value of the minimum orthogonal quality of the cell in the different grids were respectively 0.6 and 0.4. The grid independence study is performed for the highest *Re* regarding each geometry and for each flow model. It is ensured that for the highest *Re*, the value of $y^+<1$ for both fine and coarse grids. The coarse grid which is constructed for the highest *Re* of each geometry is used afterwards for the simulations of the whole range of *Re* related to that geometry.

The error caused by the discretization of the flow domain is calculated using Roache's Grid Convergence Index (GCI) [119]. It calculates an error for how far the solution is from the asymptotic numerical value. When the grids are geometrically similar, the quantity of interest depends on the grid spacing (*H*). The GCI estimates the grid refinement error theoretically. This means that the error is estimated relative to the theoretical solution on an infinitely fine grid (H=0). For any given quantity of interest, a Taylor series expansion around this theoretical solution with the same order of convergence (*p*) as the discretization scheme is developed:

$$f(H) = f(0) + \frac{\partial f}{\partial H}|_{H=0} H + \frac{1}{2!}\frac{\partial^2 f}{\partial H^2}|_{H=0} H^2 + O(H^3).$$

(2-26).

The global quantities are converged at the same order of convergence and the simulations provide the second order solutions, therefore, it is assumed that that the higher order terms are neglected. Therefore, the two remaining unknowns are identified by conducting two calculations on two different grids (fine and coarse). The first unknown, $f(0)$, is the theoretical value of the quantity of interest at zero grid spacing, and the second unknown $(\frac{\partial f}{\partial H}|_{H=0} H)$ is the partial derivative of the quantity at zero grid spacing. Afterwards, the relative error (e) between a coarse grid with rH spacing and a fine grid with H spacing are estimated from

$$e = \frac{f(rH) - f(H)}{f(H)}.$$

(2-27).

If the grid spacing for both fine and coarse grids are similar, e becomes very small. Therefore, the relative error alone is not a good indicator for grid discretization error estimation. In order to weigh the differences between the two calculations and grids, other factors such as grid refinement ratio (r) and order of convergence (p) are necessary to consider. Moreover, due to the assumptions that are made, a safety factor is required. According to Roache [119], if two grids are used and the order of convergence is assumed to be the same as the order of the discretization scheme, the safety factor (F) is recommended to be 3. Finally, the GCI on coarse grid and fine grid are calculated from (2-28) and (2-29).

$$GCI_{coarse} = F\frac{|e|r^p}{r^p - 1},$$

(2-28).

$$GCI_{fine} = F\frac{|e|}{r^p - 1},$$

(2-29).

The grid refinement ratio in this study is 2 in each direction. The relative error and GCI on coarse grid for the Colburn j factor and friction factor are tracked, and the results for the RSM model are shown in Table 2-3.

α [°]	*Re*	Fine mesh			Coarse mesh			e_j	e_f	j-GCI	f-GCI
		Grids	j	f	Grids	j	f	(%)	(%)	(%)	(%)
45	2064	44954128	0.006428	0.248527	5619266	0.006431	0.248381	0.05	-0.06	0.2	-0.23
55	2026	36099024	0.007443	0.308757	4512378	0.007430	0.308718	-0.17	-0.01	0.7	-0.05
65	1971	29769776	0.008347	0.368193	3721222	0.008366	0.367429	0.23	-0.2	0.92	-0.83
75	1903	24328960	0.009218	0.420727	3041120	0.009227	0.420555	0.098	-0.40	0.39	-0.16
90	1767	18773936	0.010251	0.467935	2327486	0.010296	0.468565	0.43	1.73	1.95	0.53
100	1659	15938656	0.010685	0.466255	1992332	0.010750	0.466998	0.60	0.16	2.42	0.63
110	1539	13301248	0.010869	0.43346	1662656	0.010944	0.434111	0.68	0.15	2.72	0.6
120	1399	11019744	0.010909	0.375978	1377468	0.010939	0.376597	0.27	0.16	1.09	0.66
125	1327	9792672	0.010694	0.341435	1224084	0.010772	0.344465	0.72	0.87	2.88	3.51
130	1251	8872368	0.010467	0.304785	1109046	0.010557	0.306491	0.85	0.55	3.41	2.22
140	1093	11731448	0.009621	0.232055	1466431	0.009679	0.233332	0.51	0.54	2.02	2.19
150	930	8646152	0.008151	0.163323	1080769	0.008177	0.162624	0.32	-0.43	1.27	-1.71

Table 2-3. Comparison of fine and coarse mesh (RSM) model.

2.3 Results and Discussion

2.3.1 Model validation

Before proceeding to the main results and discussions, it is necessary to validate the simulations with respect to the benchmark studies. The numerical model in this study is validated by both the experimental [56, 120] and numerical [121] work of other authors. The experimental work of Scott and Lobato [56, 120] has been a validation benchmark for several numerical studies of cross-corrugated plates [99, 121, 122]. Their experimental results report the mass transfer coefficient for the triangular cross-corrugated channels with an apex angle of 90°, base length of 2 mm, and different corrugation angles (0°, 45° and 90°) using electromechanical techniques [123]. They propose several correlations for the Sherwood number. The Nusselt number can be obtained from these correlations by using the analogy between heat and mass transfer [110]. The coefficients of determination (R-squared) of the correlations are higher than 0.99. The accuracy of Nusselt number correlations based on the experiment with constant properties is within ± 10% to ±15%. This order of accuracy is sufficient to calculate the heat transfer characteristics of the heat exchangers [124]. The *Re* for the aforementioned experimental study is in the range of 100–1400.

To validate the numerical model, a test case with geometrical parameters identical to the triangular cross-corrugated plate used in the experimental study of Scott and Lobato [56] is considered. In Figure 2-6, the Nusselt numbers obtained from the CFD simulations using the RSM model and the steady-state laminar model are depicted alongside the correlations of Scott and Lobato [56].

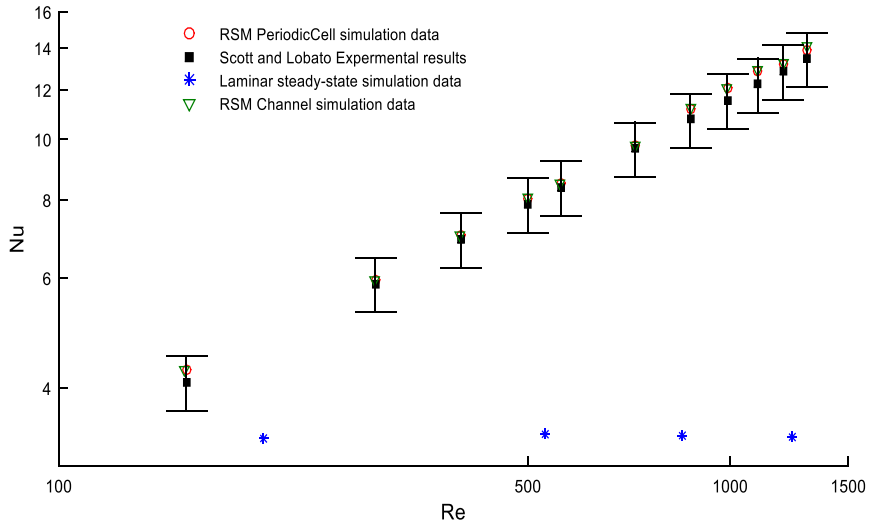

Figure 2-6. Comparison in log-log scale between CFD and experimental correlations for Nu versus Re (error bar is ±10%).

The CFD simulations using the RSM model are conducted with a periodic unitary cell and a channel with eight repetitive cells (Figure 2-2). Variations of Nu and f for each cell along the flow direction are shown for *Re*=1300 in Figure 2-7 and Figure 2-8. The boundary layer is very thin at the entrance of the channel; therefore, Nu and f are very high. The thickness of the boundary layer grows along the flow direction until the flow is fully developed (after 4–5 cells). Consequently, Nu and f decrease sharply along the first cells, and after 4–5 cells they reach a steady value and further changes are negligible. The Nu and f for the aforementioned channel are in very good agreement with the results for a unitary cell with periodic boundary conditions. The maximum deviation for Nu is 0.5% and for f is 0.02%. However, the mesh size for the channel (4051121 elements) is approximately eight times larger than that of the periodic unitary cell (507100 elements). Therefore, in this work, a unitary cell with a periodic boundary is considered for the CFD study.

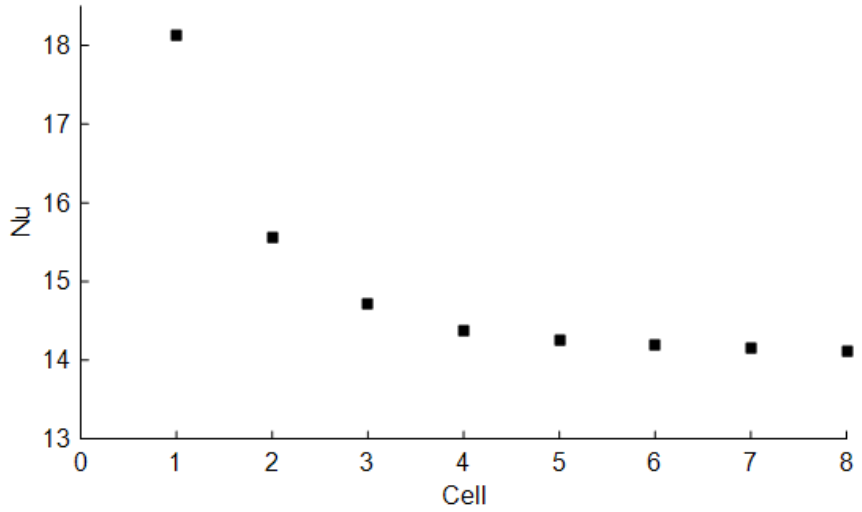

Figure 2-7. Variation of Nu along the flow direction in channel with eight cells at Re=1300.

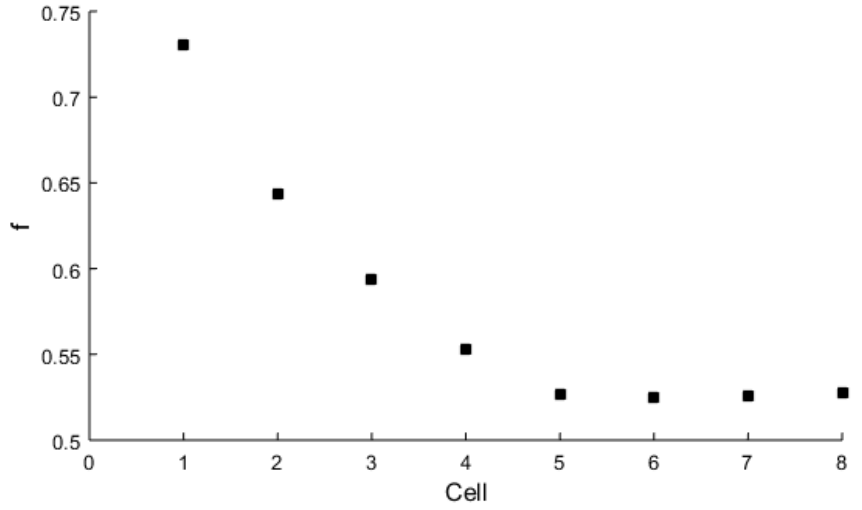

Figure 2-8. Variation of f along the flow direction in channel with eight cells at Re=1300.

The RSM results and experimental results are observed to be in very good agreement, with deviations between 0.8–4.84% (Table 2-4). The deviation values are relatively small compared to the conventional error on the experimental results, which is 10% [125].

Re	Nu (RSM periodic cell)	Nu (Scott and Lobato experiment)
154	4.27	4.08
296	5.94	5.87
397	7.02	6.91
589	8.71	8.62
721	9.74	9.66
872	11.19	10.75
990	12.06	11.54
1099	12.82	12.23
1199	13.18	12.85
1300	13.86	13.44

Table 2-4. Comparison between the RSM periodic cell results and experimental results of Scott and Lobato [56] for Nu.

Furthermore, the numerical model is compared with the numerical study of Zhang [121], which is based on a geometry with the corrugation and apex angles of 90˚ and 60˚, respectively. The *Re* in the aforementioned study is between 100 and 3000. The CFD results fit well with the data from Zhang [121] , with a maximum deviation of 2.82% for Nu (Figure 2-9). Based on the RSM results, a power law relationship is utilized to describe the variation of Nu with *Re* (Figure 2-6). To illustrate the quality of the model even further, simulations are conducted with a laminar model. The laminar model predicts a negligible change of Nu with respect to *Re*, i.e. it predicts a constant Nu (Figure 2-6). The same behaviour can be observed in a fully developed laminar flow in a duct with hexagonal cross section (Nu=3.34) [15].

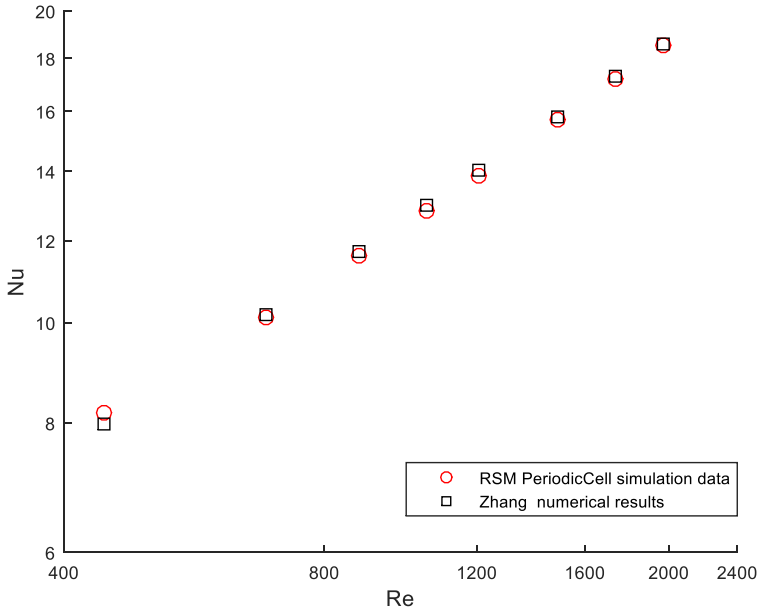

Figure 2-9. Comparison in log-log scale between CFD results and data from literature for Nu versus Re.

By further inspecting the velocity vectors (Figure 2-10) at *Re*=550, a significant difference between the laminar and RSM results can be observed, especially with regard to the vortices in the lower plate. Consequently, the laminar model leads to a thicker thermal boundary layer, as can be deducted from the temperature distributions shown in Figure 2-11. This is not surprising considering that a steady-state laminar solution resembles an RSM model at lower viscosity. This is confirmed in the significantly different recirculation flow as predicted by RSM, compared to the laminar flow simulations. These generated vortices lead to higher dissipation and shear rates in the flow resulting in further heat transfer through the thermal boundary layer. By increasing *Re* these vortices become stronger and enhance the heat transfer even further.

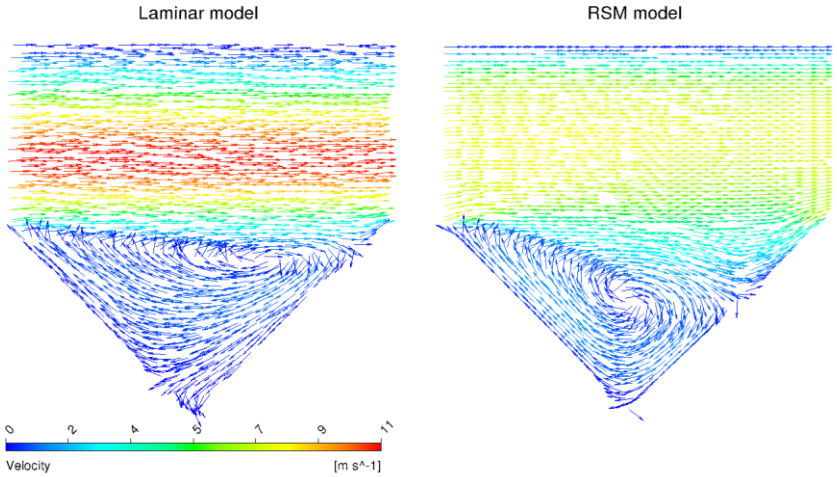

Figure 2-10. Velocity vector fields of laminar and RSM results at Re=550; colour coded by velocity magnitude.

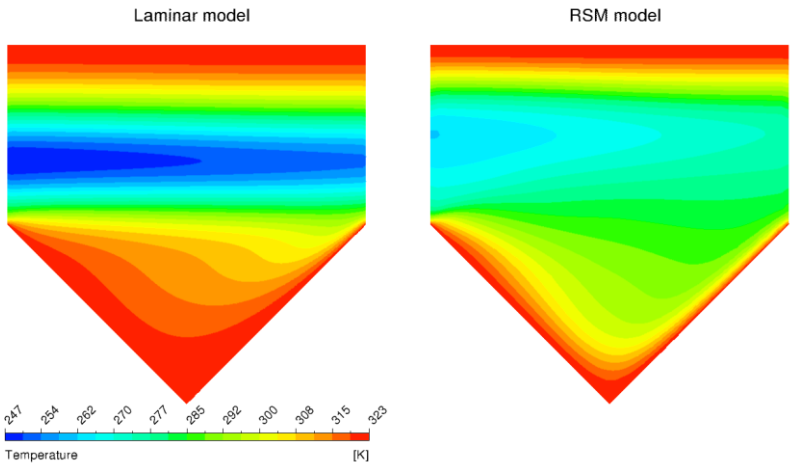

Figure 2-11. Temperature distribution at the mid plane along the flow direction for laminar and RSM models at Re=550.

2.3.2 Flow and heat transfer characteristics

It is well known that the majority of overall pressure drop in typical compact heat exchangers is due to the core frictional pressure drop [15]. Therefore, in the following, the core frictional pressure drop is analysed as the main measure of the overall pressure drop at different *Re* and for various apex angles. Furthermore, according to Paisarn [126], the pressure drop in a corrugated channel is an outcome of turbulence augmentation and the recirculation zone formed by corrugation and drag forces acting on the flow field. Accordingly, the mentioned contributions are investigated to characterise the flow and heat transfer mechanisms.

2.3.2.1 Pressure drop

For the heat exchanger geometries considered in this study, increasing the apex angle results in a smaller channel cross section and a smaller hydraulic diameter. Therefore, in order to maintain a specific *Re* for all cases, a higher mass flow rate must be imposed as the apex angle increases. In Figure 2-12, the velocity vectors at *Re*=1370 are shown for three different apex angles. The presence of a recirculation zone in the corrugation part is apparent for all of the apex angles. Furthermore, the highest core velocity is seen in the geometry with the greatest apex angle.

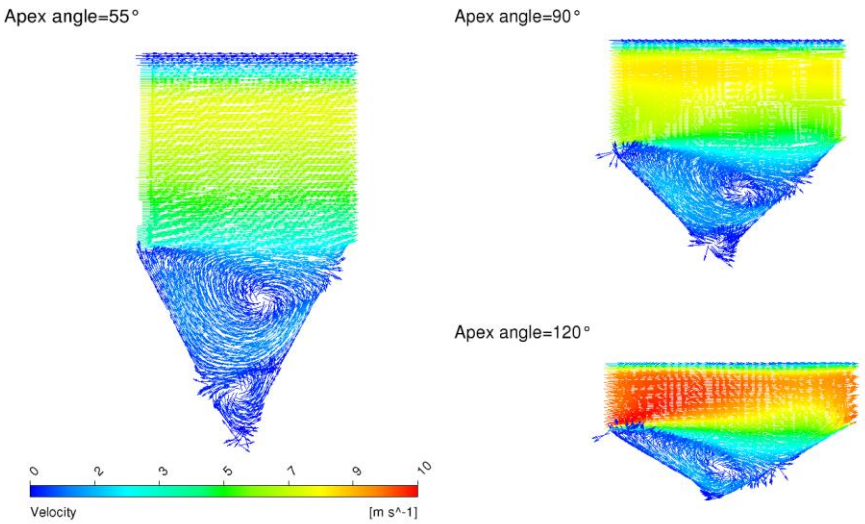

Figure 2-12. Velocity vectors at Re=1370 for different apex angles at the mid plane along the flow direction; colour coded by velocity magnitude.

For a given *Re* (=1370), by increasing the magnitude of the apex angle the drag force increases (Figure 2-13), resulting in a larger pressure drop (Figure 2-14). The pressure drop for the apex angle of 120° is higher than that arising from the angles of 90° and 55° by 109% and 474%, respectively. More insights can be gained by analysing the two components of the drag force, i.e. pressure and viscous force in the direction of the main flow. Based on the obtained results for the considered geometry, the pressure force is found to be dominant (Figure 2-15), and thus the pressure drop is determined by the pressure force. The pressure force is calculated by integration of the pressure multiplied by area normal vector of each boundary cell over the wall boundaries. This is then multiplied by the specified direction vector of the main flow. Note that this is in contrast to the pipe flow, where the viscous force is the main component of the pressure drop [111].

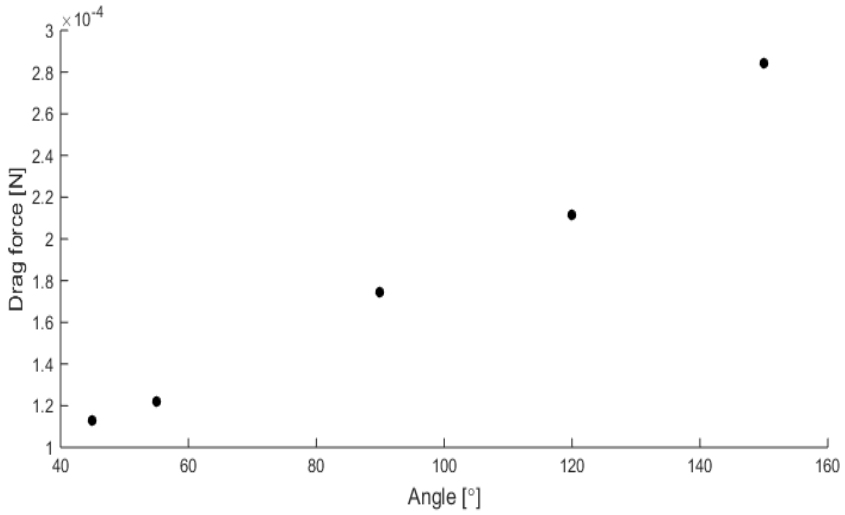

Figure 2-13. Drag force versus apex angle at Re=137

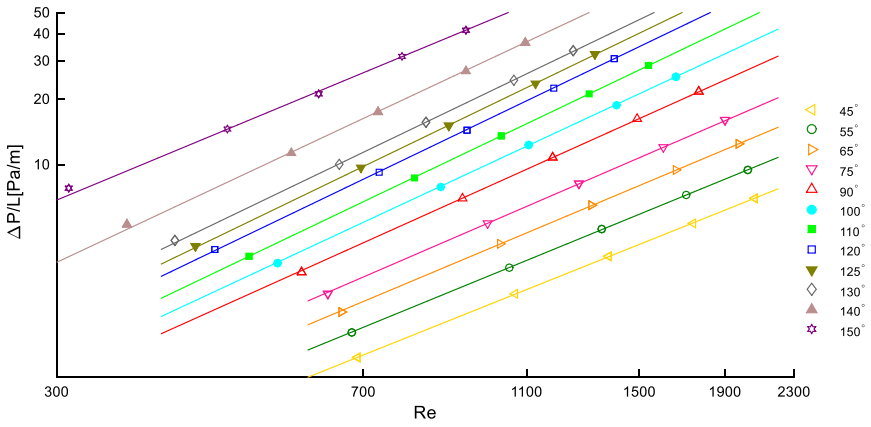

Figure 2-14. Pressure drop versus Re for different apex angles in log-log scale.

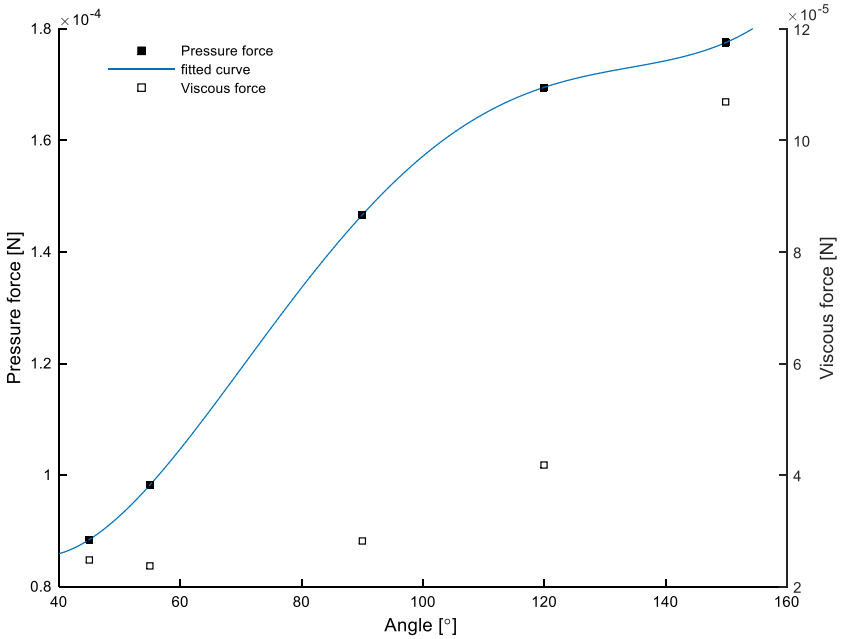

Figure 2-15. Pressure force and viscous force versus the apex angle at Re=1370.

According to the flow structures shown in Figure 2-12, the pressure force is closely connected to the vortices present in the recirculation zone. According to Greitzer et al. [127], the rate of rotation of fluid particles is quantified by the mean vorticity

magnitude along the flow direction (Figure 2-16). Vorticity magnitude increases with a greater apex angle. According to Panton [128], there is a coupling relationship between the pressure gradient and the vorticity magnitude, as the pressure gradient is necessary to sustain the flux of vorticity into the fluid. Therefore, the pressure drop also increases with greater apex angles, resulting in the highest pressure drop at the apex angle of 150° and the lowest at the apex angle of 45°.

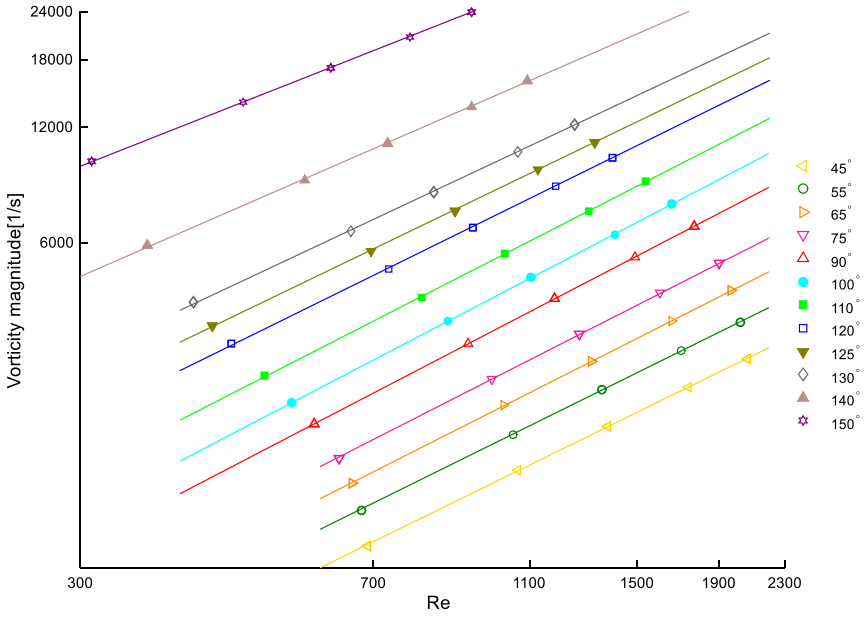

Figure 2-16. Mean vorticity magnitude along the flow direction for different apex angles versus Re in log-log scale.

2.3.2.2 Friction factor

The hydraulic performance of heat exchangers is characterized by the friction factor (f), which is a dimensionless representation of the pressure drop. The physical meaning of f is the fraction of kinetic energy that is dissipated in a unit length of the channel. The variations of f with respect to the apex angle and *Re* are demonstrated in Figure 2-17 and Figure 2-18. It can be clearly seen that f decays with respect to *Re*.

The highest and lowest hydraulic performances are obtained at the apex angles of 150° and 90°, respectively. The influence of the apex angle on f is described by two distinct trends. The first trend is related to the angles between 45° and 90°,

where f increases when the apex angle is increased. The second trend is associated with the angles between 90° and 150°, where f decreases when apex angle is increased. In the following section, the hydrodynamic justification for these two opposing trends is explained.

An explanation for the aforementioned trends is given based on the turbulence intensity. The turbulence intensity is defined as the ratio of the root-mean-square of the velocity fluctuations to the mean flow velocity [129].

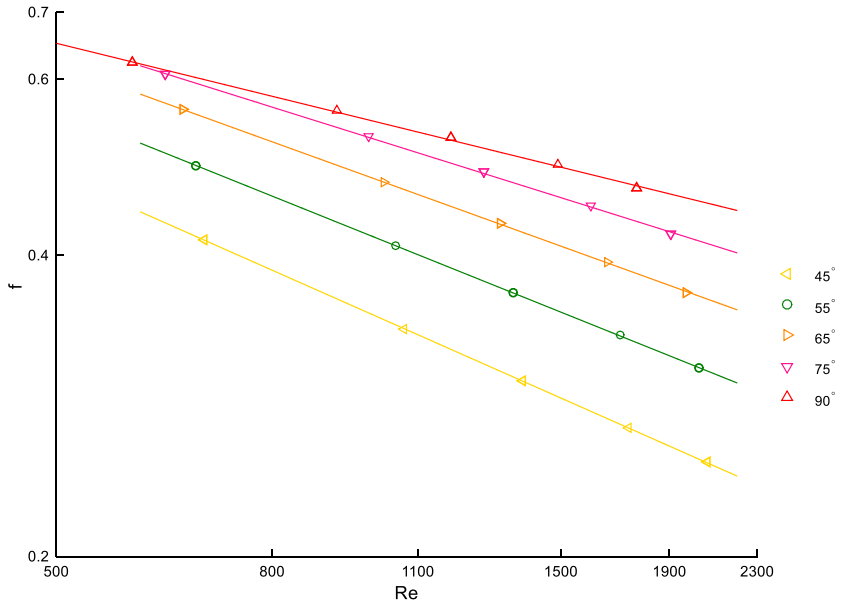

Figure 2-17. Friction factor versus Re for apex angle 45–90° in log-log scale.

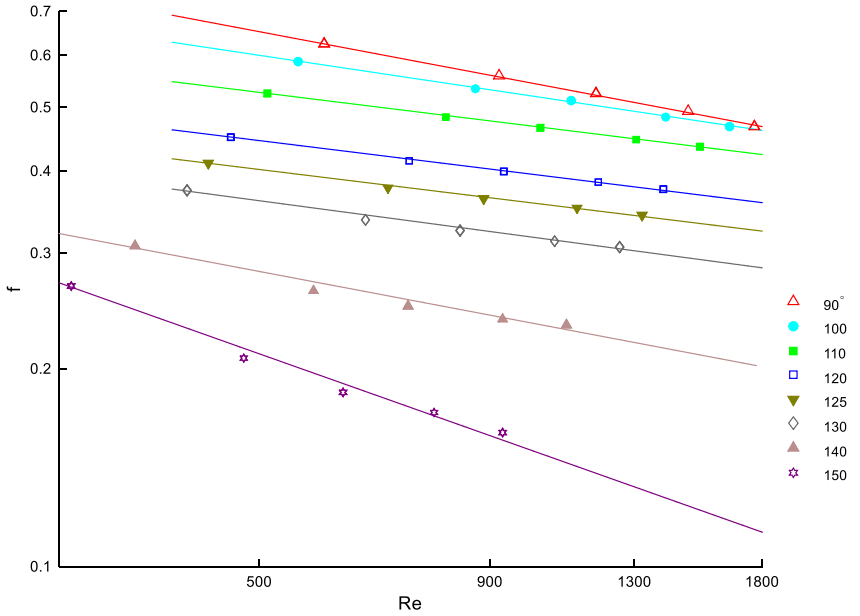

Figure 2-18. Friction factor versus Re for apex angle 90–150° in log-log scale.

The average turbulence intensity in the mid-surface along the flow direction caused by the fluid interaction is calculated for different apex angles at *Re*=1370 (Figure 2-19).

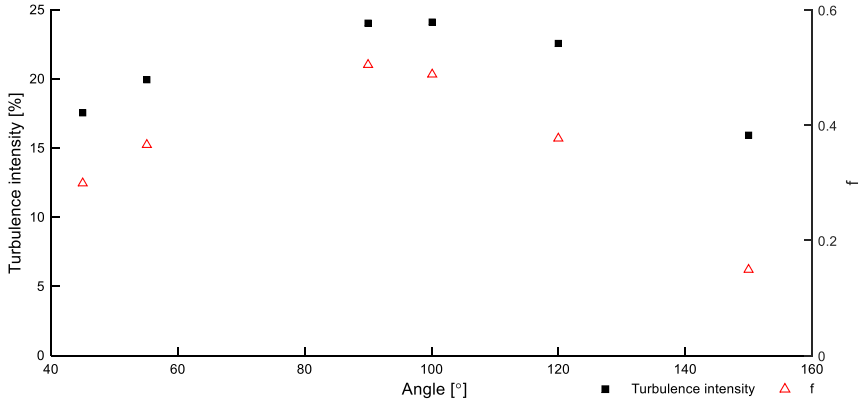

Figure 2-19. Average turbulence intensity along the flow direction at Re=1370 for different apex angles.

By increasing the angle in the first trend, the turbulence intensity increases, and thus f increases as well. However, although the vorticity magnitude increases in the second trend, the turbulence intensity decays, resulting in lower f. Therefore, for a constant *Re*, the highest f is found near an angle of 90°. Note that at higher *Re*, apex angles between 90° and 100° give similar friction factors. For example, at *Re*=1370, the variation in f from an angle of 90–100° is negligible (only 3.2%). The lowest f is found at an angle of 150°, around 70% lower than *f* for an angle of 90°. Similar trends were observed for sinusoidal cross-corrugated plate heat exchangers, where Ciofalo et al. [82] argue that when pitch to height ratio of the channel increases from 2.2 to 4 (equivalent to the dimension of a triangular cross-corrugated plate with an apex angle greater than 90°), f decreases. They associate this trend with the complexity of swirling flow and recirculation zones. Similarly, as shown in Figure 2-12, only one recirculation zone appears for the angle of 120°, while two recirculation zones are present for the angles between 55° and 90°.

According to Ciofalo et al. [82] and Zhang and Che [95], the complexity of the recirculation zones plays an important role in friction factor and Nusselt number behaviour. The swirling motion and recirculation zones are created by the pressure force. To further analyse this phenomenon, a polynomial function is fitted to the pressure force obtained from simulation data at *Re*=1370, for different apex angles (Figure 2-15). The critical point of this function is found to be at an angle of 100°, where turbulence intensity is at its peak (Figure 2-19). This means that even though the pressure force increases with the angle, the growth rate decays from angles of a magnitude of 90–150°. Moreover, it can be clearly observed in Figure 2-15 that the variation of the viscous force by increasing the angle up to 100° is negligible (14% from angles 45–90°). Conversely, in the second trend, the growth rate of the viscous force is increased significantly. For example, for angles 90–120°, the viscous force is increased by 49%; therefore, the ratio between pressure and viscous forces decays after an angle of 100°, resulting in a smaller recirculation zone and lower turbulence intensity.

2.3.2.3 Heat transfer coefficient

The heat transfer coefficient (h) in the cross-corrugated channel is controlled by the thermal boundary layer behaviour. Figure 2-20 shows the influence of the apex angle and *Re* on h.

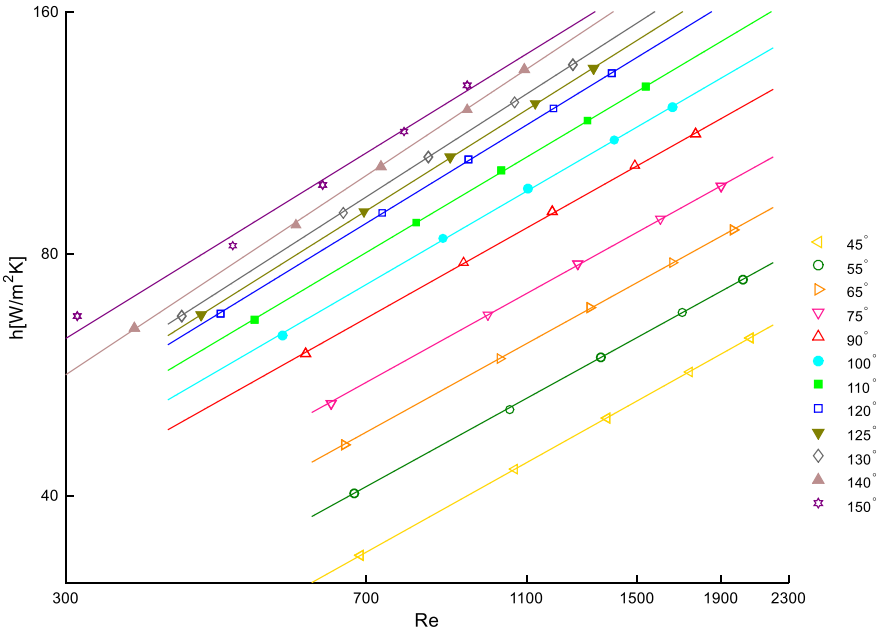

Figure 2-20. Heat transfer coefficient with respect to Re for different apex angles in log-log scale.

A clear analogy can be found between the heat transfer coefficient and the pressure drop behaviour. Furthermore, it can be seen that h increases with increasing *Re*. This can be attributed to the thickness of the thermal boundary layer decreasing in both the upper wall and the troughs of the lower one while the temperature gradient increases near the wall (see Figure 2-21). For a constant Re, a greater apex angle leads to a higher heat transfer coefficient. By inspecting the temperature distribution at different angles for *Re*=1370 (Figure 2-22), the influence of the apex angle on the thermal boundary layer becomes evident.

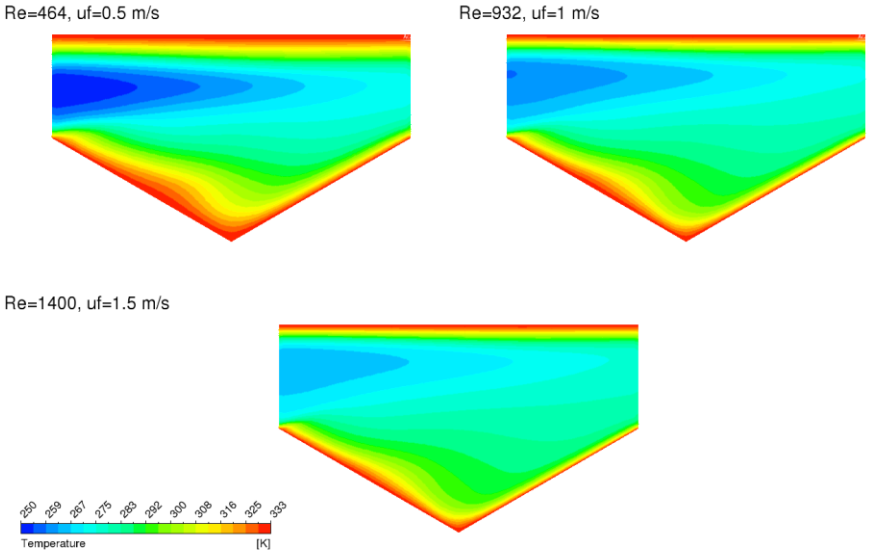

Figure 2-21. Temperature distribution at the mid plane along the flow for the apex angle 120°.

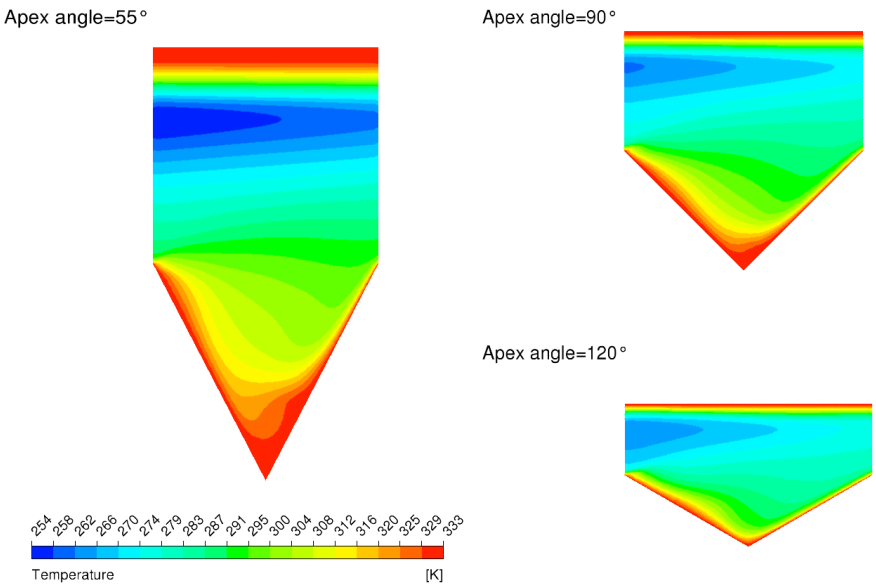

Figure 2-22. Temperature distribution at the mid plane in direction of the flow direction at Re=1370 for different apex angles.

2.3.2.4 Colburn j factor

To further analyse heat transfer performance, the Colburn j factor (j) is used. The j factor provides the ratio between the heat and momentum transfer. The influence of the apex angle on the j factor is explained in the following paragraph. In general, the same trends as seen for the friction factor can be observed in Figure 2-23 and Figure 2-24.

As expected, j decreases as *Re* increases. Following the first trend, j increases along with the apex angle up to an angle around 90–100°. Afterwards, j decreases as the apex angle grows for a constant *Re*. The highest thermal performance (j) is observed with an apex angle of around 90–100°, whereas the lowest thermal performance is associated with an apex angle of 150°. Indeed, similar to f, the two different flow patterns (characterized by turbulence intensity) lead to two different trends of j associated with increasing the apex angle. This can be explained by the fact that, in the second trend, although the heat transfer rate grows due to the change in thermal boundary layer thickness, as the channel gets smaller the mass flow rate increases as well. Again, the angles between 90° and 100° are found to be the transitional points between the two trends. Note that the variation in j from an apex angle of 90–100° is approximately 0.92%. At a *Re* of 1370, the highest j is obtained at an apex angle of 90°. Moreover, the minimum j is observed at an

angle of 150˚, which is 36% lower than the maximum. At this *Re*, the influence of the apex angle is roughly two times greater on f than on j.

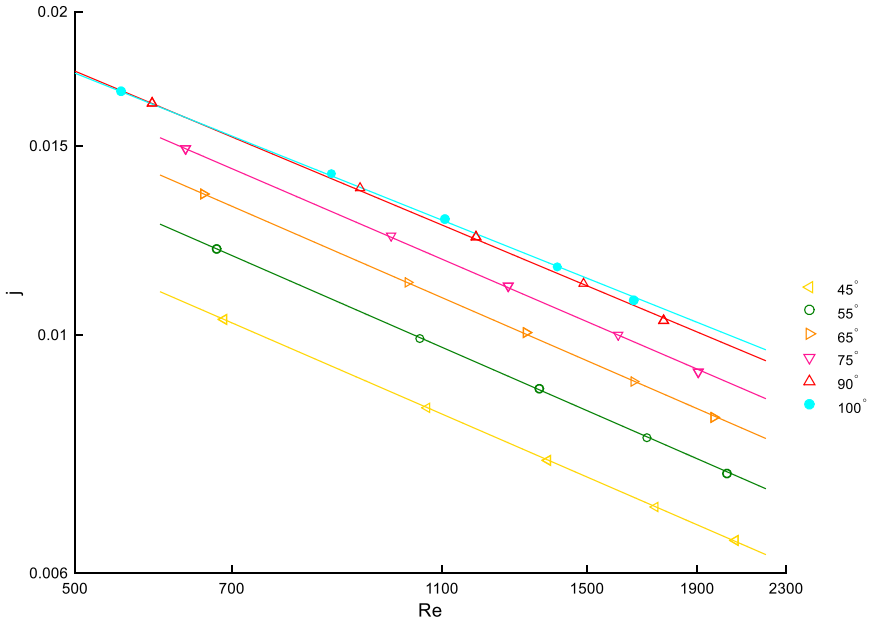

Figure 2-23. Colburn j factor versus Re for apex angle 45–100˚ in log-log scale.

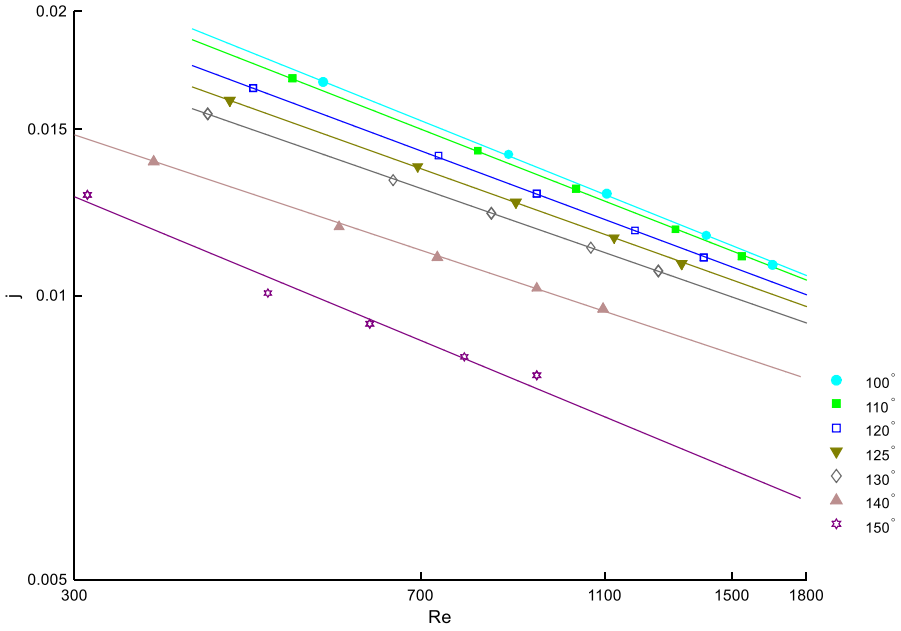

Figure 2-24. Colburn j factor versus Re for apex angle 100–150° in log-log scale.

2.3.3 Thermo-hydraulic performance

The PEC introduced by Cowell [103] is used in this study. Ameel [65] explained this method in depth in his dissertation. For a given inlet flow temperature, mass flow rate, and heat transfer rate (constant heat transfer unit), the relative heat exchanger volume (V^*) and relative pumping power (P^*) are calculated from equations (2-30) and (2-31). Contraction factor (σ) is the ratio of the minimum cross section area to the frontal area.

$$\sigma = \frac{A_c}{A_f},$$

$$V^* = \frac{D_h^2}{\sigma\, j\, Re},$$

(2-30).

$$P^* = \frac{fRe^2}{j\, D_h^2}.$$

(2-31).

Based on the PEC method mentioned earlier in this study, in order to choose the heat exchanger with the best thermo-hydraulic performance, the relative volume (V^*) of heat exchangers at different apex angles should be compared for a given pumping power and heat transfer rate. The one with the lowest V^* is the best performing.

In Figure 2-25, the relative pumping power (P^*) with respect to V^* for different heat exchangers is depicted for different apex angles and a constant heat transfer rate. For a given pumping power and similar heat transfer rate, the relative heat exchanger volume decreases by increasing the apex angle. For the heat exchanger with an apex angle of 45° and 90°, V^* is found to be 4.07 and 2.14 times larger, respectively, than the heat exchanger with an apex angle of 150°. The variation in V^* caused by increasing the apex angle for a given P^* is non-linear, and in fact can be described by an exponential function (Figure 2-26). It is important to note that V^* monotonically decreases as the apex angle increases. Therefore, among the apex angles considered in this study, the heat exchanger with the apex angle of 150° has the best thermo-hydraulic performance.

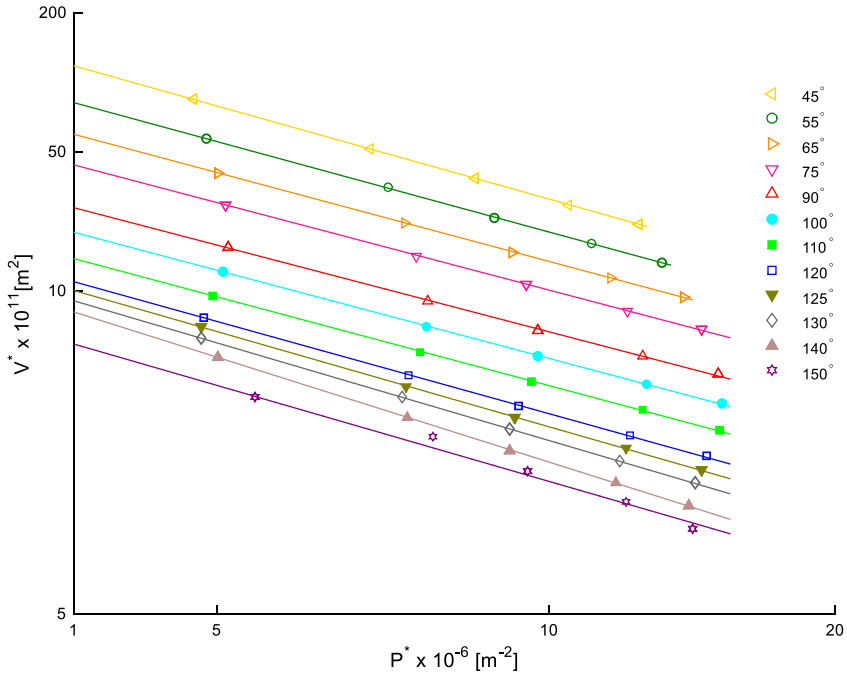

Figure 2-25. Performance plot for different apex angles in log-log scale.

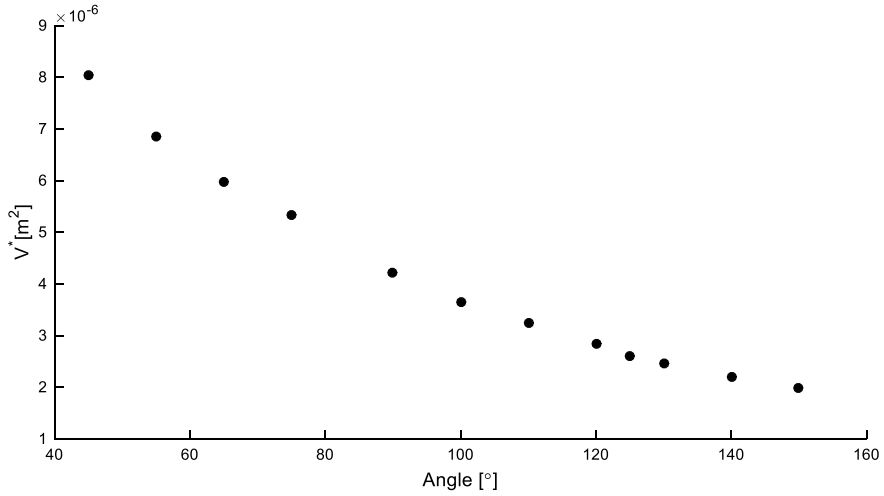

Figure 2-26. V with respect to the apex angle for a given P* and heat transfer rate.*

2.4 Summary

In this chapter, the influence of geometrical parameters on the flow and heat characteristics of cross-corrugated heat exchangers is studied, particularly the influence of apex angle (channel aspect ratio) for low *Re* applications. A wide range of apex angles from 45–150° are analysed numerically for their effects on the heat transfer and hydraulic characteristics. The choice of the flow solver as laminar versus turbulent (Reynolds stress model) for the CFD model is discussed. The results of the two CFD models with the two solvers are compared with the available experimental results. A three-dimensional computational fluid dynamics approach with the Reynolds stress model is considered to investigate the influence of the apex angle on the thermal and hydraulic features of triangular cross-corrugated heat exchangers for a range of Reynolds numbers 310-2064. The influence of the intensity and complexity of the recirculation zones along with the turbulence intensity on those characteristics and corresponding viscous and pressure forces are studied. The choice of the computational domain as a unitary cell with periodic boundary condition versus a long channel with several cells is discussed. One on one comparison between the Reynolds stress model and experimental results shows less than 5% deviation, which is within the uncertainty of the experiment. By increasing the apex angle both pressure drop and heat transfer coefficient increase, due to the increase of the pressure force and the vorticity magnitude along the flow direction. The pressure force is the dominant force, contrary to pipe flow, where the viscous force is dominant. The influence of the apex angle on the friction factor and the Colburn j factor follows two distinguished trends. The apex angles around of 90–100° are the transitional angles for the flow regime. Peak of turbulence intensity, friction factor and Colburn j factor are observed around these angles. The ratio between pressure and viscous forces decays after angle 100°, resulting in a smaller recirculation zone and lower turbulence intensity. Finally, the thermo-hydraulic performance of the considered geometries is compared with respect to each other based on a performance evaluation criterion. It is found that the geometry with the largest apex angle has the highest thermo-hydraulic performance.

3

Correlations for Cross-Corrugated Plate Heat Exchangers in Transitional Flow Regime

3.1 Introduction

According to Focke et al. [13], in comparison with smooth channels, corrugated channels offer a larger heat transfer area per unit volume of the heat exchanger. This creates a higher heat transfer rate, stronger structure, lighter weight, reduced space, and more economical design. Shah and Sekulic [15], describe the small hydraulic diameter of the channels, continuous disruption of boundary layers, and promotion of secondary flow as the reasons for the enhancement of the heat transfer rate. According to Shah and Wanniarachchi [14], Liu and Tsai [78] and Focke et al. [13], the flow in the cross-corrugated channel has a complex nature and the transition from laminar regime to turbulent regime happens at a low range of Reynolds numbers (100-1500) depending on the geometry parameters.

Accurate prediction of the flow and heat transfer characteristics of these complex geometries is very important to the design process. The aforementioned characteristics are strongly influenced by the geometric parameters of the cross-corrugated channels. Muley et al. [58], identified the geometric parameters as the corrugation angle and the channel cross section aspect ratio (the ratio of width to height).

Kakac et al. [130] stated that the available generalised correlations for the flow and heat transfer characteristics of cross-corrugated channels are limited, contrary to those pertaining to tubular heat exchangers. As it is known from the literature, the most popular corrugation profile that has been studied numerically and experimentally is sinusoidal. Authors such as Ciofalo et al. [82], Blomerius et al. [12], Mehrabian and Poulter [68], Yin et al. [79] and Freund and Kabelac [70] investigated the heat and flow characteristics of cross-corrugated plates with sinus wave corrugation (chevron plates) for a wide range of Reynolds numbers. Savostin and Tikhonov [60], Heavner et al. [59], Martin [131], Wang and Sunden [132] and Rao et al. [133] introduced generalized flow and heat transfer correlations for industrial chevron plates with different corrugation angles. However, these correlations are only valid for a specific cross-sectional aspect ratio (industrial plates) and they mainly explain the effect of different corrugation angles.

According to Liang and Li [134], and Mahmud et al. [135], with the development of membrane based technology, the use of cross-corrugated plates with triangular corrugation (triangular cross-corrugated plates) has increased in air conditioning industries. Unlike sinusoidal cross-corrugated plates, very few researchers (e.g. Scott and Lobato [56], Hall et al. [97], and Zhang [99]) have investigated both numerically and experimentally the flow and heat transfer characteristics of triangular cross-corrugated plates. The geometric parameters are the apex angle (equivalent to cross-sectional aspect ratio) and corrugation angles. Unfortunately, the majority of previously published correlations for triangular cross-corrugated plates are associated with only three apex angles of 45°, 60°, and 90°. As pointed out by Sharif et al. [136], by increasing the apex angle, the performance of triangular cross-corrugated plates improves. The database including other apex angles, especially apex angles greater than 90°, is not available for the development of previous correlations. Therefore, it is very crucial to update the existing database and develop new correlations to include a wider range of apex angles.

3.2 Nu and f Correlations

The Nu (calculated from equation (2-11)) and f (calculated from equation (2-14)) data from numerical simulations are presented respectively in Figure 3-1 and Figure 3-2. The solid black lines and dashed blue lines describe the relationship between Nu and f with *Re* for each apex angle (Figure 3-1 and Figure 3-2). As variations in Nu and f with *Re* for each apex angle follow log-linear lines (solid black lines and dashed blue lines) with a constant slope, the use of a power law expression in equation (3-1) is justified. Figure 3-3 and Figure 3-4 show the simulation results for f and Nu as a function of α. The relationship between the Nu and f with α can be describe with a sine function. This is chosen as it is the simplest function to describe this relationship. It is scientifically always best to choose the simplest model that fits the data point. This is in line with Occam's razor principle (attributed to the 14th century English philosopher, William of Occam), which states that, "Pluralitas non est ponenda sine necessitate," or "Entities should not be multiplied unnecessarily".

It is evident that Nu and f are functionally related to *Re* and α. The general form of this function is expressed in equation (3-1).

$$\begin{cases} X = (\mathrm{asin}(\alpha) + b)\, Re^{c} \\ X = f \text{ or } Nu \end{cases} . \qquad (3\text{-}1).$$

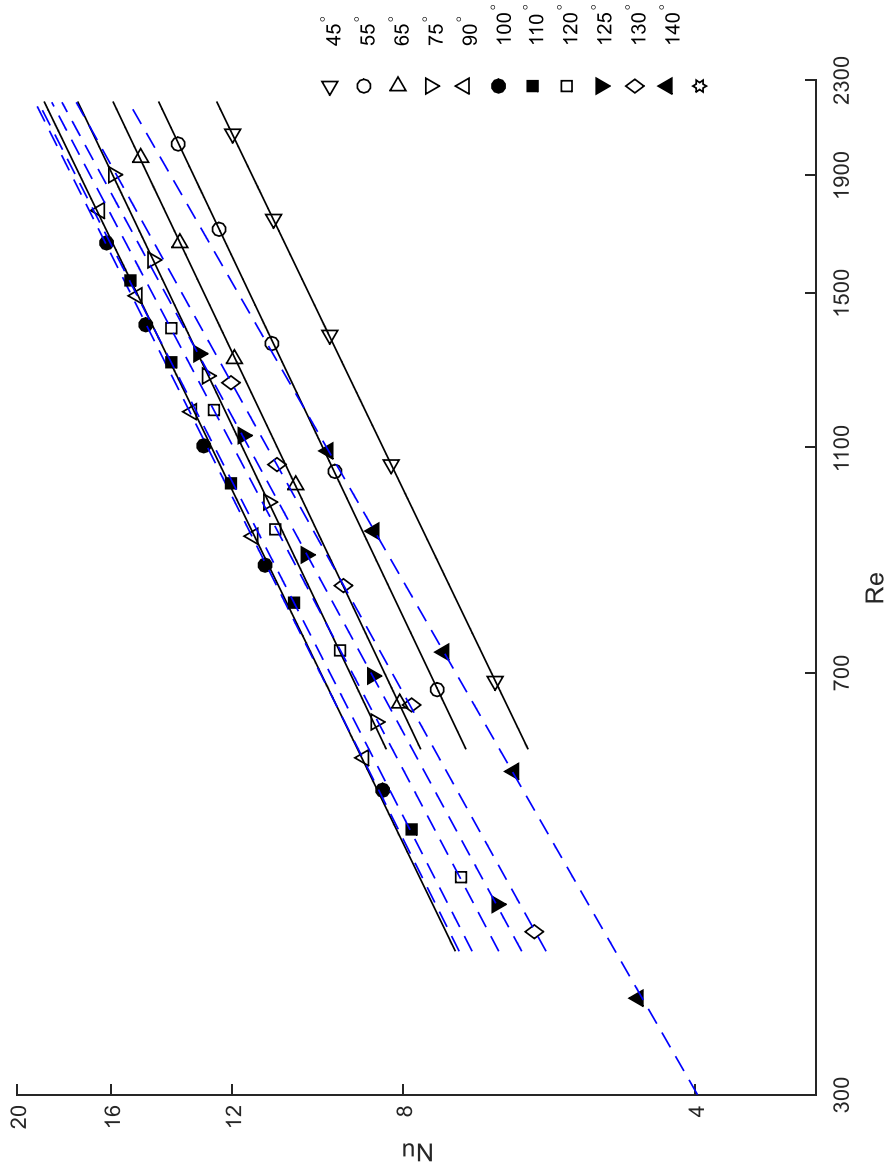

Figure 3-1. Nu versus Re for apex angles 45–140°.

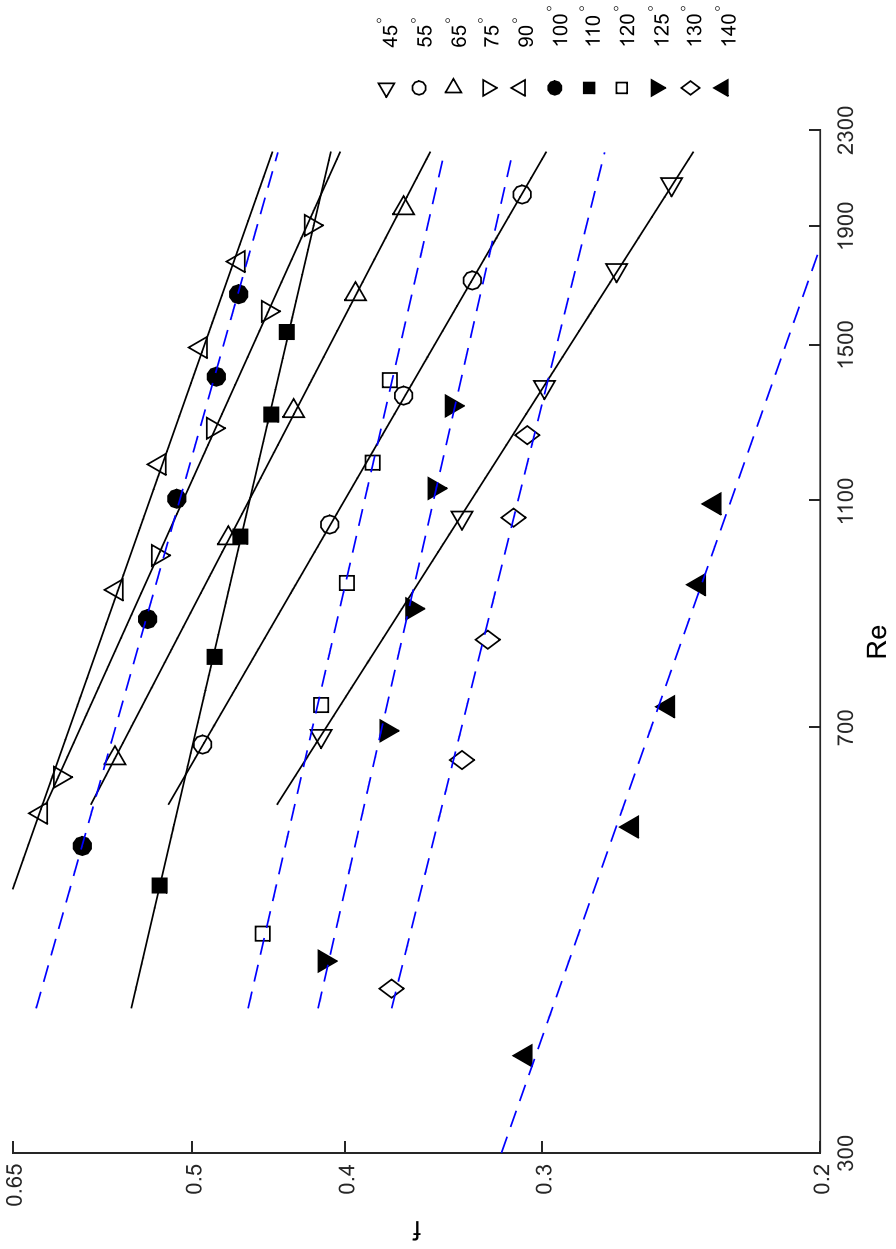

Figure 3-2. f versus Re for apex angle 45–140° in log-log scale.

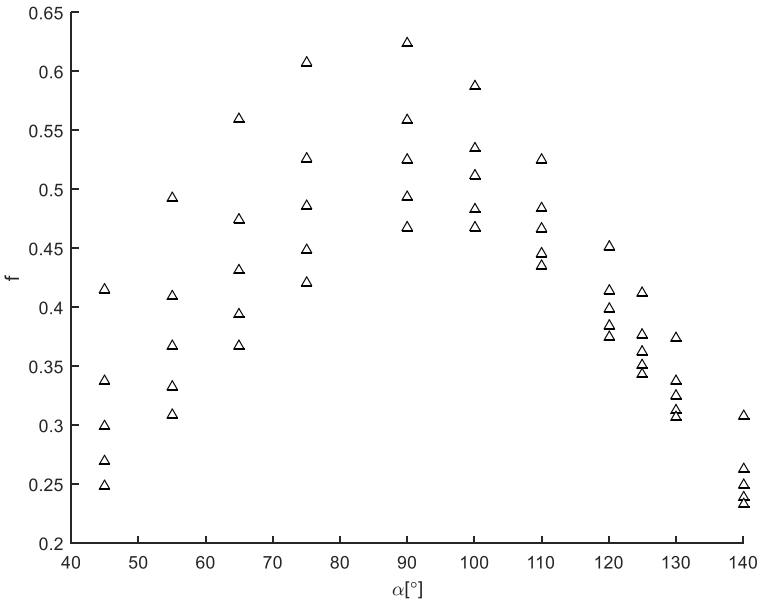

Figure 3-3. Simulation results for f.

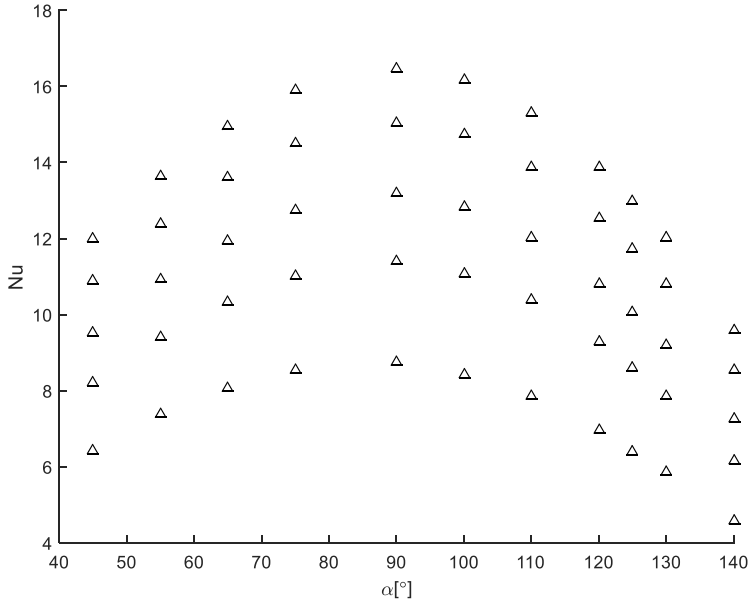

Figure 3-4. Simulation results for Nu.

According to Figure 3-1 and Figure 3-2, for the apex angle between 45° and 90° (trend 1), the solid black lines are approximately parallel to each other. Moreover, for apex angles in the range of 100–140° (trend 2), the dashed blue lines display almost the same slope. The influence of the apex angle on f and Nu following two distinct trends is explained in section 2.3.2. By increasing the apex angle in the first trend, both f and Nu increase, while in the second trend, both aforementioned characteristics decrease.

The least squares approach described in [137] is used to develop a generalized correlation for Nu (equation (3-2)) and f (equation (3-3)) based on equation (3-1).

In equations (3-2) and (3-3) the unit of α is in radians.

$$Nu = 0.3673 \sin(\alpha)\, Re^{0.5084}, \tag{3-2}$$

(3-2).

$$f = \begin{cases} (6.315 \sin(\alpha) - 1.33)\, Re^{-0.3222} & 45° < \alpha < 90^{\circ} \quad trend1 \\ (2.438 \sin(\alpha) - 0.8539)\, Re^{-0.1638} & 100° < \alpha < 140^{\circ} \quad trend2 \end{cases}, \tag{3-3}$$

(3-3).

In Figure 3-5 and Figure 3-6, the simulation results and the values predicted by the correlations (3-2) and (3-3) are illustrated. The maximum deviations between simulation results and the values predicted by the correlations for Nu and f are 13% and 11.7% respectively. The minimum deviations for Nu and f are 0.13% and 0.05%, respectively. The coefficient of determination (R-squared) for Nu, f (trend 1) and f (trend 2) are 0.94, 0.97 and 0.98, respectively. The root mean square error of the estimates for Nu, f (trend 1) and f (trend 2) are 0.7, 0.018 and 0.013, respectively. The aforementioned generalized correlations ((3-2) and (3-3)), provide an appropriate level of accuracy for engineering applications.

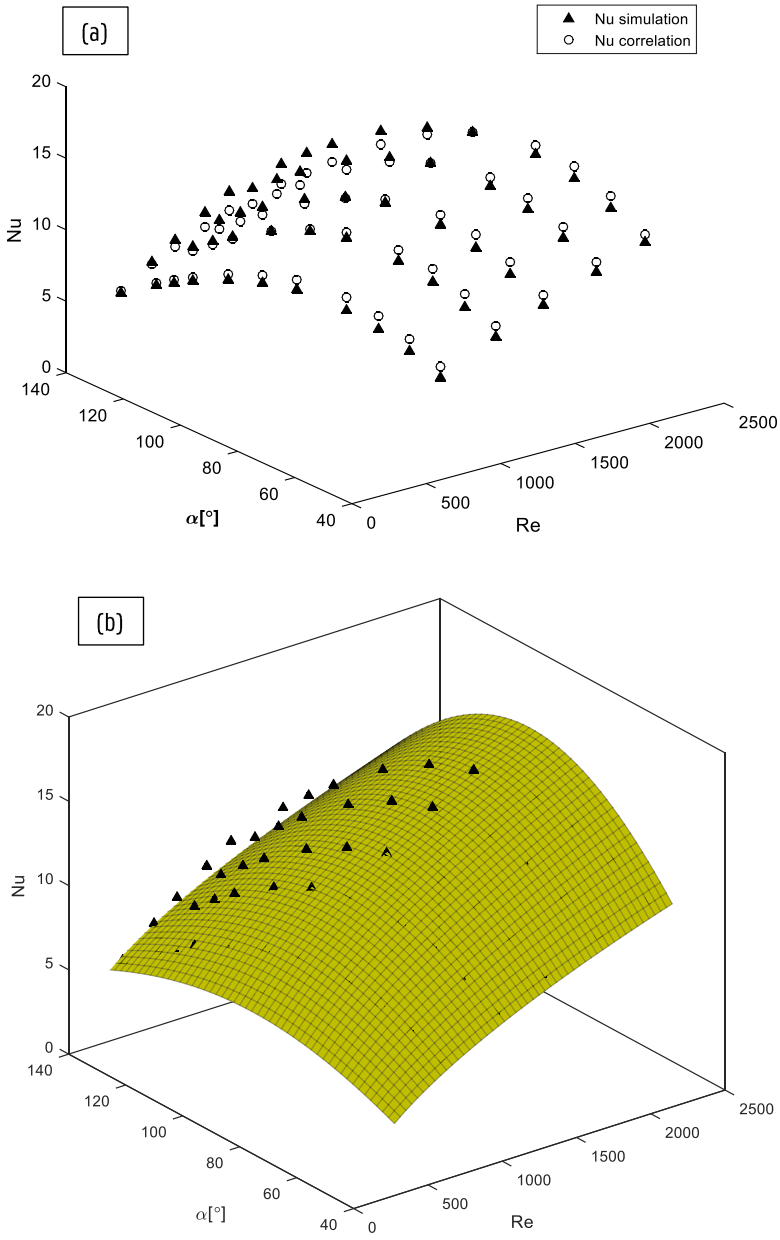

Figure 3-5. Comparison between simulation results and values predicted by Nu correlations (3-2): (a) point cloud (b) surface is added to the correlation points

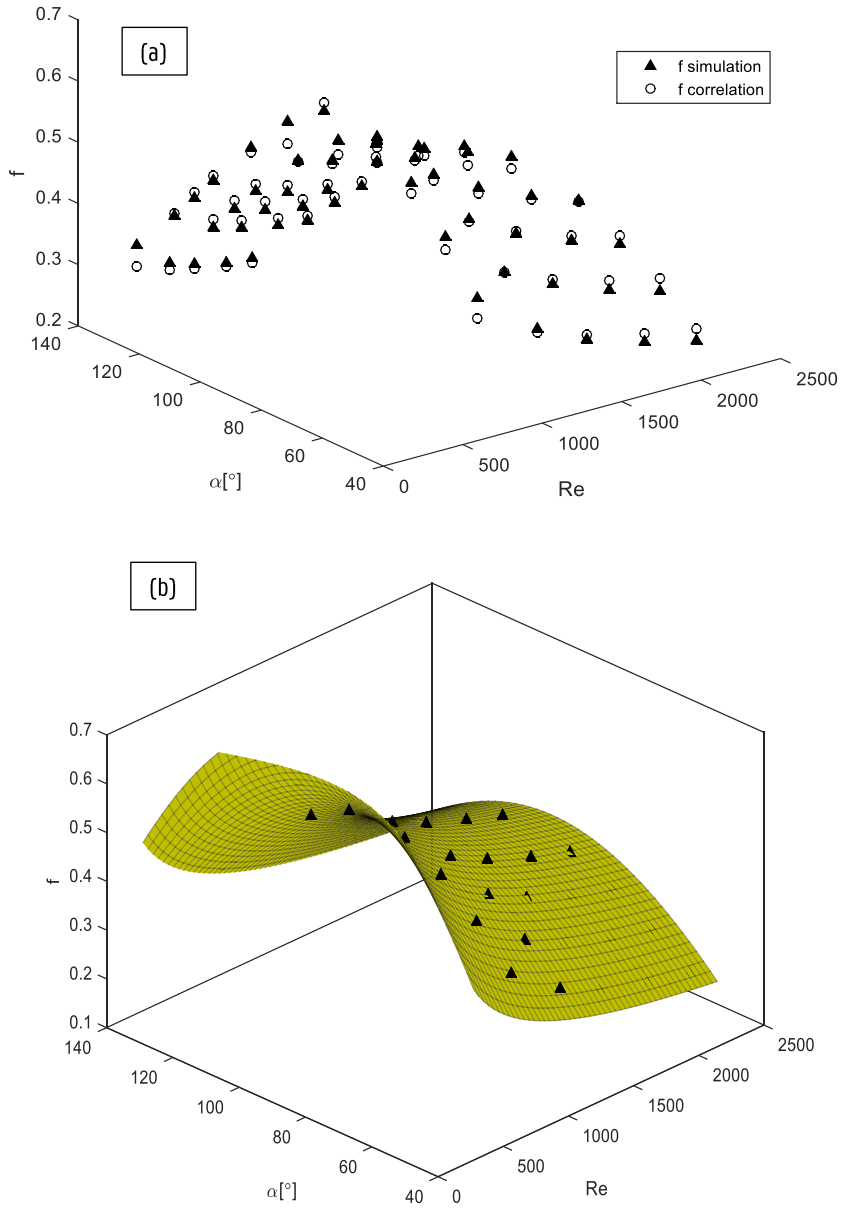

Figure 3-6. Comparison between simulation results and values predicted by f correlations (3-3): (a) cloud point, (b) surface is added to the correlation points.

The more accurate correlations can be derived for f and Nu as a function of *Re* for each apex angle. These correlations are shown in Table 3-1. The standard errors for Nu and f correlations for each geometry are described in Table 3-2. The maximum standard error for Nu is 0.005 and for f is 0.02. The maximum deviations between the simulation results and the values predicted by the correlations for each apex angle for Nu and f are 0.84% and 4%, respectively. The R-squared for all correlations is higher than 0.98.

α [°]	*f-Correlation*	*Nu-Correlation*
45	$8.8Re^{-0.47}$	$0.157Re^{0.568}$
55	$7.87Re^{-0.43}$	$0.19Re^{0.561}$
65	$6.73Re^{-0.38}$	$0.211Re^{0.562}$
75	$5.21Re^{-0.33}$	$0.227Re^{0.563}$
90	$3.3Re^{-0.26}$	$0.23Re^{0.572}$
100	$2.16Re^{-0.21}$	$0.204Re^{0.59}$
110	$1.51Re^{-0.17}$	$0.182Re^{0.604}$
120	$1.27Re^{-0.169}$	$0.15Re^{0.625}$
125	$1.14Re^{-0.168}$	$0.129Re^{0.642}$
130	$1.12Re^{-0.18}$	$0.114Re^{0.653}$
140	$1.38Re^{-0.26}$	$0.087Re^{0.671}$

Table 3-1. Correlations for f and Nu for each geometry.

α	45°	55°	65°	75°	90°	100°	110°	120°	125°	130°	140°
Nu	1e-3	2.3e-3	2.1e-3	3.2e-3	5e-3	4.5e-3	3e-3	3e-3	2e-3	1.5e-3	5e-3
Standard error											
f	1.5e-3	1.2e-3	2.7e-3	4e-3	5.4e-3	3.6e-3	3e-6	5e-3	7e-3	1e-2	2e-2
Standard error											

Table 3-2. Accuracy of the correlations for Nu and f for each geometry (correlations are described in Table 3-1).

3.3 Summary

The main goal of this chapter is to develop heat transfer and pressure drop correlations for triangular cross-corrugated heat exchangers. More specifically, this chapter focuses on the triangular cross-corrugated plates with an orientation angle of 90° and an apex angle in the range of 45–140°. By using the least squares approach several correlations for both Nu and f as the function of *Re* are proposed for each apex angle separately. The numerical results of Nusselt number and friction factor reported in Chapter 2 (55 simulations) are used for this purpose. Moreover, generalized correlations for Nu and f are presented to specifically take into account the effect of the apex angle. The data from the simulations and generalized correlations are in a good agreement, with a maximum deviation of 13% for Nu and 11.7% for f.

4

Thermal Performance Assessment of Polymeric Cross-Corrugated Plate Heat Exchangers

4.1 Introduction

Metallic materials have high thermal conductivity and high material strength. These properties are favourable for designing heat exchangers with a wide range of pressure and temperature ratings for many different industrial applications [138]. Factors such as the 2020 targets of the EU on climate change and energy (Figure 1-3), the scarcity of precious materials, and the heavy weight and high capital cost of metallic heat exchangers are all incentives towards considering alternative polymeric/composite heat exchangers [22].

Polymeric/composite heat exchangers can be a good replacement for the metallic ones, once the following criteria are met in terms of their performance. First, they are required to provide the minimum required thermo-hydraulic performance for their specific application that are designed for. Second, they must provide a structural performance which can withstand the temperature and pressure loads of their specific application. Third, the polymeric processing techniques must be exploited in such a way that manufacturability is optimised while costs are minimised.

Over the years, the heat exchanger market has focused on the development and enhancement of cross-corrugated plate heat exchangers for a wide range of applications due to their high thermal performance and compactness [139]. Until now, the cross-corrugated plates have been primarily manufactured using precious metallic materials, namely steel, copper, or aluminium for different applications such as heat recovery, air conditioning, and electronics cooling [17]. The performance of the metallic cross-corrugated plates has been extensively discussed in Chapter 2. While metallic materials remain the first choice for cross-corrugated plates, recent advances in the development of thermally enhanced polymer composites raises the possibility of lighter, more energy-efficient, mouldable polymeric cross-corrugated plates with thermal performance appropriate for commercial applications [140].

As mentioned earlier in Chapter 1, there are a very limited number of studies on polymeric cross-corrugated plates. The only available studies are Burns and Jachuck [27], Zaheed and Jachuck [16] and Zaheed-Maheswaran [51]. These studies are published by a research group in the University of Newcastle. They proposed for the first time to use PEEK (Polyetheretherketone) as an alternative to metallic materials for the construction of cross-corrugated plates in HVAC and process intensification applications. Process intensification is an approach in chemical engineering that aims for substantially smaller, cleaner, safer, and more energy-efficient design [141]. The aforementioned research group applied a film processing method to produce seven thin PEEK sheets of 13.5 cm wide by 13.5 cm long with a thickness of 100 μm (non-corrugated plate) that were subsequently corrugated and stacked into a cross flow configuration (Figure 4-1). The wall thickness of the corrugated plate was 53 μm. Moreover, they investigated the thermal and hydraulic characteristics of this heat exchanger with six fluid systems: air/air, water/water, and four thickened water systems mixed with glycerol experimentally. It was found that the constructed heat exchanger could withstand mechanical pressures up to 10 bar at atmospheric conditions. Furthermore, it provides the same thermal performance as metallic heat exchangers.

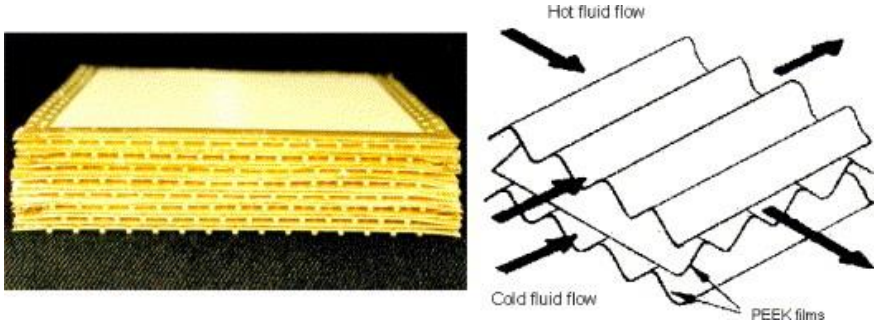

Figure 4-1. PEEK cross-corrugated plate heat exchanger proposed by Zaheed-Maheswaran [51] (colour figure available online.).

The selection of PEEK was due to its high thermal performance, its chemical, fouling and fatigue resistance, and its stability at a high working temperature (up to 220 ˚C) compared to the other polymeric materials [142]. A very thin wall was designed to enhance the thermal performance (100 μm non-corrugated plate). However, there is a trade-off between the thermal and mechanical performance. By decreasing the wall thickness, the mechanical performance decreases while the thermal performance increases. PEEK has the highest yield tensile strength among the widely used polymers in the design of heat exchangers such as Teflon or PTFE (polytetrafluoroethylene), PP (polypropylene), PE (polyethylene), PC (polycarbonate), PPS (polyphenylene sulphide), and PA6 (Polyamide) [24]. Therefore, the design of cross-corrugated plates with the other common polymeric materials cannot sustain identical mechanical pressure at such a minimal wall thickness without reinforcement [32]. Also, the high cost of PEEK and its associated processing costs indicate that PEEK may be unsuitable for low-cost applications [143]. Last but not least, manufacturing a corrugated plate with such a thin wall requires using micro-injection and micro-extrusion. In these cases, processing problems may occur because the polymer flow in microchannels is significantly different from the flow in normal size cavities. Some important properties are affected by the micro environment [144-146]. Such issues prompt the further investigation of the thermal performance of thicker walls, which require a much simpler manufacturing process. Therefore, the feasibility of the design of a polymeric triangular cross-corrugated plate heat exchanger with a thicker wall than the limit identified by Zaheed and Jachuck [16]) is investigated. This is the main objective of this thesis.

As discussed earlier, no study to date has addressed the use of alternative materials other than PEEK or alternative design parameters for cross-corrugated plate geometry. Advances in materials science and engineering have made it possible to overcome the typical limitations associated with using cheaper thermoplastics in

heat exchangers. Development of thermally enhanced polymers (composites) by the addition of suitable fillers that possess high thermal conductivity can increase the thermal and structural performance of the heat exchanger while also increasing the chemical resistance [25]. Therefore, it is interesting to investigate the thermal performance of cross-corrugated plates with composite materials to understand to which extent these materials enhance the thermal performance of cross-corrugated plate heat exchangers. This is one of the objectives of this thesis.

In this situation, the numerical approach is the most reliable to investigate the local heat transfer coefficient. Rapidly-improving CFD technology offers a numerical means to study in detail the flow and heat transfer processes that take place inside polymeric cross-corrugated heat exchangers [147]. The use of CFD offers a very detailed solution containing local values of variables that are difficult to measure, such as inner pressure and temperature. In the literature to date, there is no CFD study applied to polymeric or composite cross-corrugated heat exchangers. The aim of this Chapter is to establish an appropriate three-dimensional CFD model to obtain a detailed solution containing local values of variables that are difficult to measure, such as temperature and afterwards establish a method to analyse the flow and heat transfer characteristics of polymeric cross-corrugated heat exchangers accurately.

4.2 Methods

4.2.1 Solid and fluid materials

Depending on the application, several different polymer materials can be considered for building heat exchangers. T'Joen et al. [17] reported the merits of polymeric heat exchangers for HVAC applications. The thermal and mechanical properties and cost index of common polymers used in heat exchanger design are shown in Table 4-1 [148, 149]. The cost index is calculated based on the price per kilogram of bulk materials. As shown in Table 4-2 most polymer materials exhibit a thermal conductivity between 0.1 and 0.3 W/mK, which is two orders of magnitude lower than steel (50 W/mK) or three orders of magnitude lower than copper (400 W/mK) and aluminium (200 W/mK) [52]. The densities of these polymers are in the range of 1000–2000 kg/m^3. This is 4 to 8 times lower than steel. Moreover, their strength, stiffness, and melting temperatures are generally much lower. The low thermal conductivity of pure polymers is a major impediment to their application in heat exchangers. A description of this issue and solutions to overcome it are presented in section 4.2.2.

	Thermal Conductivity (W/mK)	Tensile strength, ultimate (MPa)	Tensile modulus (GPa)	Density (kg/m³)	Deflection temperature at 1.8 MPa, °C	Cost index
PP	0.11	36.8	1.9	937	49-60	1
PPS	0.3	86.7	3.6	1430	100-135	3
PA-6,6	0.26	73.1	2.1	1120	56-80	2
PC	0.2	64	2.3	1200	120-135	2
PTFE	0.27	33.6	0.61	2170	46	3
PEEK	0.25	110	4.5	1330	150-204	5
PFA	0.20	27	0.7	2150	48	4

Table 4-1. Thermal and mechanical properties at 25 ˚C and cost index of polymers [148]. (Cost index: 1. Less than 1.6 €/kg; 2. 1.6 - 4 €/kg; 3. 3 to 11 €/kg; 4. 10 to 25 €/kg; 5. More than 25 €/kg) [149].

Next to pure polymers, thermally enhanced polymers using fillers (composites) have been developed. Composites are made of two or more materials, commonly referred to as constituents. The constituent that is continuous and which is often, but not always, present in greatest quantity in the composite is termed the matrix. The second constituent is termed the reinforcement or filler. Fillers reinforce or improve the properties of the matrix [150]. The special chemical and physical properties of such a composite matrix shows great promise for heat exchangers to be adapted to satisfy the unique application needs [151]. Composites have thermal conductivities ranging from 1–25 $\mathrm{W/mK}$. Additionally, the thermal conductivities of composites are anisotropic, more specifically orthotropic, depending on the orientations of the fillers inside the composite matrix [23]. According to Bar-Cohen et al. [54], the anisotropic thermal conductivity of the composites is defined by a transversely isotropic thermal conductivity tensor (equation (4-1)), where $K_{11} = K_{xx} = K_{zz} = K_{33}$ correspond to in-plane thermal conductivity, and $K_{22} = K_{yy}$ corresponds to through-plane thermal conductivity.

$$[K_{ij}] = \begin{bmatrix} K_{11} & 0 & 0 \\ 0 & K_{22} & 0 \\ 0 & 0 & K_{33} \end{bmatrix}, \qquad (4\text{-}1).$$

Table 4-2 shows the orthotropic thermal conductivities of a set of commercially available composites with different matrices [152].

Vendor	Matrix	In-plane TC (W/mK)	through-plane TC (W/mK)
RTP 299 X	PA-6,6	10.01	2
RTP 399 X 137054	PC	4	0.7
RTP 4099 X 137099 D	PPA	6	1.2
RTP 1399 X 137162 E	PPS	5	1.2

Table 4-2. Orthotropic thermal conductivity of commercial composites [152].

Table 4-3 shows the thermal and mechanical properties of a set of commercially available composites. These conductivities are generally highly orthotropic, and the given figures are usually the highest directional value. These composites exhibit higher thermal and structural properties than the pure polymers [31].

Vendor	Matrix	Thermal Conductivity (W/mK)	Tensile strength, ultimate (MPa)	Tensile modulus (GPa)	Density (kg/m³)	Deflection temperature at 1.8 MPa, ˚C
Cool Polymers	PP	5	25	5.2	1380	-
Cool Polymers	PPS	20	45	13	1700	260
Sabic IP	PPS	7/2.2	139	27.6	1740	270
Sabic IP	PA-6,6	1.2	95	11.9	2004	216
Ovation Polymers	PC	6.1	59	6.9	1450	136
RTP	PPS	2.31	62	26.2	1700	260
PolyOne	PPS	10-11	100	26.2	1700	260

Table 4-3. Thermal and mechanical properties of composites [31].

In this study, air at atmospheric pressure and with constant properties is chosen as the primary and secondary flow in the cross-corrugated heat exchanger (similar to the air properties used in the simulation of the metallic cross-corrugated plate heat exchanger in section 2.2.2). The structural and chemical performance of the heat exchanger is not the subject of this study. For the thermal design of solid parts, the only important property of the solid is its thermal conductivity. Both pure polymers and composites with orthotropic thermal conductivity are considered for the solid part of the cross-corrugated plate heat exchanger in the CFD model. Through-plane thermal conductivity plays an important role in heat transfer for composite materials. Table 4-4 presents the value of thermal conductivity of solid

materials implemented in the CFD model. Both isotropic and anisotropic thermal conductivities are studied. The values for isotropic thermal conductivities are 0.2 or 0.6 W/mK, which are lower than the minimum through-plane thermal conductivity mentioned in Table 4-2. The through-plane thermal conductivity values are 0.2 or 0.6 W/mK and the in-plane thermal conductivity values are 2 or 10 W/mK for anisotropic materials. The solid materials are named based on the value of the through-plane and in-plane thermal conductivity.

Name	Through-plane TC (W/mK)	In-plane TC (W/mK)
TC 0.2	0.2	0.2
TC 0.2,2	0.2	2
TC 0.6	0.6	0.6
TC 0.6,2	0.6	2
TC 0.6,10	0.6	10

Table 4-4. Thermal conductivity associated with the solid materials implemented in the CFD model.

4.2.2 Thermal design calculations

The thermal performance of a heat exchanger is determined by its thermal conductance (UA), which gives the relation between the logarithmic mean temperature difference and the heat transfer rate.

This thermal conductance UA equation (4-2) is governed by a series of thermal resistances (Figure 4-2), namely the convective resistance on the primary fluid side (R_1), the conductive resistance over the wall which separates both fluids (R_w), and finally the convective resistance on the secondary fluid side (R_2), when the fouling resistances are neglected.

$$UA = \frac{1}{R_1 + R_w + R_2} = \frac{1}{\frac{1}{h_1 A_1} + \frac{t}{K_w A_w} + \frac{1}{h_2 A_2}}, \quad (4\text{-}2).$$

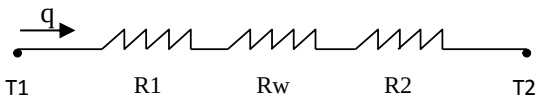

Figure 4-2. The thermal resistance network of heat transfer through a plane wall.

Thermal performance is dictated by the dominant thermal resistance. Therefore, in order to improve the thermal performance, the dominant resistance must be decreased. Typically for metallic heat exchangers, due to the very high thermal conductivity of the wall, the conductive resistance is several orders of magnitude smaller than the convective resistance and can be considered negligible. For the polymeric heat exchanger, the low wall thermal conductivity (K_w) increases the conductive resistance, creating an impact on thermal performance.

To overcome this impediment to the design of polymeric heat exchangers for a given thermal conductivity, either the wall thickness (t) needs to be decreased or the heat transfer area increased. However, there is a limitation on how far the thickness of the wall can be decreased because a very thin polymeric wall cannot typically withstand a high stress. This is the reason that Zaheed-Maheswaran [51] used PEEK material for the design of a cross-corrugated heat exchanger with a very thin wall.

4.2.2.1 Biot number analysis

It is possible to determine the significance of the conductive resistance (R_w) relative to the convective ($R_1, R_2 = R_{conv}$) resistance using a dimensionless parameter called Biot number (Bi) for heat transfer, equation (4-3). For high Biot numbers (Bi>>0.1), the conductive resistance is dominant over the convective resistance, while the convective resistance is dominant over the conductive resistance for low Biot numbers (Bi<<0.1) [110].

$$Bi = \frac{R_w}{R_{conv}} = \frac{ht}{K_w}, \qquad (4\text{-}3).$$

By assuming that the cross-corrugated plate heat exchanger is made of a polymeric wall with a thickness of 0.5 mm and a thermal conductivity of 0.2 W/mK, the Biot number for heat transfer can be calculated for different working fluids such as low pressure gases and liquids. Based on the Figure 2-20, the heat transfer coefficients of air in cross-corrugated channels with different apex angles are comprised from 34 to 139 W/m^{2}K. Also, Hesselgreaves et al. [9] stated that for the low pressure gases such as air, the heat transfer coefficients are comprised between 50 and 100 W/m^{2}K. Contrary to the low pressure gases, the heat transfer coefficients for liquids are typically comprised between 2000 and 5000 W/m^{2}K [9]. In the following paragraphs, different scenarios for the convective heat transfer coefficient of the flow on each fluid side within the aforementioned ranges for the convective heat transfer for air and liquids are considered and the relative importance of the conductive resistance compared to the convective one is assessed. For the cases where the convective heat transfer coefficients is the same on both fluid sides, due to the symmetry, the conductive resistance (equation (4-3)), is calculated based on the half of the wall thickness.

Scenario one: air is considered as the flow for hot and cold sides of the heat exchanger. For this scenario, 3 cases are defined as indicated in Table 4-5. First, the heat transfer coefficient is considered equal for both air sides (case 1-1 and case 1-2). Considering the aforementioned heat transfer coefficient range of air (34<h<139 W/m^{2}K), the calculated Biot numbers are respectively 0.0425–0.3475. This means that when the convective heat transfer coefficient is low, the conductive resistance becomes negligible compared to the convective resistance. This statement will be confirmed by the conjugate CFD study later in the section 4.4. Second, in the case 2, on one side of the flow the highest heat transfer coefficient is assigned (139 W/m^{2}K) and on the other side the lowest one (34 W/m^{2}K). The Biot numbers are respectively 0.3475 and 0.085.

	Case 1-1	Case 1-2	Case 2
Air side 1 heat transfer coefficient [W/m^{2}K]	34	139	34
Air side 2 heat transfer coefficient [W/m^{2}K]	34	139	139

Table 4-5. The different cases for the working fluids in the scenario one.

The ratios between each resistance and the total resistance for each case are shown in Figure 4-3. The wall thermal resistance varies from 2–8%. For all the cases the dominant resistance is on the air side. For the case 2, the dominant resistance is on the side 1 with the lower convective coefficient and the resistance on the side 2 is 3 times higher than the wall resistance. By increasing the heat transfer coefficient, Bi increases but it is still small and the conductive resistance can be considered as negligible.

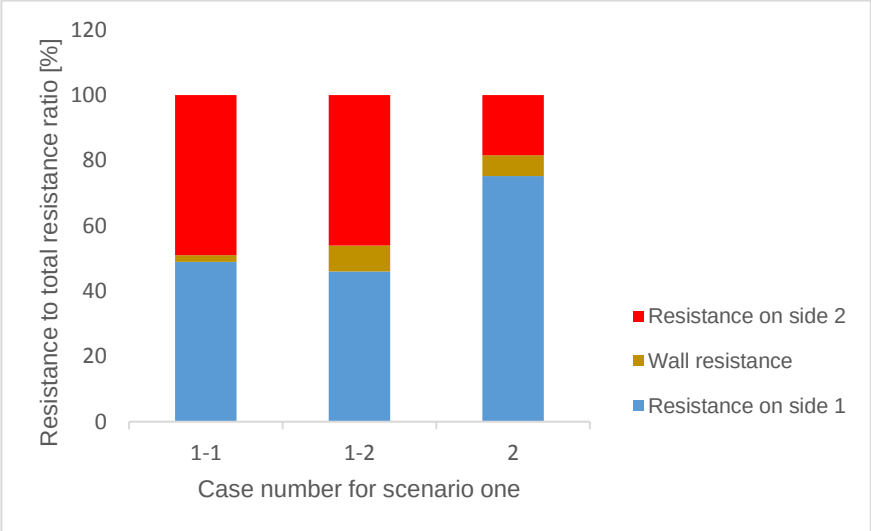

Figure 4-3. Ratio of each resistance to the total resistance for the cases described in Table 4-5.

Scenario two: liquids with the heat transfer coefficients in the range of 2000–5000 W/m^2K are considered as the working flow on both sides of the heat exchanger. For this scenario, 3 cases are considered as shown in Table 4-6.

	Case 1-1	Case 1-2	Case 2
liquid side 1 heat transfer coefficient [W/m^2K]	2000	5000	2000
Liquid side 2 heat transfer coefficient [W/m^2K]	2000	5000	5000

Table 4-6. The different cases for the working fluids in the scenario two.

By assuming the same heat transfer coefficient on both sides (case 1-1 and case 1-2), the Biots are in the range of 2.5–12.5. This means that the Biot numbers for liquids tend to be larger compared to air. The ratios between each resistance and the total resistance for each case are shown Figure 4-4. It is observed that, the conductive resistance is the dominant resistance for all the case and it varies from 55.5% to 78%. Thus, for the cases with liquids as working fluid, the conductive resistance cannot be ignored and must be included in the calculation of the thermal conductance.

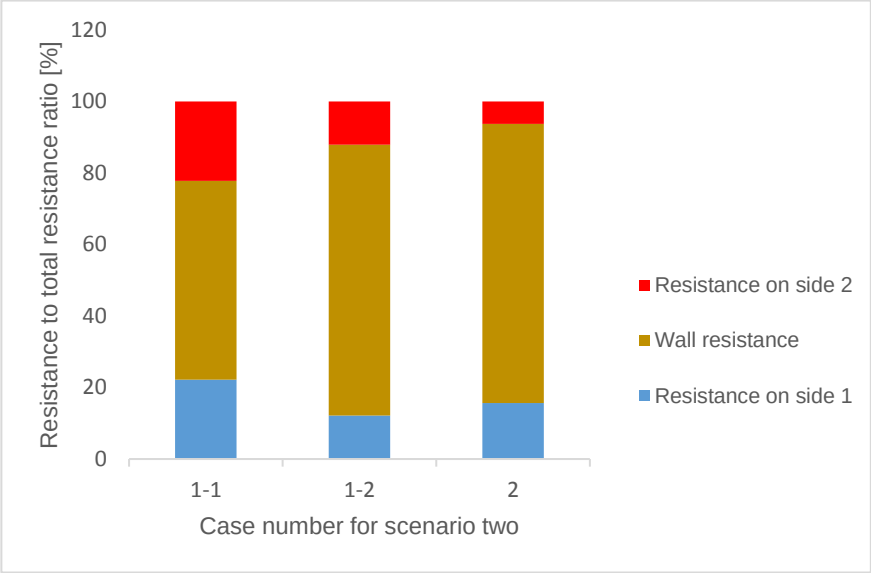

Figure 4-4. Ratio of each resistance to the total resistance for the cases described in Table 4-6.

Scenario three: on one side of the heat exchanger, air is used as the working fluid and liquids are used on the other side. For this scenario, 4 cases are considered as shown in Table 4-7.

	Case 1	Case 2	Case 3	Case 4
Air side heat transfer coefficient [W/m^{2}K]	34	34	139	139
Liquid side heat transfer coefficient [W/m^{2}K]	5000	2000	2000	5000

Table 4-7. The different cases for the working fluids in the scenario three.

The ratios between each resistance and the total resistance for each case are shown in Figure 4-5. For all the cases, the resistance on the liquid side is less than 5%, and can therefore be considered negligible. The wall thermal resistance varies from 7.7–25.3%. For the first two cases, the wall thermal resistance can be disregarded, as the resistance on the air sides are higher than 90% of the total resistance. However, in the case 3 and case 4, the wall thermal resistance must be

considered in the thermal conductance calculation as it includes approximately 25% of the total resistance.

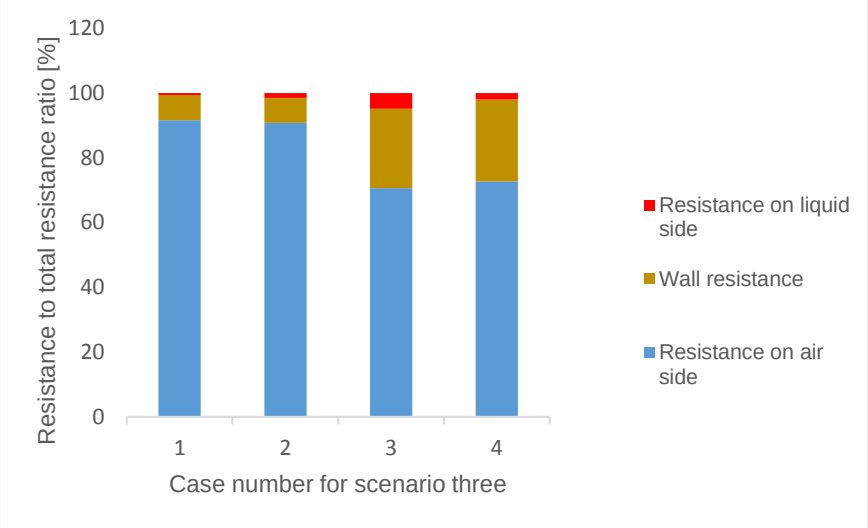

Figure 4-5. Ratio of each resistance to the total resistance for the cases described in Table 4-7.

4.2.2.2 Heat transfer coefficient calculation

Previously, in section 2.2.4, for metallic heat exchangers the reduced equation for LMTD called $LMTD_{sim}$ is used to calculate the average heat transfer coefficient. In this formula, it is assumed that the heat transfer coefficient is constant and uniform throughout the heat exchanger, also the wall temperature. Therefore, in CFD simulations the integration of the wall temperature adjacent to the fluid is assumed constant, and this constant wall temperature is implemented in the $LMTD_{sim}$ formula to calculate the average heat transfer coefficient of the heat exchanger, as it is shown in formula (2-12). However, this approach may not be valid in the case of polymeric heat exchangers, as the wall temperature may not be constant along the length of heat exchanger and consequently the heat transfer coefficient may varies along the length of heat exchanger [15]. According to Shah and Sekulic [15], where the heat transfer coefficient is not constant along the length of heat exchanger, the best way to explain the complex heat transfer phenomena is to define the local heat transfer coefficient based on Newton's law of cooling (equation (4-4)). This local heat transfer coefficient expresses the convective heat flux (area weighted averaged heat flux over the walls of each cell) per unit temperature difference (temperature potential) between the wall (T_w) and

fluid (T_{ref}) in each repetitive cell of the heat exchanger. A schematic view of a channel of the heat exchanger with several repetitive cells are shown in Figure 4-6.

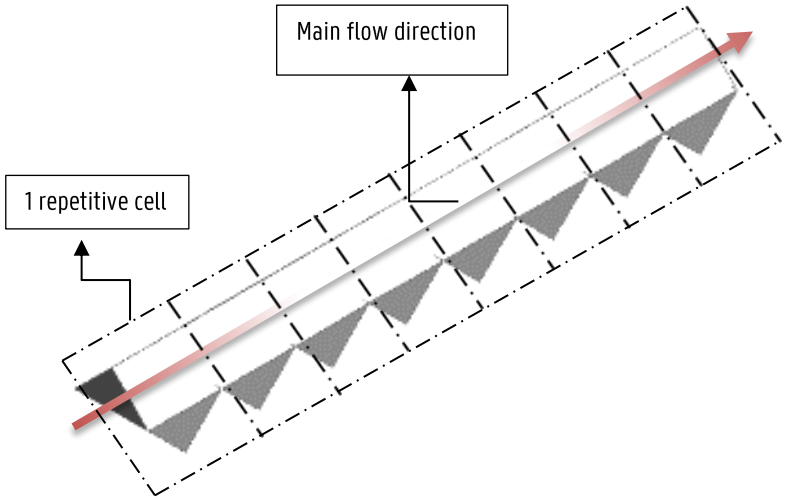

Figure 4-6. A schematic view of a channel of the heat exchanger with several repetitive cells including the control volume for calculation of local heat transfer coefficient in each cell.

$$q = h(T_w - T_{ref}),$$

(4-4).

The wall temperature (T_w) is the area weighted average temperature on the wall surfaces (A) of each repetitive cell.

The best choice for temperature reference (T_{ref}) depends on the application in question. For external flows such as a flow over a flat plate, the free stream temperature is used as a reference temperature and the reference temperature for internal flows is the local bulk temperature (T_b). The bulk fluid temperature is the mixed mean temperature over a minimum flow section in each repetitive cell.

Therefore, for the purpose of this study, a better-suited alternative for the calculation of the average heat transfer coefficient of the whole channel is to first determine the local heat transfer coefficients for each cell (equation (4-5)) and then average them out over the entire cells (equation (4-6)) [15]. In this thesis, we call this procedure, average of local heat transfer coefficients. The local heat transfer coefficient ($h(x^*)$) is calculated for each repetitive cell based on the local bulk temperature (mixed mean temperature over a minimum flow section in each repetitive cell) and local wall temperature (area weighted average temperature on the wall surfaces) of each repetitive cell. In the following equations, $x^*$is the dimensionless coordinate along the main flow direction, N is the number of repetitive cells and L is length of full channel. From now on in this chapter, the average heat transfer coefficient $\bar{h}$ is simply written as heat transfer coefficient (h). The local heat transfer coefficient in each repetitive cell is explicitly called local heat transfer coefficient.

$$h(x^*) = \frac{q_w}{T_w(x^*) - T_b(x^*)},$$

(4-5).

$$\bar{h} = \frac{\sum_0^1 h(x^*)}{N},$$

(4-6).

$$x^* = \frac{x - x_{leadingedge}}{L},$$

(4-7).

4.2.3 Computational domain and boundary conditions

Two geometries are considered as the computational domain for the conjugate heat transfer simulations in a cross-corrugated heat exchanger. Depending on the shape of the mould used during the manufacturing process, the corrugation shape can be sharp (triangular shape) or smooth (sinusoidal curve). Kanaris et al. [153] have proven that the shape of the corrugation profile only influences the pressure drop, not the heat transfer. Therefore, in order to minimise complexity, the triangular corrugation was chosen.

Previously, in section 2.2.1, the geometric parameters and the flow directions for cross-corrugated plates with triangular corrugation were defined in Figure 2-2. Two sets of corrugation parameters are considered for the simulations. For both

sets, the corrugation angle is 90° and the aspect ratio is 2 (apex angle of 90°). For the set that is used for the experimental validation of the CFD model, the corrugation base (B) is 2 mm and the thickness is 0.053 mm. For the other set, the base is 5 mm and the thickness is set to 0.5 mm.

The first geometry (Geometry1) is a periodic unitary cell as shown in Figure 4-7. It is similar to the unitary cell considered in Chapter 2, while the solid part is included.

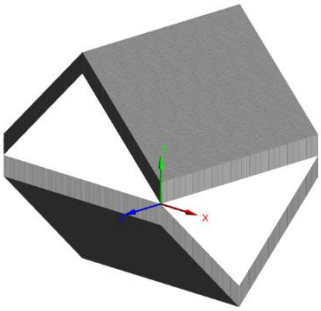

Figure 4-7. A periodic unitary cell with solid (Geometry1).

The boundary conditions for a unitary cell without solid walls are explained in Chapter 2, section 2.2.2. Here, the same boundary conditions are applied. However, by adding the solid wall to the model, the coupled wall boundary conditions are imposed at the interface between the solid and fluid.

The second geometry (Geometry2), is shown in Figure 4-8. This is representative of the entire heat exchanger, considering both cold and hot flows. In general, a heat exchanger consists of several plates stacked on top of each other (Figure 2-1). Each channel consists of several repetitive cells with the same length. However, it is very expensive in terms of calculation time to consider all of these stacked plates in the computational domain. Therefore, the periodicity in vertical direction (Y axes) is used to capture the flow and heat transfer characteristics at the core of the heat exchanger. In order to reach this goal, only the hot and cold channels (one layer of each) in the core of the heat exchanger are simulated. Three stacked plates are considered in the computational domain. The periodic boundary conditions at half of the wall thickness of the top and bottom plate are applied ('periodic BC at half thickness of solid wall'). Essentially, the wall thicknesses of the top and bottom plates are half the value of the wall thickness of the middle plate. The length of each channel is seven times longer than the base of a unitary cell. This is similar to the length of the heat exchanger designed by Zaheed-Maheswaran [51].

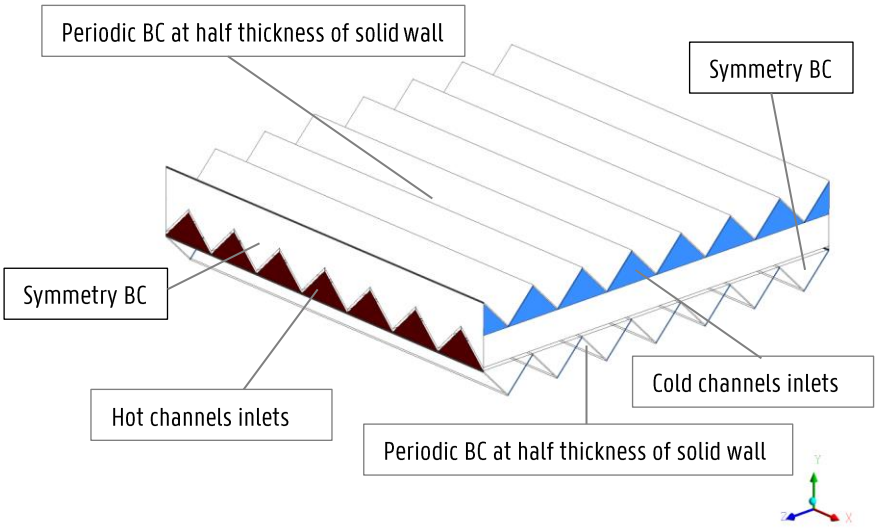

Figure 4-8. A representative of the HEX with hot and cold channels (Geometry2).

At the inlets of the channels, a uniform velocity with a constant temperature is imposed. At the outlets of the channels, the atmospheric pressure is applied. The 'coupled wall boundary conditions' are applied at the interface of the solids and fluids. This requires the heat flux and temperature to be continuous at the interface. Furthermore, the flow velocity at the interface is equal to zero. The normal velocity components are set to zero at the lateral boundaries of each domain and the normal component of the gradient of all scalar quantities is also set equal to zero. This implies no flow and no flux across the boundaries ('symmetry BC').

The meshing method explained in section 2.2.6 is used for meshing both of the computational domains with bases of 2 and 5 mm. For both geometries, the element size described in section 2.2.6 is used. The number of elements for Geometry1 and Geometry2 with a base of 5 mm are 1.5 million and 24.38 million, respectively. The GCI and the relative errors for a base of 5 mm are calculated in section 2.2.6. For geometries with a base of 2 mm, the number of elements for Geometry1 and Geometry2 are 1.2 million and 17.5 million, respectively. The GCI for heat transfer coefficients and friction factors for the highest Reynolds number used in this study are respectively 2.23% and 4.3%.

4.2.4 Conjugate Heat Transfer CFD Model

The steady-state three-dimensional numerical simulations of flow and combined convection-conduction heat transfer in the corrugated channel are obtained with the aid of the commercial CFD code FLUENT 16.2. In Chapter 2, the flow phenomena and the convection heat transfer problem are explained in detail. As discussed in section 2.2.5, the RSM turbulence model is chosen as the flow solver. The conduction heat transfer is described by Fourier's law defining the conductive heat flux where q is proportional to the temperature gradient, as shown in the equation below

$$q_{w_i} = -K_{ij} \frac{\partial T}{\partial x_j}$$

(4-8).

As explained in section 4.2.1, the thermal conductivities for the composites are defined by equation (4-1).

4.3 Choice of Computational Domain

4.3.1 Conjugate heat transfer CFD model validation

In order to validate the CFD model, a one-on-one comparison of the simulation data with the available experimental data is necessary [77]. For this purpose, the numerical data for the two computational domains are compared with the experimental work of Zaheed-Maheswaran [51].

4.3.1.1 Experimental study details

As previously mentioned, the experimental work of Zaheed-Maheswaran [51] is the only available report on the heat transfer and pressure drop characteristics of a polymeric cross-corrugated heat exchanger with wavy corrugation. The corrugation width is 2 mm, the corrugation height is 1 mm, and the wall thickness is 0.053 mm (0.1 mm for non-corrugated plate). The length of the heat exchanger is 13.5 mm. The corrugation angle is 90˚. The corrugation width is considered as hydraulic diameter. The flow system is air/air and the solid material is pure PEEK. Moreover, Zaheed-Maheswaran [51] reports that the experimental error on the calculated h and f are respectively 10% and 13% based on an uncertainty analysis [154]. The *Re* for the aforementioned experimental study is in the range of 510–2370. The author calculated the average heat transfer coefficient based on the ε-NTU method and no data is reported regarding the local values. As discussed

earlier in section 4.2.2.2, in this approach it is ideal that the heat transfer coefficient is constant and uniform throughout the heat exchanger. However, for the sake of the validation of the CFD simulations with the experimental work, the average heat transfer coefficient is also calculated using this approach.

The air properties in the experimental study are described in Table 4-8. These properties are used only to validate the CFD models with the experimental study. For the rest of the simulations, the constant air properties mentioned in section 2.2.2 are used.

ρ (kg/m3)	cp (J/kg K)	K (W/m K)	μ (kg/m s)	Pr
1.29	1047	0.05	3.15e-5	0.7

Table 4-8. Air properties for experimental study.

4.3.1.2 Pressure drop comparison

In Figure 4-9, the friction factor is calculated based on the conjugate heat transfer CFD simulations using both computational domains (Geometry1 and Geometry2) discussed in section 4.2.3. These friction factors are plotted next to the those reported for the experimental work of Zaheed-Maheswaran [51]. The circle and triangle symbols represent the CFD simulations with Geometry2 and Geometry1, respectively, and the square symbols represent the experimental data. The uncertainty errors are indicated on the experimental data. As shown, the simulated results agree well with the experimental results within the examined uncertainty range. Moreover, the friction factors calculated for the two computational domains are in a very good agreement, with less than 4% deviation. This is lower than the GCI, which is 4.3%. This indicates that the fully developed condition for the velocity profile is achieved in the CFD model with Geometry2. Therefore, the model using Geometry1 is able to predict the friction factor correctly, and is faster than the other model in terms of computational time. It is noted that the model using Geometry1 systematically predicts a lower friction than the model using Geometry2. This is understandable considering that the periodic boundary condition is explicitly imposed at the inlet and outlet of the domain of the model using Geometry1. With imposing this boundary condition, it is assumed that the heat exchanger is long enough, and the entrance effect does not have influence on the flow and heat transfer characteristics. It is well known that the entrance effect increases the friction and heat transfer characteristics. Therefore, as in the model using Geometry2, the channel has an entrance region, the entrance effect can lead to a slightly higher pressure drop.

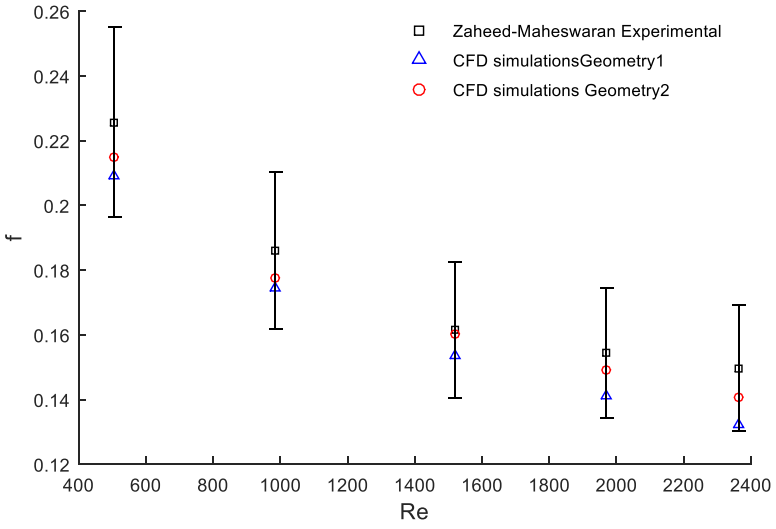

*Figure 4-9. Friction factor (**f**) comparison between CFD and experimental results of Zaheed-Maheswaran [51].*

4.3.1.3 Heat transfer coefficient comparison

In Figure 4-10, the heat transfer coefficients obtained from the simulations and experimental results are depicted. As mentioned earlier, the average heat transfer coefficient is calculated based on $LMTD_{sim}$ formula, where the wall temperature is averaged out over the full channel surface.

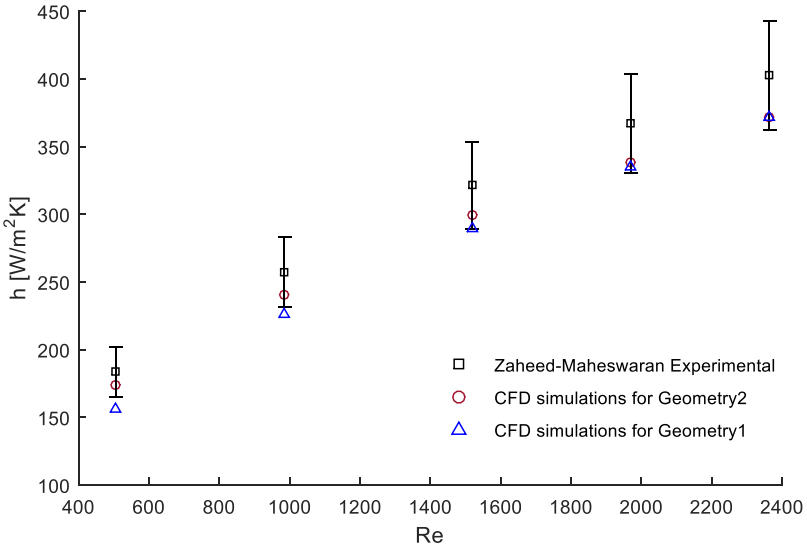

*Figure 4-10. Heat transfer coefficient (**h**) comparison between CFD and experimental results of Zaheed-Maheswaran [51].*

As shown, the CFD results using Geometry2 and the experimental results are in very good agreement, with deviations between 1.25 and 4.24 %. The CFD results using Geometry1 are in agreement with the experimental results and the other CFD model only at the higher *Re* (2370 and 1970). The deviations between the CFD results using Geometry1 from the experimental results and other CFD model depend on *Re*. The deviations compared to the experimental results are 14%, 13%, 11%, 9% and 8% for *Re* of 510, 987, 1525, 1970 and 2370, respectively. The CFD model using Geometry1 compared to the model using Geometry2 underpredicts the heat transfer coefficient with the respective deviations of 14%, 10%, 7%, 5% and 4%. Especially at the higher *Re*, these deviations are much higher than the GCI error for the heat transfer coefficient (2.23%). It seems that by increasing *Re*, the CFD results using Geometry1 are converging towards both the CFD results using Geometry2 and the experimental results. The possible reasons for these discrepancies are investigated in the following sections.

4.3.2 Temperature and velocity distribution in the middle channel

The first hypothesis to test is that the temperature profile is not fully developed. Zaheed and Jachuck [16] mentioned that the reason for the high heat transfer coefficient in this heat exchanger at low *Re* (laminar flow) is that the flow is still developing due to the short length of the heat exchanger. It is well known that the average heat transfer coefficient for a developing flow is higher than for a fully developed flow. However, as discussed in Chapter 2, the flow is periodic in this heat exchanger. According to Shah and Sekulic [15], for the periodic flow, the conventional definition of fully developed laminar or turbulent flow does not exist and sufficiently downstream of the heat exchanger, the velocity and dimensionless temperature profiles are invariant (previously discussed in section 2.2.1). Usually, depending on the geometry, after 2–8 repetitions the periodic conditions for thermal and hydraulic characteristics are achieved [15]. Earlier, in section 2.3.1, it is shown that after 5 repetitions (5 cells), the Nusselt number and friction factor remain constant. Therefore, in the CFD model using Geometry1, the flow is assumed to be periodic for the whole range of *Re*. This assumption is applied in the model by imposing the periodic boundary conditions at the inlet and outlet. Moreover, it is seen in Figure 4-9 that the results for the friction factors calculated based on Geometry1 and Geometry2 are in a good agreement (less than 4% deviation). This confirms that the velocity profile is periodic. As for air, the Prandtl number is less than 1. It is expected that for Geometry2, the temperature profile repeats after 5 cells and the average heat transfer coefficient for Geometry1 and Geometry2 are in agreement for all ranges of *Re*. More insights can be gained by analysing the local heat transfer coefficient along the length of heat exchanger, as well as the temperature and velocity distributions along the flow length at the core of the heat exchanger.

The cross section of velocity and temperature contours from across the middle hot channel of Geometry2 are shown in Figure 4-11 and Figure 4-12 for the lowest and highest *Re* (510 and 2370), respectively. Note that in Figure 4-11 the velocity is zero on the solid parts shown in grey. It is observed that for both *Re*, the velocity profiles are periodic. This confirms the earlier finding that the friction factors derived from both computational domains are in agreement.

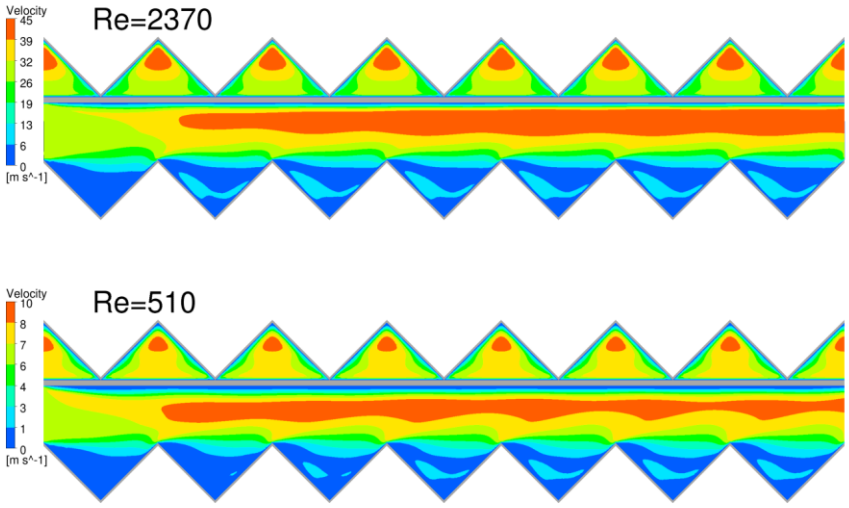

Figure 4-11. Cross section of velocity contours across the middle hot channel centre plane for Re=510 and 2370.

By inspecting the temperature contours (Figure 4-12), it is seen that the temperature component also possesses a periodic nature. Therefore, it is expected that the values of the heat transfer coefficient calculated from Geometry1 are in agreement with the ones calculated from Geometry2, as this is the case for the friction factor. The temperature profile on the wall adjacent to the fluid is not uniform. To further study this, the local wall temperatures adjacent to the fluid along the length of the channel for all *Re* are plotted in Figure 4-13. The local wall temperature refers to the average wall temperature adjacent to the fluid over the wall surfaces of each repetitive cell.

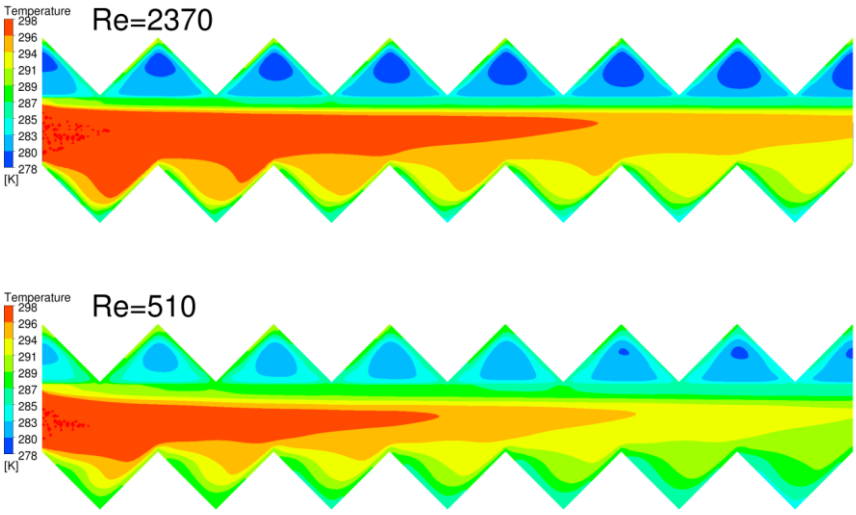

Figure 4-12. Cross section of temperature contours across the middle hot channel centre plane for Re=510 and 2370.

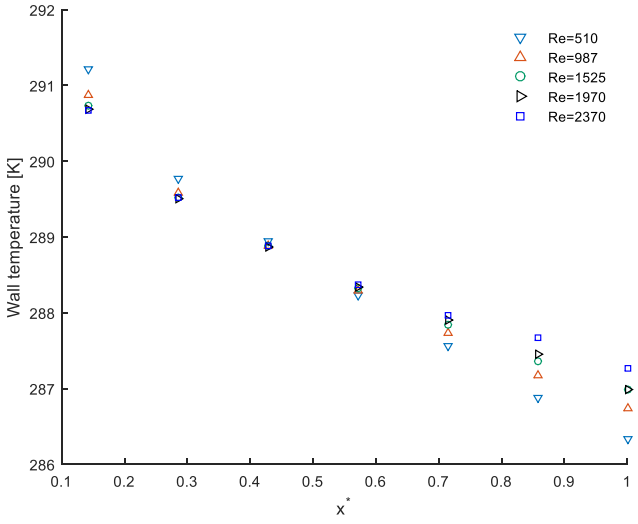

Figure 4-13. Local wall temperatures adjacent to fluid along the flow length for all Re.

As shown, for the lowest *Re* of 510, the wall temperature adjacent to the fluid changes from 291 K at the beginning of the channel (cell 1) to 286 K at the outlet of the channel (cell 7). For a Reynolds number of 2370, the change in temperature between cell 1 and cell 7 is around 3 K. It stands to reason that by increasing the Reynolds number, the intense mixing of the fluid particles enhances the heat and momentum transfer between fluid particles and reduces the temperature gradient in the flow field along the wall. For the lowest *Re* of 510 and the highest *Re* of 2370, the vorticity magnitudes along the flow direction in the channel are 15387 1/s and 75917 1/s, respectively.

Therefore, it is also interesting to look at the local heat transfer coefficients along the flow length and investigate the influence of the non-uniformity of wall temperature adjacent to the fluid on the local heat transfer coefficients.

It is worthwhile to mention that the change in temperature through the wall is negligible (approximately 0.5K) as the thickness of the wall is 0.053 mm. This is observed by zooming in on the temperature contour plots of the last cells (Figure 4-12) shown in Figure 4-14 and Figure 4-15. The conductive resistance is 0.007% of the total resistance and the convective resistance on each fluid side is 49.99%. This demonstrates that the total heat transfer in the heat exchanger is dominated by the convention phenomena.

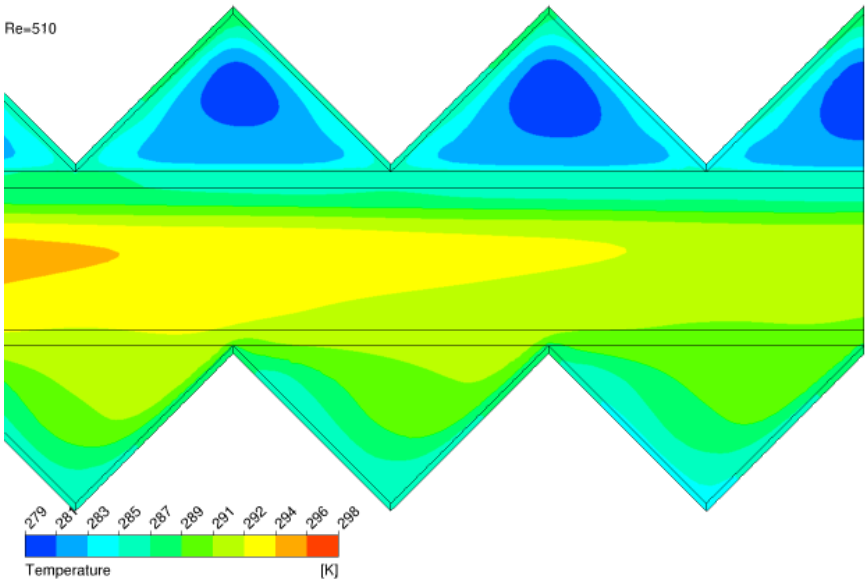

Figure 4-14. Zoomed in temperature through the wall for Re=510.

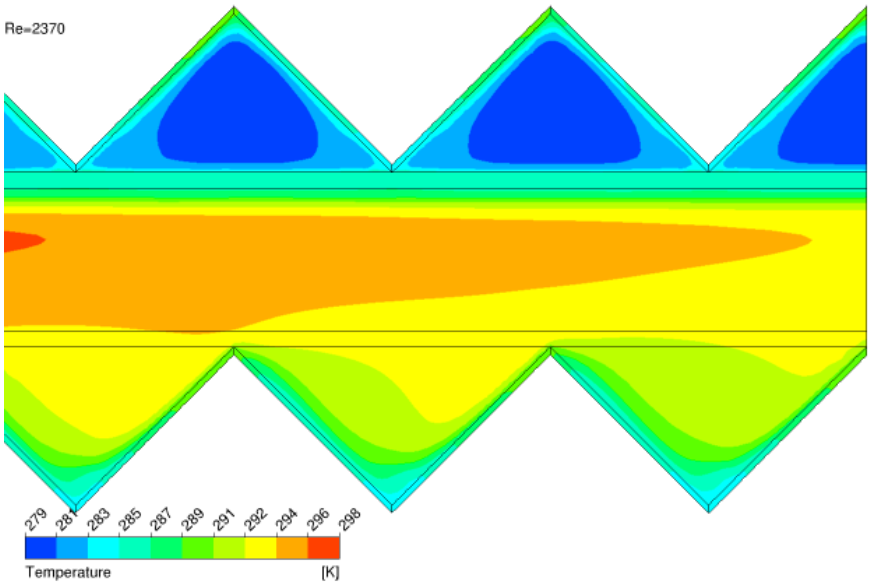

Figure 4-15. Zoomed in temperature through the wall for Re=2370.

4.3.3 Local heat transfer coefficients in the middle channel

As explained in section 4.2.2.2, the best approach to determining the average heat transfer coefficient in a channel with non-uniform wall temperature is to average the local heat transfer coefficients. For each *Re*, the local heat transfer coefficients for each repetitive cell are determined based on Geometry2 simulations along the flow length (different symbols) and their averaged heat transfer coefficient (solid lines) are plotted in Figure 4-16 (equations (4-5) to ((4-7)). The average heat transfer coefficients determined using Geometry1 are represented using dashed lines.

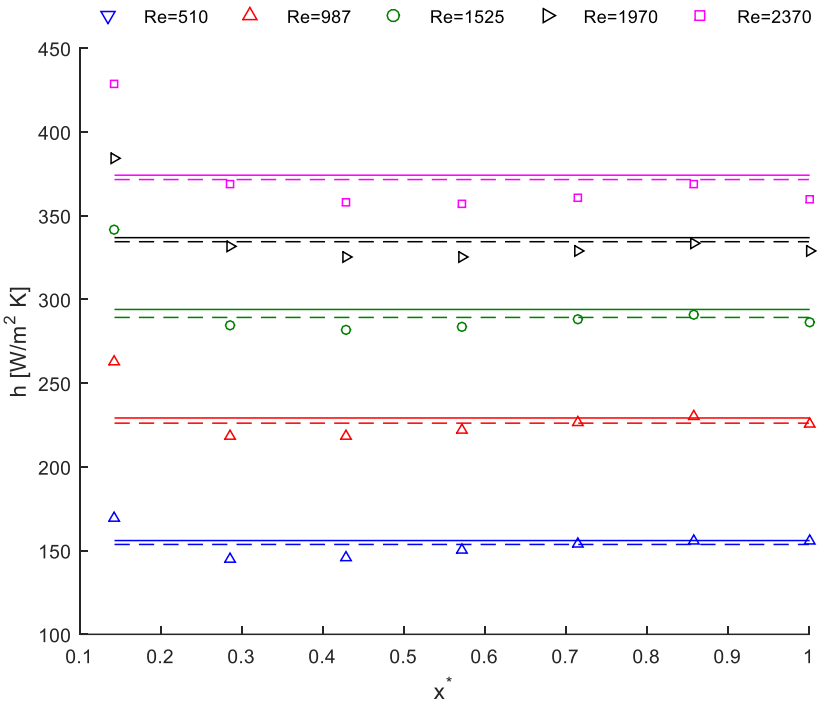

Figure 4-16. Local heat transfer coefficients along the flow length (symbols) and their averaged-out heat transfer coefficient calculated using Geometry2 (solid lines) and the heat transfer coefficient calculated using Geometry1 (dashed lines) - polymeric materials.

It is observed that after a few cells, the local heat transfer coefficients approach a constant value for the entire Reynolds number range. This confirms that the heat transfer coefficient also has a periodic nature. Moreover, the average heat transfer coefficients for the whole range of *Re* determined by averaging the local values (solid lines) are in agreement with the heat transfer coefficients calculated using Geometry1 with a maximum deviation of 1.7%, which is smaller than the GCI error for the heat transfer coefficient.

As observed earlier in Figure 4-10, by increasing the Reynolds number, the deviations between the results of the simulations with Geometry1 and the results derived using $LMTD_{sim}$ formula (Geometry2 and experiment) are reduced. This is due to the fact that by increasing *Re*, the temperature change along the wall decreases or the wall temperature approaches more uniformity due to turbulent mixing.

4.4 Composite Materials and Wall Thickness

The earlier results comparing the two CFD models utilizing different computational domains (Geometry1 and Geometry2) indicate that the CFD model that utilizes Geometry1 is a computationally cost-effective model for the prediction of the average heat transfer coefficient and friction factor in cross-corrugated plates with polymeric materials. Therefore, in this section, the CFD model with Geometry1 is used to investigate the influence of different thermal conductivities and wall thicknesses on the heat transfer coefficient of a heat exchanger with a specific Reynolds number. As the Reynolds number is the same for all simulations, the same meshing method and element size are used to eliminate the error caused by different meshes. The corrugation base is set at 5 mm for all cases. The solid wall thickness is set to 0.053 or 0.5 mm.

The heat transfer coefficient results from the simulation of different wall thicknesses and thermal conductivities are plotted in Figure 4-17. It is observed that for a very thin wall (0.053mm), improving the thermal conductivity of polymer materials will not contribute further to a higher heat transfer coefficient. The heat transfer coefficient of the composite heat exchanger named TC 0.6,10 is higher than that of the pure polymeric heat exchanger (TC 0.2) by 0.3%, which is negligible. By increasing the wall thickness of the heat exchanger by a factor of approximately 10 (from 0.053 to 0.5 mm), the influence of thermal conductivity on the heat transfer becomes slightly more noticeable. For a wall thickness of 0.5 mm, enhancing the thermal conductivity of the heat exchanger from TC 0.6,10 to TC 0.2 only improves the thermal performance by 1.3%. These results indicate that increases in thermal conductivity do not significantly improve heat exchanger thermal performance since the controlling resistance for heat transfer becomes the air-side convection resistance. It should be noted that this conclusion concerning the relative importance of wall material thermal conductivity and the convective heat transfer coefficient is dependent upon the geometry and the fluid.

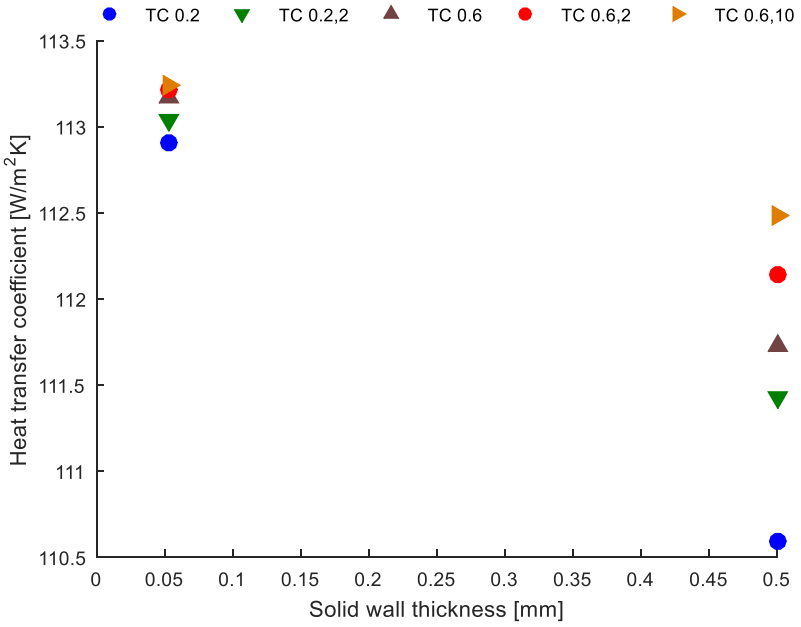

Figure 4-17. Heat transfer coefficients calculated based on different wall thickness and thermal conductivity.

The convective thermal resistances on both fluid sides and the conductive thermal resistance for the model with metallic material and polymeric material with the worst-case thermal conductivity are illustrated in Figure 4-18. For the model with metallic material, a TC of 200 W/mK and a wall thickness of 0.5 mm are considered. A thermal conductivity of 0.2 W/mK and a wall thickness of 0.5 and 0.053 mm are set for the model with polymeric material. As the same mass flow rate is imposed for both primary and secondary flows, the same convective resistance is achieved. It is seen that by increasing the wall thickness for the composite materials, the conductive resistance rises from 0.73% to 6.7%. Decreasing the thermal conductivity changes the conductive resistance from 0.007% to 0.73%. However, the convective resistance is dominant for all cases and it determines the overall thermal performance (UA).

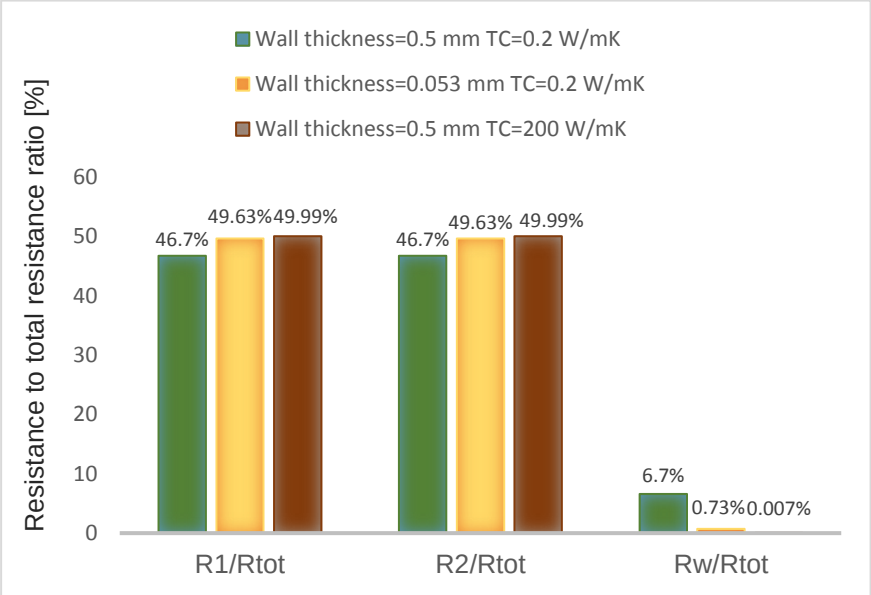

Figure 4-18. Resistance to total resistance ratio for different wall and thermal conductivity.

In conclusion, in order to design the cross-corrugated plates from polymeric materials for low *Re* applications, the following considerations and steps are necessary.

As far as the HVAC applications with working fluids of air are concerned, the dominant resistance is on the air side, therefore application of a very thin wall (for example 0.053 mm) is not necessary. This finding is confirmed by other authors for other types of heat exchangers [155, 156]. As explained earlier, the higher wall thickness contributes to the higher structural performance. Moreover, the fabrication of cross-corrugated plates with higher thickness using conventional extrusion techniques and tools is easier than the thin film processing. If the wall thickness of a cross-corrugated heat exchanger increases from 0.053 mm to 0.5 mm, depending on the thermal conductivity of the material (Table 4-4) the thermal performance will decrease by 2% for the lowest wall thermal conductivity (TC 0.2) and 0.3% for the best thermal conductivity (TC 0.6,10). Therefore, if the wall thickness is within such an interval, it is not necessary to use composite materials to improve the thermal performance as the pure polymers provides almost the same thermal performance. The cost calculation of heat exchangers built from composite materials is complex, and a detailed analysis of this is beyond the scope of this work. However, it should be noted that the addition of thermally conductive fillers in composite materials can increase the cost of manufacturing significantly,

while fabricating a heat exchanger from pure polymeric materials can reduce the cost [17]. Moreover, as the influence of the composite materials on thermal performance for the proposed design is negligible, they should be considered only if they contribute to the structural performance of the heat exchanger.

In order to calculate the thermal performance of the heat exchanger, both CFD models proposed in the section of 4.2.3 can be used. If the average heat transfer coefficient is the value of interest for the periodic flow, considering the number of grids that are used in the CFD models of Geometry1 and Geometry2, the CFD model using Geometry1 provides more cost-effective solution in terms of calculation time. The number of elements of Geometry1 is approximately 17 times lower than that of Geometry2. However, if the local heat transfer characteristics and wall temperature are the subjects of interest or the flow is not fully developed, then the computational model with Geometry2 provides the best solution. And yet, the implementation of the periodic boundary condition on the half thickness of the solid walls leads to less computational time when compared to a domain with several stacked layers. Moreover, if the CFD model using Geometry2 is used to solve the temperature and heat flux field, the average heat transfer coefficient must be calculated by averaging of local heat transfer coefficients as explained in section 4.2.2.2 instead of the $LMTD_{sim}$ formula. The reason is to include the influence of temperature gradient over the wall adjacent to the fluid in the average heat transfer calculation. It is concluded that the average heat transfer coefficient value calculated from the $LMTD_{sim}$ formula (equation (2-12)) which have the constant integration of wall temperature assumption, is artificially higher than the value calculated by averaging the local heat transfer coefficient in this study specifically at lower *Re* (Figure 4-10) for the polymeric cross-corrugated plate heat exchangers. As explained earlier, for the average heat transfer calculation, the deviation between the $LMTD_{sim}$ formula values and the values obtained from the procedure of calculating the average heat transfer coefficient by averaging the local heat transfer coefficient (introduced in section 4.2.2.2) are 14%, 10%, 7%, 5% and 4% for *Re* of 510, 987, 1525, 1970 and 2370 respectively.

4.5 Summary

In this chapter, the combined convection-conduction (conjugate) heat transfer problems on cross-corrugated plates is studied with the aid of CFD. This CFD model specifically takes into account the thermal properties of the heat exchanger material (pure polymer and composite). The feasibility of the application of the CFD model to solve the flow and conjugate heat transfer problems of polymeric cross-corrugated heat exchangers is validated against experimental results. The choice of two different computational domains for the CFD model and their advantages are discussed. It is found that the wall temperature distribution is not uniform specifically at lower Reynolds number for the polymeric heat exchanger. Therefore, the constant wall temperature assumption in the $LMTD_{sim}$ formula overpredict the heat transfer coefficients in this study specifically at lower *Re* for the polymeric cross-corrugated plate heat exchangers. This study appears to provide the first reported data set on the wall temperature distribution along the flow length and the local heat transfer coefficients of polymeric cross-corrugated heat exchangers. The thermal performance of a new polymeric cross-corrugated heat exchanger designed to be thermally competitive with a metallic one at the component level is studied. Furthermore, the influence of wall thickness and thermal conductivity on thermal performance are investigated. In conclusion, the new design for a polymeric cross-corrugated heat exchanger has great potential to replace the metallic cross-corrugate for a wide range of applications due to its advantages regarding fouling, corrosion, and manufacturing cost. The proposed CFD model is able to accurately predict the performance of this type of geometries composed of polymeric material. However, it should be ensured that for each specific application the structural performance, cost analysis of composite materials and material performance in terms of permeability and absorption are coupled with the proposed CFD thermal model.

5

Conclusions and Future Recommendations

5.1 Conclusions

The main objective of this work is to predict the thermal hydraulic performance of cross-corrugated plate heat exchangers fabricated from polymeric/composite materials using numerical method. Due to the low thermal conductivity of polymeric/composite compounds, the combined conduction-convection problems are solved using the three-dimensional CFD model. However, in order to achieve the main objective, first a better understanding of the convection problem in this geometry is necessary. This is another objective of this doctoral work. Moreover, the influences of the geometrical parameters, more specifically channel aspect ratio (for triangular corrugation profile is equal to the apex angle) on the thermal hydraulic performance of cross-corrugated plate heat exchangers.

First, a simplified CFD model is developed to only solve the convection problem with the assumption that the heat exchanger is built from metallic materials with high thermal conductivity. Thanks to this CFD model a thorough numerical study of convection heat transfer and flow phenomena governing the performance of triangular cross-corrugated heat exchangers with a large range of apex angles (45–150°) is conducted. In order to isolate the heat transfer problem to convection phenomena, it is assumed that the heat exchanger is made of metallic materials. The accuracy of the numerical results based on a steady-state laminar model and

RSM are examined by the available experimental and numerical correlations for a triangular cross-corrugated plate with the apex angles of 90° and 60°. It is shown that for the considered range of *Re* (310–2064), the steady-state laminar model fails to provide accurate Nu behaviour. The RSM model gives rise to a power law relationship between Nu and *Re* which is in agreement with the experimental results (less than 5% deviation) and numerical correlations (maximum deviation: 2.82%). The deviation between the numerical and experimental results is less than the uncertainty of experimental measurements. Moreover, it is proven that the use of a periodic unitary cell as the computational domain instead of a long channel with several cells is appropriate for the convection heat transfer problem. The results for both computational domains (periodic unitary cell and long channel) are found to be in very good agreement. The maximum deviation for Nu is 0.5% and for f is 0.02%. However, the mesh size for the long channel is approximately eight times larger than that of the periodic unitary cell. Therefore, the results of the periodic unitary cell have been investigated for the convection heat transfer problem.

Second, several three-dimensional steady-state simulations are carried out using the RSM model in order to investigate the influence of the apex angle on the convection heat transfer and flow characteristics. It is found that the increase of the apex angle from 45° to 150° results in the growth of the pressure drop and the heat transfer coefficient. This is due to the increase of the vorticity magnitude along the flow direction, as well as the pressure force. Contrary to pipe flow, the pressure force is the dominant force. Moreover, the thickness of the thermal boundary layer decreases in both the upper wall and in the troughs of the lower one, while the temperature gradient increases near the wall. The highest pressure drop and heat transfer coefficient are related to an apex angle of 150°, while the lowest ones are found at an angle of 45°.

The influence of the apex angle on the friction factor and the Colburn j factor follows two distinct trends. The first trend is related to the angle interval of 45–90° (100°), within which an increase in the apex angle causes the friction factor and the Colburn j factor to grow. The second one is associated with the larger angles between 90° (100°) and 150°, where an increase in the apex angle causes the friction factor and the Colburn j factor to decrease. Even though the heat transfer rate grows due to the change in thermal boundary layer thickness, as the channel gets smaller, the mass flowrate increases as well. This is associated with the complexity of the recirculation zones in the lower plate and the alteration of the turbulence intensity. It is observed that for an angle of 120°, only one recirculation zone appears, while two recirculation zones are present for the angles in the first trend. By increasing the angle in the first trend, the turbulence intensity increases and thus f increases as well. However, in the second trend, even though the

vorticity magnitude increases, the turbulence intensity decays resulting in lower f. The complexity of the recirculation zones is linked to the pressure force. It is observed that the rate at which the pressure force increases is not linear and thus the variation of pressure force with respect to the angle is fitted by a polynomial function. The critical point of this function is found to be around an angle of 100°, which is the angle with the peak turbulence intensity. The variation of the viscous force caused by increasing the angle up to 100° is negligible. Conversely, in the second trend, the growth rate of the viscous force is increased significantly by 49%. Hence the ratio between pressure and viscous forces decays after angle 100°, resulting in a smaller recirculation zone and lower turbulence intensity. Therefore, it is concluded that the apex angles around 90–100° are the transitional angles for the flow pattern, the trend of the turbulence intensity, and the corresponding forces (i.e. pressure and viscous forces). Around this range of angle, the highest friction factor and the Colburn j are observed. The minimum j and f are observed at the angle of 150° which are respectively 36% and 70% lower than the maximum for *Re*=1370. This shows that in the second trend, increasing the apex angle has stronger influence on f than on j.

Third, the heat exchanger with an apex angle of 150° is found to have the highest performance according to the comprehensive evaluation criteria introduced by Cowell [42]. This is because the relative volume required for this heat exchanger is the minimum for the given pumping power and heat transfer rate. It is important to note that the thermo-hydraulic performance monotonically increases as the apex angle is increased. This is in line with the earlier conclusion that in the second trend (90–150°), as the apex angle increases, f decreases at a higher rate compared to j.

Fourth, a generalized correlation for Nu and f as a function of *Re* and apex angle are developed. The deviations of the simulation and predicted value from the generalized correlations for Nu and f are 13% and 11.7%, respectively. Moreover, more accurate correlations for Nu and f as a function of *Re* for each apex angle are proposed. The maximum deviations between the specific correlation for each apex angle and the simulation data for Nu and f are 0.84% and 4%, respectively.

The aforementioned findings and the CFD model for the convection problem can contribute significantly to the work of heat exchanger designer and manufacturer of cross-corrugated plate heat exchangers for low Reynolds applications, such as HVAC applications and in compressed air systems. This extensive analysis and correlations allow the designer predict the thermal hydraulic performance accurately to avoid the over sizing mistake which can lead to the financial and energy loss.

Once the convection problem is fully understood in cross-corrugated plate heat exchangers, the combined convection-conduction (conjugate) heat transfer problems on cross-corrugated plates is solved with the aid of CFD. It is assumed that the heat exchanger is made of polymeric materials. The influence of two different computational domains and boundary conditions named Geometry1 (a unitary cell with solid wall) and Geometry2 (consisting of several hot and cold channels) on the heat and flow characteristics are studied. The two aforementioned computational domains are explained in detail in section 4.2.3. The results of friction factor and heat transfer coefficient calculated based on the conjugate heat transfer CFD models agree well with the experimental correlations within the considered uncertainty range. It is found that the local wall temperature adjacent to flow is not uniform, especially at lower *Re*, for the CFD model with Geometry2. The change of wall temperature along the flow direction between inlet and outlet is 5 K for *Re* of 510. By increasing the *Re*, this wall temperature becomes more uniform due to turbulent mixing. It is observed that after a few cells, the local heat transfer coefficients approach a constant value for all *Re* in the channel. This confirms that the heat transfer has a periodic nature. Moreover, it is concluded that the correct approach to determining the average heat transfer coefficients for Geometry2 for the whole range of *Re* is to average the local values over the length of the channel. Therefore, assuming the constant wall temperature for the whole heat exchanger in the $LMTD_{sim}$ formula is not valid for calculation of the average heat transfer coefficient of heat exchangers with polymeric materials. The results of both CFD models are found to be in very good agreement in terms of heat transfer coefficient and friction factor, with deviation of less than 1.7% and 4%, respectively. Furthermore, considering the number of grids that are used for each CFD model (Geometry1 and Geometry2), the CFD model with Geometry1 is superior and more cost-effective in terms of calculation time compared to the Geometry2.

A new design for a polymeric cross-corrugated heat exchanger with triangular corrugation for HVAC applications is proposed. The corrugation base is 5 mm and the aspect ratio is 2. The thickness of the wall is 0.5 mm. The conjugate CFD model shows that the thermal performance of the proposed polymeric heat exchanger is competitive with the metallic one with very low thermal conductivity. The proposed CFD model in this dissertation has great potential to accurately predict the thermo-hydraulic behaviour of polymeric cross-corrugated heat exchangers. As far as the HVAC applications with working fluid of air are concerned, the dominant resistance is on the air side; therefore, application of a very thin wall (thickness of 0.053 mm.) is not necessary for thermal enhancement unless it is required to meet the structural performance. This thicker wall (0.5 mm) has two advantages. First, it allows manufacturer to apply conventional extrusion techniques and tools instead of investing in the thin film processing method.

Second, it improves the structural performance. Even though composite materials have been developed to attain very high thermal conductivities, for the new design proposed in this thesis, the composite materials do not specially improve the thermal performance. The influence of the composite materials on thermal performance becomes more noticeable as wall thickness is increased. It is noted that the composite materials are superior to the pure polymeric materials for the proposed design when high structural performance is required. On the other hand, care has to be taken in making composite material because adding the thermal enhanced fillers to polymers increases the cost of heat exchanger manufacturing, while the fabrication of heat exchangers from pure polymers decreases the cost. Therefore, depending on the application and structural performance requirements, fabrication of this type of heat exchanger from composites must be evaluated in terms of production cost. It is concluded that for HVAC applications operating with air at low temperature and pressure conditions (temperature lower than 60°C and atmospheric pressure), for example building applications, the proposed design in this dissertation using pure polymers could produce an economical commercial heat exchanger. It should be noted that this conclusion concerning the relative importance of wall material thermal conductivity and the convective heat transfer coefficient is dependent upon the geometry and fluid.

5.2 Future Recommendations

The flow in a cross-corrugated plate heat exchanger displays a three-dimensional behaviour. The main part of it follows the upper corrugation area of the channel and a small part of it impinges into the lower corrugation area of the channel. The behaviour of the flow in the upper area is similar to pipe flow. It is observed that the complexity of the vortices in the lower part of the channel contribute mostly to the high pressure drop and heat transfer coefficient. There is a hypothesis that if a larger part of the flow diverges towards the lower corrugation part this can lead to the creation of stronger vortices in the lower part, and consequently an improved thermo-hydraulic performance. Therefore, it is recommended to investigate the influence of adding a vortex generator, baffle, or dimple to the upper corrugation part on the thermo-hydraulic characteristics of heat exchanger. This can be simply implemented in the proposed CFD model for convection described in this dissertation

Additionally, due to the lack of experimental data on polymeric cross-corrugated heat exchangers, it is recommended that a set of experimental measurements be conducted for the virtual polymeric heat exchanger design from this dissertation in future. The availability of more data and exposing the production challenges of this heat exchanger in reality will open the new opportunities for the heat

exchanger market to benefit from the advantages of new polymeric technologies especially for compact cross-corrugated geometries.

Furthermore, it is recommended that industrial applications operating in a high range of temperatures or pressures where the analytical structural performance correlations are not able to predict the strength of polymeric cross-corrugated heat exchanger (specifically for the new generation of composite materials) integrate the conjugated CFD model developed in this dissertation with finite element model for structural analysis.

Finally, in the case of the production of cross-corrugated heat exchangers from composite materials, it is recommended to define an optimisation tool in which thermal performance (UA) is the goal function and the constraints are the pressure drop, strength, and costs requirements. Solving this optimisation problem ensures that all requirements are met, and the design parameters are efficiently chosen for the specific application. Consequently, this tool can validate whether the replacement of metallic materials with pure polymers or composites is feasible. This provides a strong incentive for industries to move towards new polymeric heat exchanger technologies for better energy efficiency, as well as fouling and corrosion resistance. Likewise, it diminishes the mainstream obstacles defined against the use of polymeric or composite materials for heat exchangers.

A

Publications

Related Publications in Peer-Reviewed International Journals

- Sharif, Asal, Bernd Ameel, Ilya T'Jollyn, Steven Lecompte, and Michel De Paepe. 2018. "Comparative Performance Assessment of Plate Heat Exchangers with Triangular Corrugation." Applied Thermal Engineering 141: 186–199.

- Sharif, Asal and Michel De Paepe. 2019. "Heat transfer and pressure drop correlations for triangular cross-corrugated plates in transitional flow regime". Computational Thermal Science (approved by editor, in possession of editor in chief).

Related Publications in Proceedings of Conferences as First Author

- Sharif, Asal, Bernd Ameel, Sven De Schampheleire, Özer Bağci, Lenka Bokisova, and Michel De Paepe. 2016. "Feasibility study of a plastic helical coil heat exchanger for a domestic storage tank." In Proceedings of the 12th International Conference on Heat Transfer, Fluid Mechanics and Thermodynamics, 949 – 954.
- Sharif, Asal, Bernd Ameel, Özer Bağci, Lenka Bokisova, and Michel De Paepe. 2017. "Influence of Apex Angle on Thermal Hydraulic Behavior of a Polymeric Triangular Cross-corrugated Plate." In Advances in Computational Heat Transfer. Begell House.

- Sharif, Asal, Özer Bağci, Bernd Ameel, Lenka Bokisova, and Michel De Paepe. 2017. "Parametric Study of a Triangular Cross-corrugated Plate" In Proceedings of the 13th International Conference on Heat Transfer, Fluid Mechanics and Thermodynamics, 716–721.

- Sharif, Asal, and Michel De Paepe. 2018. "Thermal Hydraulic Characteristic of a Triangular Cross-corrugated Plate." In Proceedings of the International Heat Transfer Conferences, 2919–2927.

Publications in Proceedings of Conferences as Co-author

- De Schampheleire, S., De Kerpel, K., Ameel, B., Sharif, A., Bagci, O. and De Paepe, M., 2016. On the numerical simulation of fins in natural convection. In Proceedings of the 12th International Conference on Heat Transfer, Fluid Mechanics and Thermodynamics. HEFAT 2016.

- Bokiskova, Lenka, Özer Bağci, Asal Sharif, Dieter Daenens, Wim Beyne, and Michel De Paepe. 2017. "Plastic helical coil heat exchanger as an alternative for a domestic water storage tank." In proceedings of 13th International Conference on Heat Transfer, Fluid Mechanics and Thermodynamics. HEFAT 2017.

- Bağci, Özer, Asal Sharif, Bernd Ameel, and Michel De Paepe. 2016. "Comparison of Heat Transfer and Pressure Drop Between Analytical and Computational Approaches: a Preliminary Study for Optimal Heat Exchanger Design." In Proceedings of the 12th International Conference on Heat Transfer, Fluid Mechanics and Thermodynamics. HEFAT 2016.

- De Schampheleire, Sven, Kathleen De Kerpel, Bernd Ameel, Asal Sharif, Özer Bağci, and Michel De Paepe. 2016. "How to Perform Numerical Simulations on Fins in Buoyancy-driven Heat Transfer?" In 7th European Thermal-Sciences Conference.

References

[1] F. Birol, World energy outlook 2010, International Energy Agency, 1(3) (2010).

[2] S. Bruce, International law and renewable energy: Facilitating sustainable energy for all, Melb. J. Int'l L., 14 (2013) 18.

[3] I.E.A. (IEA), Global Energy and CO2 Status Report in, International Energy Agency (IEA), 2018.

[4] European Union, The EU climate and energy package, in.

[5] E. Thorin, Basics of energy, (2014).

[6] European Commission, Communication from the commission to the European Parliament, the council, the European Economic and social committee of the regions- An EU Strategy on Heating and Cooling, 2016.

[7] Frost&Sullivan, Trends in Heat Exchangers - Technology Market Penetration and Roadmapping, 2011.

[8] G.B.M. Market, Acmite market intelligence, Ratingen, Germany, (2013).

[9] J.E. Hesselgreaves, R. Law, D. Reay, Compact heat exchangers: selection, design and operation, Butterworth-Heinemann, 2016.

[10] D.P. Sekulic, Compact heat exchangers, Handbook of Thermal Science and Engineering, (2017) 1-20.

[11] W. Focke, P. Knibbe, Flow visualization in parallel-plate ducts with corrugated walls, Journal of Fluid Mechanics, 165 (1986) 73-77.

[12] H. Blomerius, C. Holsken, N. Mitra, Numerical investigation of flow field and heat transfer in cross-corrugated ducts, Journal of heat transfer, 121(2) (1999) 314-321.

[13] W. Focke, J. Zachariades, I. Olivier, The effect of the corrugation inclination angle on the thermohydraulic performance of plate heat exchangers, International Journal of Heat and Mass Transfer, 28(8) (1985) 1469-1479.

[14] R. Shah, A. Wanniarachchi, Plate heat exchanger design theory, in: J.M. Buchlin (Ed.) Industrial Heat Exchangers, Lecture Series 1991–04, VKI Industrial Heat Exchangers, Rhode-Saint-Genese, Belgium, 1991.

[15] R.K. Shah, D.P. Sekulic, Fundamentals of heat exchanger design, John Wiley & Sons, 2003, pp. 28.

[16] L. Zaheed, R. Jachuck, Review of polymer compact heat exchangers, with special emphasis on a polymer film unit, Applied thermal engineering, 24(16) (2004) 2323-2358.

[17] C. T'Joen, Y. Park, Q. Wang, A. Sommers, X. Han, A. Jacobi, A review on polymer heat exchangers for HVAC&R applications, International journal of refrigeration, 32(5) (2009) 763-779.

[18] H.T. El-Dessouky, H.M. Ettouney, Plastic/compact heat exchangers for single-effect desalination systems, Desalination, 122(2-3) (1999) 271-289.

[19] J. Zhao, B. Li, X. Li, Y. Qin, C. Li, S. Wang, Numerical simulation of novel polypropylene hollow fiber heat exchanger and analysis of its characteristics, Applied Thermal Engineering, 59(1-2) (2013) 134-141.

[20] R. Bahadur, A. Bar-Cohen, Thermal design and optimization of natural convection polymer pin fin heat sinks, IEEE transactions on components and packaging technologies, 28(2) (2005) 238-246.

[21] A. Mannoni, D. Vitali, Development of All-Nylon Charge Air Cooler for Automotive Applications, 0148-7191, SAE Technical Paper, 2001.

[22] D. Reay, The use of polymers in heat exchangers, Heat Recovery Systems and CHP, 9(3) (1989) 209-216.

[23] J.G. Cevallos, A.E. Bergles, A. Bar-Cohen, P. Rodgers, S.K. Gupta, Polymer heat exchangers—history, opportunities, and challenges, Heat Transfer Engineering, 33(13) (2012) 1075-1093.

[24] X. Chen, Y. Su, D. Reay, S. Riffat, Recent research developments in polymer heat exchangers–A review, Renewable and Sustainable Energy Reviews, 60 (2016) 1367-1386.

[25] A.R.J. Hussain, A.A. Alahyari, S.A. Eastman, C. Thibaud-Erkey, S. Johnston, M.J. Sobkowicz, Review of polymers for heat exchanger applications: Factors concerning thermal conductivity, Applied Thermal Engineering, 113 (2017) 1118-1127.

[26] D.C. Deisenroth, R. Moradi, A.H. Shooshtari, F. Singer, A. Bar-Cohen, M. Ohadi, Review of heat exchangers enabled by polymer and polymer composite additive manufacturing, Heat Transfer Engineering, 39(19) (2018) 1652-1668.

[27] J. Burns, R. Jachuck, Condensation studies using cross-corrugated polymer film compact heat exchanger, Applied Thermal Engineering, 21(4) (2001) 495-510.

[28] A. Lowenstein, S. Slayzak, E. Kozubal, A zero carryover liquid-desiccant air conditioner for solar applications, in: ASME 2006 International Solar Energy Conference, American Society of Mechanical Engineers, 2006, pp. 397-407.

[29] L. Cheng, C.W.V.D. GELD, Experimental study of heat transfer and pressure drop characteristics of air/water and air-steam/water heat exchange in a polymer compact heat exchanger, Heat transfer engineering, 26(2) (2005) 18-27.

[30] P.W. Luckow, Minimum Energy Design of Seawater Heat Exchangers, 2009.

[31] A. Bar-Cohen, P. Rodgers, J. Cevallos, Application of thermally enhanced thermoplastics to seawater-cooled liquid-liquid heat exchangers, in: Proceedings 5th European Thermal-Sciences Conference, Citeseer, 2008.

[32] D. Laaber, H.-J. Bart, Chemical and pressure stress resistance of polymer films, Polymer Testing, 40 (2014) 280-285.

[33] J.B. Christmann, L.J. Krätz, H.-J. Bart, Falling film evaporation with polymeric heat transfer surfaces, Desalination, 308 (2013) 56-62.

[34] J.B. Christmann, L.J. Krätz, H.-J. Bart, Novel polymer film heat exchangers for seawater desalination, Desalination and Water Treatment, 21(1-3) (2010) 162-174.

[35] S. Alizadeh, A feasibility study of using solar liquid-desiccant air conditioner in Queensland, Australia, Journal of Solar Energy Engineering, 130(2) (2008) 021005.

[36] C. Harris, M. Despa, K. Kelly, Design and fabrication of a cross flow micro heat exchanger, Journal of Microelectromechanical Systems, 9(4) (2000) 502-508.

[37] P. Glouannec, P. Chauvelon, J.-F. Feller, H. Noel, J.-P. Ploteau, Current passage tubes in conductive polymer composite for fluid heating, Energy Conversion and Management, 49(4) (2008) 493-505.

[38] H. Noel, P. Glouannec, J.-P. Ploteau, P. Chauvelon, J.-F. Feller, Design and study of an electrical liquid heater using conductive polymer composite tubes, Applied Thermal Engineering, 54(2) (2013) 507-515.

[39] K. Bourouni, R. Martin, L. Tadrist, H. Tadrist, Experimental investigation of evaporation performances of a desalination prototype using the aero-evapo-condensation process, Desalination, 114(2) (1997) 111-128.

[40] B. Ghosh, W. Yousef, M. Al Jaberi, N. Al Hajeri, A. Al Braiki, V. Eveloy, P. Rodgers, Design and Investigation into the Thermal and Mechanical Performance of a Polymer Composite Prototype Gas-Liquid Heat Exchanger: Int, Int. J. of Thermal & Environmental Engineering, 11(1) (2016) 51-59.

[41] J. Cevallos, A. Bar-Cohen, D.C. Deisenroth, Thermal performance of a polymer composite webbed-tube heat exchanger, International Journal of Heat and Mass Transfer, 98 (2016) 845-856.

[42] L. Chen, Z. Li, Z.-Y. Guo, Experimental investigation of plastic finned-tube heat exchangers, with emphasis on material thermal conductivity, Experimental Thermal and Fluid Science, 33(5) (2009) 922-928.

[43] L. Song, B. Li, D. Zarkadas, S. Christian, K.K. Sirkar, Polymeric hollow-fiber heat exchangers for thermal desalination processes, Industrial & Engineering Chemistry Research, 49(23) (2010) 11961-11977.

[44] W. Liu, J. Davidson, S. Mantell, Thermal analysis of polymer heat exchangers for solar water heating: a case study, TRANSACTIONS-AMERICAN SOCIETY OF MECHANICAL ENGINEERS JOURNAL OF SOLAR ENERGY ENGINEERING, 122(2) (2000) 84-91.

[45] C. Wu, S.C. Mantell, J. Davidson, Polymers for solar domestic hot water: long-term performance of PB and nylon 6, 6 tubing in hot water, Journal of solar energy engineering, 126(1) (2004) 581-586.

[46] D.M. Zarkadas, K.K. Sirkar, Cooling crystallization of paracetamol in hollow fiber devices, Industrial & engineering chemistry research, 46(10) (2007) 2928-2935.

[47] X. Yan, B. Li, B. Liu, J. Zhao, Y. Wang, H. Li, Analysis of improved novel hollow fiber heat exchanger, Applied Thermal Engineering, 67(1-2) (2014) 114-121.

[48] G. Shives, J. Norley, M. Smalc, G. Chen, J. Capp, Comparative thermal performance evaluation of graphite/epoxy fin heat sinks, in: The Ninth Intersociety Conference on Thermal and Thermomechanical Phenomena In Electronic Systems (IEEE Cat. No. 04CH37543), IEEE, 2004, pp. 410-417.

[49] K. Kasza, I. Królikowski, Optimization of pin fin heat sink by application of CFD simulations and DOE methodology with neural network approximation, International Journal of Applied Mechanics and Engineering, 18(2) (2013) 365-381.

[50] J. Hoerber, M. Mueller, J. Franke, F. Ranft, C. Heinle, D. Drummer, Assembly and interconnection technologies for MID based on thermally conductive plastics for heat dissipation, in: Proceedings of the 2011 34th International Spring Seminar on Electronics Technology (ISSE), IEEE, 2011, pp. 103-108.

[51] L. Zaheed-Maheswaran, Process intensification: cross-corrugated polymer film compact heat exchanger (PFCHE), Newcastle University, 2003.

[52] F. Mazzolani, Aluminium alloy structures, CRC Press, 1994.

[53] L.-Z. Zhang, C.-H. Liang, L.-X. Pei, Conjugate heat and mass transfer in membrane-formed channels in all entry regions, International Journal of Heat and Mass Transfer, 53(5-6) (2010) 815-824.

[54] A. Bar-Cohen, P. Luckow, J.G. Cevallos, S. Gupta, Thermal Anisotropy in Injection Molded Polymer Composite Fins, in: 2010 14th International Heat Transfer Conference, American Society of Mechanical Engineers, 2010, pp. 405-416.

[55] L.-z. Zhang, Z.-y. Chen, Convective heat transfer in cross-corrugated triangular ducts under uniform heat flux boundary conditions, International Journal of Heat and Mass Transfer, 54(1-3) (2011) 597-605.

[56] K. Scott, J. Lobato, Mass transport in cross-corrugated membranes and the influence of TiO2 for separation processes, Industrial & engineering chemistry research, 42(22) (2003) 5697-5701.

[57] S. Etemad, B. Sundén, Hydraulic and Thermal Simulations of a Cross-Corrugated Plate Heat Exchanger Unitary Cell, Heat Transfer Engineering, 37(5) (2016) 475-486.

[58] A. Muley, R. Manglik, H. Metwally, Enhanced heat transfer characteristics of viscous liquid flows in a chevron plate heat exchanger, Journal of Heat Transfer, 121(4) (1999) 1011-1017.

[59] R. Heavner, H. Kumar, A. Wanniarachchi, Performance of an industrial plate heat exchanger: effect of chevron angle, in: AIChE Symposium Series, American Institute of Chemical Engineers, 1993, pp. 262-262.

[60] A. Savostin, A. Tikhonov, Investigation of characteristics of plate-type heating surfaces, Thermal Engineering, 17(9) (1970) 113-&.

[61] B. Sundén, R.M. Manglik, Plate heat exchangers: design, applications and performance, Wit Press, 2007.

[62] eurostat. Final energy consumption by sector (EuroStat dataset). http://ec.europa.eu/eurostat/tgm/table.do?tab= table&plugin=1&language=en&pcode=tsdpc320. Accessed: 21-06-2019.

[63] 2050 low-carbon economy — Climate Action. https://ec. europa.eu/clima/policies/strategies/2050_en. Accessed: 21-06-2019

[64] A.S.o. Heating, Refrigerating, A.-C. Engineers, A.N.S. Institute, Thermal environmental conditions for human occupancy, American Society of Heating, Refrigerating and Air-Conditioning Engineers, 2004.

[65] B. Ameel, Optimisation of compound louvred fin and vortex generator heat exchangers, Ghent University, 2014.

[66] L. Pérez-Lombard, J. Ortiz, C. Pout, A review on buildings energy consumption information, Energy and buildings, 40(3) (2008) 394-398.

[67] R. Shah, W. Focke, Plate heat exchangers and their design theory, Heat Transfer Equipment Design, 227 (1988) 254.

[68] M. Mehrabian, R. Poulter, Hydrodynamics and thermal characteristics of corrugated channels: computational approach, Applied Mathematical Modelling, 24(5) (2000) 343-364.

[69] C.S. Fernandes, R.P. Dias, J.M. Nóbrega, J.M. Maia, Laminar flow in chevron-type plate heat exchangers: CFD analysis of tortuosity, shape factor and friction factor, Chemical Engineering and Processing: Process Intensification, 46(9) (2007) 825-833.

[70] S. Freund, S. Kabelac, Investigation of local heat transfer coefficients in plate heat exchangers with temperature oscillation IR thermography and CFD, International Journal of Heat and Mass Transfer, 53(19) (2010) 3764-3781.

[71] W. Han, K. Saleh, V. Aute, G. Ding, Y. Hwang, R. Radermacher, Numerical simulation and optimization of single-phase turbulent flow in chevron-type plate heat exchanger with sinusoidal corrugations, HVAC&R Research, 17(2) (2011) 186-197.

[72] N. Ghaddar, K. Korczak, B. Mikic, A. Patera, Numerical investigation of incompressible flow in grooved channels. Part 1. Stability

and self-sustained oscillations, Journal of Fluid Mechanics, 163 (1986) 99-127.

[73] B. Sundén, S. Trollheden, Periodic laminar flow and heat transfer in a corrugated two-dimensional channel, International Communications in Heat and Mass Transfer, 16(2) (1989) 215-225.

[74] J. Pereira, J. Sousa, Finite volume calculations of self-sustained oscillations in a grooved channel, Journal of Computational Physics, 106(1) (1993) 19-29.

[75] T. Adachi, H. Uehara, Correlation between heat transfer and pressure drop in channels with periodically grooved parts, International Journal of Heat and Mass Transfer, 44(22) (2001) 4333-4343.

[76] P. Heggs, P. Sandham, R. Hallam, C. Walton, Local transfer coefficients in corrugated plate heat exchanger channels, Chemical Engineering Research and Design, 75(7) (1997) 641-645.

[77] R. Shah, M. Heikal, B. Thonon, P. Tochon, Progress in the numerical analysis of compact heat exchanger surfaces, Advances in heat transfer, 34 (2001) 363-443.

[78] F.-B. Liu, Y.-C. Tsai, An experimental and numerical investigation of fluid flow in a cross-corrugated channel, Heat and Mass Transfer, 46(5) (2010) 585-593.

[79] J. Yin, G. Li, Z. Feng, Effects of intersection angles on flow and heat transfer in corrugated-undulated channels with sinusoidal waves, Journal of heat transfer, 128(8) (2006) 819-828.

[80] Z. Guo-Yan, T. Shan-Tung, M. Hu-Gen, Numerical and Experimental Study on the Heat Transfer and Pressure Drop of Compact Cross-Corrugated Recuperators, Journal of Heat Transfer, 136(7) (2014) 071801.

[81] Z. Chen, Laminar forced flow and heat transfer in cross-corrugated triangular ducts, Heat Transfer Engineering, 37(16) (2016) 1392-1400.

[82] M. Ciofalo, J. Stasiek, M. Collins, Investigation of flow and heat transfer in corrugated passages—II. Numerical simulations, International Journal of Heat and Mass Transfer, 39(1) (1996) 165-192.

[83] M. Ciofalo, M. Collins, J. Stasiek, Flow and heat transfer predictions in flow passages of air preheaters- Assessment of alternative modeling approaches, Computer simulations in compact heat exchangers(A 99-14847 02-34), Southampton, United Kingdom and Boston, MA, Computational Mechanics Publications, 1998, (1998) 169-225.

[84] M. Ciofalo, I. Di Piazza, J. Stasiek, Investigation of flow and heat transfer in corrugated-undulated plate heat exchangers, Heat and Mass Transfer, 36(5) (2000) 449-462.

[85] A. Kanaris, A. Mouza, S. Paras, Optimal design of a plate heat exchanger with undulated surfaces, International Journal of Thermal Sciences, 48(6) (2009) 1184-1195.

[86] O. Pelletier, F. Strömer, A. Carlson, CFD Simulation of Heat Transfer in Compact Brazed Plate Heat Exchangers, ASHRAE Transactions, 111(1) (2005) 846-854.

[87] C.F. Dietz, S. Olaf Neumann, B. Weigand, A comparative study of the performance of explicit algebraic models for the turbulent heat flux, Numerical Heat Transfer, Part A: Applications, 52(2) (2007) 101-126.

[88] B.E. Launder, Second-moment closure and its use in modelling turbulent industrial flows, International Journal for Numerical Methods in Fluids, 9(8) (1989) 963-985.

[89] D. Dovic, S. Svaic, Experimental and numerical study of the flow and heat transfer in plate heat exchanger channels, (2004).

[90] X. Liu, J. Niu, Effects of geometrical parameters on the thermohydraulic characteristics of periodic cross-corrugated channels, International Journal of Heat and Mass Transfer, 84 (2015) 542-549.

[91] V. Yakhot, S. Orszag, S. Thangam, T. Gatski, C. Speziale, Development of turbulence models for shear flows by a double expansion technique, Physics of Fluids A: Fluid Dynamics, 4(7) (1992) 1510-1520.

[92] M.-A. Hessami, An experimental investigation of the performance of cross-corrugated plate heat exchangers, Journal of enhanced heat transfer, 10(4) (2003).

[93] T. Khan, M. Khan, M.-C. Chyu, Z. Ayub, Experimental investigation of single phase convective heat transfer coefficient in a corrugated plate heat exchanger for multiple plate configurations, Applied Thermal Engineering, 30(8-9) (2010) 1058-1065.

[94] F. Warnakulasuriya, W. Worek, Heat transfer and pressure drop properties of high viscous solutions in plate heat exchangers, International Journal of Heat and Mass Transfer, 51(1-2) (2008) 52-67.

[95] L. Zhang, D. Che, Influence of corrugation profile on the thermalhydraulic performance of cross-corrugated plates, Numerical Heat Transfer, Part A: Applications, 59(4) (2011) 267-296.

[96] K. Scott, A. Mahmood, R. Jachuck, B. Hu, Intensified membrane filtration with corrugated membranes, Journal of Membrane Science, 173(1) (2000) 1-16.

[97] D. Hall, K. Scott, R. Jachuck, Determination of mass transfer coefficient of a cross-corrugated membrane reactor by the limiting-current technique, International journal of heat and mass transfer, 44(12) (2001) 2201-2207.

[98] C. Leung, S. Probert, Forced-convective turbulent-flows through horizontal ducts with isosceles-triangular internal cross-sections, Applied Energy, 57(1) (1997) 13-24.

[99] L. Zhang, Numerical study of periodically fully developed flow and heat transfer in cross-corrugated triangular channels in transitional flow regime, Numerical Heat Transfer, Part A: Applications, 48(4) (2005) 387-405.

[100] A.L. London, Compact heat exchangers; Part 1-Design theory, Mechanical engineering, (1964) 47-51.

[101] R. Webb, Performance evaluation criteria for use of enhanced heat transfer surfaces in heat exchanger design, International Journal of Heat and Mass Transfer, 24(4) (1981) 715-726.

[102] B. Ameel, J. Degroote, C. T'Joen, P. De Jaeger, H. Huisseune, S. De Schampheleire, J. Vierendeels, M. De Paepe, Optimization of X-shaped louvered fin and tube heat exchangers while maintaining the physical meaning of the performance evaluation criterion, Applied Thermal Engineering, 58(1) (2013) 136-145.

[103] T. Cowell, A general method for the comparison of compact heat transfer surfaces, ASME J. Heat Transfer, 112(2) (1990) 288-294.

[104] H. Huisseune, S. De Schampheleire, B. Ameel, M. De Paepe, Comparison of metal foam heat exchangers to a finned heat exchanger for low Reynolds number applications, International Journal of Heat and Mass Transfer, 89 (2015) 1-9.

[105] H. Huisseune, Performance evaluation of louvered fin compact heat exchangers with vortex generators, Ghent University, 2011.

[106] R. Bowman, A. Mueller, u. WM Nagle, Mean Temperature Difference in Design, Trans. Amer. Soc. Mech. Engrs.(ASME), 62 (1940) 283.

[107] O. Reynolds, XXIX. An experimental investigation of the circumstances which determine whether the motion of water shall be direct or sinuous, and of the law of resistance in parallel channels, Philosophical Transactions of the Royal society of London, (174) (1883) 935-982.

[108] W. Malalasekera, H. Versteeg, An introduction to computational fluid dynamics: the finite volume method, PEARSON Prentice Hall, 2007.

[109] H. Schlichting, K. Gersten, Boundary-layer theory, Springer, 2016.

[110] F.P. Incropera, A.S. Lavine, T.L. Bergman, D.P. DeWitt, Fundamentals of heat and mass transfer, Wiley, 2007.

[111] S.B. Pope, Turbulent Flows, Cambridge University Press, 2001, pp. 454-458.

[112] M. Gibson, B. Launder, Ground effects on pressure fluctuations in the atmospheric boundary layer, Journal of Fluid Mechanics, 86(3) (1978) 491-511.

[113] F.-S. Lien, M. Leschziner, Assessment of turbulence-transport models including non-linear RNG eddy-viscosity formulation and second-moment closure for flow over a backward-facing step, Computers & Fluids, 23(8) (1994) 983-1004.

[114] B.J. Daly, F.H. Harlow, Transport equations in turbulence, The Physics of Fluids, 13(11) (1970) 2634-2649.

[115] S. Fu, B. Launder, M. Leschziner, Modelling strongly swirling recirculating jet flow with Reynolds-stress transport closures, in: 6th Symposium on Turbulent Shear Flows, 1987, pp. 17-16.

[116] S. Sarkar, L. Balakrishnan, Application of a Reynolds stress turbulence model to the compressible shear layer, (1990).

[117] W. Rodi, Experience with two-layer models combining the k-epsilon model with a one-equation model near the wall, in: 29th Aerospace sciences meeting, 1991, pp. 216.

[118] S.E. Rogers, D. Kwak, J.L. Chang, Numerical Solution Of Navier-Stokes Equations, (1989).

[119] P.J. Roache, Perspective: a method for uniform reporting of grid refinement studies, Transactions-American Society of Mechanical Engineers Journal of Fluids Engineering, 116 (1994) 405-405.

[120] K. Scott, J. Lobato, Mass transfer characteristics of cross-corrugated membranes, Desalination, 146(1-3) (2002) 255-258.

[121] L. Zhang, Convective mass transport in cross-corrugated membrane exchangers, Journal of membrane science, 260(1) (2005) 75-83.

[122] Z. Li, Y. Gao, Numerical study of turbulent flow and heat transfer in cross-corrugated triangular ducts with delta-shaped baffles, International Journal of Heat and Mass Transfer, 108 (2017) 658-670.

[123] A. Wragg, A. Leontaritis, Mass transfer measurements in a parallel cell using the limiting current technique, DECHEMA Monogr, 123 (1991) 345.

[124] S. Kakac, Y. Yener, A. Pramuanjaroenkij, Convective heat transfer, CRC press, 2013.

[125] L.M. Jiji, L.M. Jiji, Heat convection, Springer, 2006.

[126] N. Paisarn, Study on the heat-transfer characteristics and pressure drop in channels with arc-shaped wavy plates, Journal of Engineering Physics and Thermophysics, 83(5) (2010) 1061-1069.

[127] E.M. Greitzer, C.S. Tan, M.B. Graf, Internal flow: concepts and applications, Cambridge University Press, 2007, pp. 104-163.

[128] R.L. Panton, Incompressible flow, John Wiley & Sons, 2006, pp. 333-335.

[129] R.S. McQuivey, Principles and measuring techniques of turbulence characteristics in open-channel flows, US Government Printing Office, 1973.

[130] S. Kakac, H. Liu, A. Pramuanjaroenkij, Heat exchangers: selection, rating, and thermal design, CRC press, 2012.

[131] H. Martin, A theoretical approach to predict the performance of chevron-type plate heat exchangers, Chemical Engineering and Processing: Process Intensification, 35(4) (1996) 301-310.

[132] L. Wang, B. Sunden, Optimal design of plate heat exchangers with and without pressure drop specifications, Applied Thermal Engineering, 23(3) (2003) 295-311.

[133] B.P. Rao, B. Sunden, S.K. Das, An experimental and theoretical investigation of the effect of flow maldistribution on the thermal performance of plate heat exchangers, Journal of heat transfer, 127(3) (2005) 332-343.

[134] C. Liang, Z. Li, Conjugate heat transfer in a total heat exchanger with cross-corrugated triangular ducts in laminar flow, Journal of Thermal Science and Technology, 10(1) (2015) JTST0015-JTST0015.

[135] K. Mahmud, G.I. Mahmood, C.J. Simonson, R.W. Besant, Performance testing of a counter-cross-flow run-around membrane

energy exchanger (RAMEE) system for HVAC applications, Energy and Buildings, 42(7) (2010) 1139-1147.

[136] A. Sharif, B. Ameel, I. T'Jollyn, S. Lecompte, M. De Paepe, Comparative performance assessment of plate heat exchangers with triangular corrugation, Applied Thermal Engineering, (2018).

[137] I. SAS, SAS User's Guide: Statistics, version 5, SAS Institute Inc., Cary, NC, (1985) 433-506.

[138] P.A. Schweitzer, Metallic materials: physical, mechanical, and corrosion properties, CRC press, 2003.

[139] T.M.A. Elmaaty, A. Kabeel, M. Mahgoub, Corrugated plate heat exchanger review, Renewable and Sustainable Energy Reviews, 70 (2017) 852-860.

[140] X. Yang, C. Liang, T. Ma, Y. Guo, J. Kong, J. Gu, M. Chen, J. Zhu, A review on thermally conductive polymeric composites: classification, measurement, model and equations, mechanism and fabrication methods, Advanced Composites and Hybrid Materials, 1(2) (2018) 207-230.

[141] D. Reay, C. Ramshaw, A. Harvey, Process Intensification: Engineering for efficiency, sustainability and flexibility, Butterworth-Heinemann, 2013.

[142] L. McKeen, Fluorinated Coatings and Finishes Handbook, ; William Andrew, Inc.: Wilmington, DC, USA, (2006).

[143] R. Raman, S. Mantell, J. Davidson, C. Wu, G. Jorgensen, A review of polymer materials for solar water heating systems, Transactions-American Society of Mechanical Engineers Journal of Solar Energy Engineering, 122(2) (2000) 92-100.

[144] S. Gepp, T. Ottnad, O. Kessling, F. Irlinger, T.C. Lüth, Pressure dependency of mass flow rate of polypropylene melts through micro nozzles smaller than 500 µm, Chemie Ingenieur Technik, 83(4) (2011) 552-557.

[145] D. Zhao, Y. Jin, M. Wang, Study on viscosity of polymer melt flowing through microchannels considering the wall-slip effect, Polymer Engineering & Science, 52(8) (2012) 1806-1814.

[146] N. Zhang, M. Gilchrist, Characterization of thermo-rheological behavior of polymer melts during the micro injection moulding process, Polymer testing, 31(6) (2012) 748-758.

[147] M.M.A. Bhutta, N. Hayat, M.H. Bashir, A.R. Khan, K.N. Ahmad, S. Khan, CFD applications in various heat exchangers design: A review, Applied Thermal Engineering, 32 (2012) 1-12.

[148] P.A. Schweitzer, Mechanical and corrosion-resistant properties of plastics and elastomers, CRC Press, 2000.

[149] Omnexus, Omnexus: plastics & polymers solutions, in.

[150] R. Haftka, Z. Gürdal, P. Hajela, Design and Optimization of Laminated Composite Materials, TA418, 9 (1999) L3.

[151] C. Zweben, Emerging high-volume applications for advanced thermally conductive materials, in: Proceedings of the 49th International SAMPE Symposium and Exhibition, 2004, pp. 4061-4072.

[152] rtpcompany, Thermally Conductive Compounds, in, 2017.

[153] A.G. Kanaris, A.A. Mouza, S.V. Paras, Flow and heat transfer prediction in a corrugated plate heat exchanger using a CFD code, Chemical Engineering & Technology: Industrial Chemistry-Plant Equipment-Process Engineering-Biotechnology, 29(8) (2006) 923-930.

[154] H.W. Coleman, W.G. Steele, Experimentation, validation, and uncertainty analysis for engineers, John Wiley & Sons, 2018.

[155] N.H.M.Q.R. Al, Structural and Thermal Analysis of Heat Exchanger with Tubes of Elliptical Shape, Iraqi journal of mechanical and material engineering, 8(3) (2008) 257-271.

[156] R. Trojanowski, T. Butcher, M. Worek, G. Wei, Polymer heat exchanger design for condensing boiler applications, Applied Thermal Engineering, 103 (2016) 150-1